Design of a rapid heating/cooling system: control of the properties of micro-injection molded parts

Annarita De Meo

UNIVERSITY OF SALERNO

DEPARTMENT OF INDUSTRIAL ENGINEERING

Ph.D. Course in Industrial Engineering
Curriculum in Chemical Engineering - XXXII Cycle

Design of a rapid heating/cooling system: control the properties of micro-injection molded parts

Supervisor
Prof. Roberto Pantani

Ph.D. student
Annarita De Meo

Scientific Referees
Prof. Ben Whiteside
Dr. Felice De Santis

Ph.D. Course Coordinator
Prof. Francesco Donsì

Acknowledgement

A dream come true. Nobody will never know how happy I have been when I found out I had the possibility for this PhD course. I have enjoyed every moment and accepted the challenges of a not easy journey.

A lot of resistances burned during the first year. My friends, the night, were used to ask me when the smoke from the university would end up because everybody knew I was not very confident with the heaters at the beginning. Later I realized that the thermocouples I used were responsible of the heaters failure, the hot joint like a little ball strongly compressed in the mold damaged the grids and the resistances stopped working. Then the few times the things work, it could happen that the polymer goes not into the cavity because you may have not aligned the blocks during the closure. So many days were spent to try to recover heaters and thermocouples covered with undesired polymer injected behind the cavity. With patience, I took the welder and tried to clean to save my resistances. Felice sometimes came and called me crazy. In the troubles, I developed a special attitude to the precision and calmness and modestly I was known as a real watchmaking in the lab. As months go, I was able to recognize the signs of weakness of every part in the system and produce some good samples. I always thought working hard all the difficulties would be overcome, no matter if a lot of experiments will be never published or you performed fifty simulations and maybe present just one. It was part of the game, it is called research because you do not know what you are searching for and when you finally obtain results the eyes shine and the dream continues.

There was one who observed my way of working during the bachelor and offered me scholarships allowing me to dedicate my time to the education and the research. Professor Roberto Pantani, for everything you taught me these years I want to thank and say you are the best professor I have ever known. You are wise and virtuous and inspired me during my career. Thank you for trusting me and involved me in your projects these years. Thanks for all the time you have given and having encouraged me when I was afraid not to make it.

I had a great mentor during the master and the PhD. He derided me when I was not able to use the tools and how to connect two wires. He dedicated his time with patience and transmitted his precision and accuracy in research. He was always present and willing to help me. He has been my angel and he is a good friend. Thank you for everything, Felice.

I want to thank Ben Whiteside and Phil Coates for welcoming me in their laboratories in Bradford where I learned more about micro-injection molding and allowed me carrying out experiments for my thesis.

Thanks Vito for having helped me to carry out the simulations, the AFM analysis and for everything. Valentina Iozzino, thanks not only for the hydrolysis experiments, Valentina Volpe and Fabiana Foglia, not only for the characterization tests, and Sara Liparoti, thank you all for the time spent together in the lab.

I want to express my gratitude also to Carmine Donadio (E.C.S. Stampi) for having manufactured my insert only in two days from the delivery of the drawings saving me from long waits and retardation of my work.

Thanks Rocco Di Girolamo for some of the X-Ray analysis presented in my thesis.

I would thank Professor Giuseppe Titomanlio and Andrea Sorrentino for the good advices they gave me.

I want to thank all the members of the lab where I spent the last 8 years, the ones that are gone and the ones who arrived and the students who worked with me for their thesis.

To all my friends, thank you.

Endless thanks to my mother and Carmine for the moral support for putting up with me in tough times with love and understanding. Thank you.

Publications list

- De Meo, A., De Santis, F., Pantani, R., Local control of crystallinity in PLA microparts (in preparation).
- Foglia, F., De Meo A., Iozzino V., Volpe, V., Pantani, R., Isothermal crystallization of PLA: Nucleation density and growth rates of α and α’ phases (in press).
- Liparoti, S., Speranza, V., De Meo, A., De Santis, F., & Pantani, R. (2020). Prediction of the maximum flow length of a thin injection molded part. Journal of Polymer Engineering, 1 https://doi.org/10.1515/polyeng-2019-0292.
- De Meo, A., De Santis, F., Pantani, R., POLYM. ENG. SCI., 58:586–591, 2018 https://doi.org/10.1002/pen.24784.
- De Meo, A., Iozzino, V., & Pantani, R., Frontiers in Materials, 6, 305, 2019 https://doi.org/10.3389/fmats.2019.00305.
- De Meo, A., De Santis, F., & Pantani, R. (2020, January). In AIP Conference Proceedings 2205, 020016, AIP Publishing.
- De Meo, A., De Santis, F., Iozzino, V., & Pantani, R. (2019, August). In AIP Conference Proceedings (Vol. 2139, No. 1, p. 120002). AIP Publishing.
- De Meo, A., De Santis, F., & Pantani, R. (2018, July). In AIP Conference Proceedings (Vol. 1981, No. 1, p. 020085). AIP Publishing.
- De Meo, A., De Santis, F., Speranza, V., Whiteside, B., Coates, P. D., & Pantani, R. (2019, February). In AIP Conference Proceedings (Vol. 2065, No. 1, p. 040002). AIP Publishing.
- F. De Santis, A. De Meo, R. Pantani, Contribution on POLYMERS: Site of Advanced Horizons and Ambits ISBN 978-80-7454-729-4, May 21-25, 2018 (Zlin, CZ)
- R. Pantani, A. De Meo, F. De Santis, S. Liparoti, V. Speranza, G. Titomanlio, Proceedings of the First International Conference on 4D Materials and Systems, August 26-30, 2018 (Yonezawa, JA).
- R. Pantani, A. De Meo, F. De Santis, S. Liparoti, V. Speranza, G. Titomanlio, Proceedings of the Workshop on Polymer Crystallization, September 3-5, 2018 (Genova, IT).

- F. De Santis, A. De Meo, R. Pantani, Conference Paper, Proceedings of PMI 2018 International Conference on polymers and moulds innovations; 19-21 Sep 2018
- Rochman A., Bezzina M., Vella P., Pantani R., De Meo A., Conference Paper, Proceedings of PMI 2018 International Conference on polymers and moulds innovations; 19-21 Sep 2018.
- Bezzina M., Rochman A., Vella P., Zammit Tabona T., De Meo A., Pantani R., Proceedings of WCMNM 2019, World Congress on Micro and Nano Manufacturing, 10-12 Sep 2019.

Table of contents

List of Figures

List of Tables

Abstract

Microinjection molding (μIM) is one of the most efficient processes for wide scale production of thermoplastic polymer microparts. In order to produce high-quality microinjection-molded components, a crucial aspect to be fully understood and optimized is the filling of the cavity by the polymer. The standard injection molding process with constant mold temperature control suffers from problems caused by the large temperature difference between the mold and the incoming polymer. The mold temperature appears to be a key parameter for the fabrication of microparts of a more large range of materials. Even though variotherm technology has existed for decades and includes many kinds of heating methods, it is still not a proven one for use with μIM. Therefore, in the literature, the polymer melt flow phenomenon in a cavity for μIM with rapid variations of temperature is still not well discussed.

In this thesis, a special surface-conditioning concept that fulfils rapid temperature evolutions during the μIM is designed and adopted to extend the freezing time and affect the morphology of semicrystalline polymers. The dynamic temperature concept is based on a multilayer cavity with thin heating elements, thermocouples and insulation layers: it permits to increase the temperature of an amount of 100°C in a few seconds and obtain a cooling time of about 10 s. The system is used for the μIM of a poly-lactid acid (PLA) and an isotactic polypropylene (iPP).

The PLA is a biodegradable polymer with a low crystallization rate. Calorimetric analysis on pellets of PLA permitted to study the crystallization behavior in quiescent conditions and set a temperature for the annealing steps during the process. In this manner, the system for the temperature control was adopted to influence the final crystallinity of the PLA, by applying isothermal steps. Furthermore, the system was used to apply different thermal histories in different zones of the sample after the solidification in the microcavity and generate a crystalline phase and an amorphous one in the same part. Morphology modifications were analyzed by means of optical observations, calorimetric analysis, X-ray and IR spectra. To study the effect of the morphology on the biodegradation rate, experiments of hydrolysis were also carried out revealing that the parts exhibit different degradation kinetics and different mechanical behavior.

The potentiality of the system for the rapid temperature control was verified for a thin cavity with a geometry characterized by two entrances. The iPP was considered as material for the tests and the effect of the application of different temperature of the cavity on the weld line formation was studied. The effect of the temperature on the weld line formation is remarkable: increasing the value of the cavity temperature the weld line appear less evident and tends to disappear at 130°C. Morphological investigations represented a

key factor to determine the effect of the different thermal histories on the final mechanical properties.

By means of Moldflow simulations, a mold for industrial scale was studied. In this case, to minimize the thermal dispersion, a moving system for the cavity seat was created. The study demonstrates that during the heating step, the use of the system allows the reduction of the thermal dispersion and the achievement of a temperature increase of the order of one hundred degrees at the cavity surfaces. Furthermore, the high thermal conductivity of the cavity permits to obtain a fast cooling when the mold is closed.

Overview of the thesis

The objective of this thesis is the development of a system for rapid and local temperature control to affect the final properties of semicrystalline polymers. The book is structured in seven chapters, after an introductive chapter on the Micro-injection molding technique, Chapters II describes the control system developed and adopted for this thesis, the Chapters III to VI give examples of applications. Since the issues investigated and the materials and thermal histories adopted are different, each chapter has its own state of art and set of experiments and analysis. A short overview is given below.

In the first chapter, *"Micro-injection Molding"* an overview of the micro-injection molding technology is given: examples of application, working principle and issues. Some of the problems or defects in microparts, like premature solidification, are related to the temperature of the mold.

In the second chapter, *"Study and development of a system for the rapid temperature control"*, dynamic mold temperature control systems will be reviewed and the system developed in this work will be described and simulated.

The simulations and the preliminary results confirm the system can be used to investigate different interesting aspects that are examined in the following chapters. They include the effects of cavity temperature on the final lengths of the parts, how to tune the final properties by promoting the crystallization phenomenon, also, locally that is only in one zone of the cavity and check the effect on the degradation of the part. The mold temperature represents a key parameter also for the mixing of the flow fronts during the injection: they can prematurely solidify with the formation of the weld lines that represent aesthetical defects but also critical regions in terms of mechanical properties. Since the experiments described in the thesis were carried out with a laboratory injection molding machine, a part of the work involved the study and the simulation of the system for the rapid temperature control in the case a mold of industrial scale is considered.

In the third chapter, *"Effects of cavity temperature variations on filling and orientation properties of micro-injection molded PLA parts"*, the effect of the temperature of the surfaces on the filling behavior and the final orientation of a relatively high viscous polymer is studied applying fast temperature variations. An injection molding grade Poly-Lactid Acid (PLA) was chosen for this study.

The effect of different thermal histories in different positions of the cavity on the final morphology of PLA parts is presented in the fourth chapter, *"Application of the system to locally control the properties of PLA micro-parts"*. In this case, the study of the crystallization kinetics permitted the identification of the most favorable condition to obtain a large amount of crystalline structures (Part 1 of the chapter) and this result was used to obtain biphasic samples with different properties along the length (Part 2 of the chapter).

In the fifth chapter, "*Micromolded PLA with selective degradation rate"*, the possibility to obtain biphasic parts, as described in the fourth chapter, was used to verify the effects on the degradation kinetics of PLA.

In the sixth chapter, *"Effect of dynamic thermal variations on the morphology and the weld line in iPP microparts"*, the method for the rapid control of the temperature was adopted for a different geometry to generate weld lines into the parts: the part 1 of the chapter focuses on the filling of the geometry and the predictions by Moldflow. The effect of different thermal conditions on the final properties of a Polypropylene are verified in the second part of the chapter. The effect of different cavity temperatures during the filling and packing stage on the weld line appearance, the morphology and mechanical properties have been investigated.

The design of a mold with the rapid temperature control system for industrial scale was studied in the seventh chapter, *"Innovative design and simulation study of a mold for rapid temperature control in micro-injection molding"*, to verify the potentiality of the system when a different volume of the mold is considered and a moving insert method is used.

The last chapter *"Future research"* contains the possible future developments of the work.

Chapter I. Microinjection Molding

The production of parts with a scale and intricate level of detail is not feasible adopting conventional injection molding techniques but requires the use of the Micro-injection molding (μIM). According to the definition gave by Whiteside et al. (Whiteside *et al.*, 2004) a micro part has these characteristics:

- The mass of the order of a few milligrams.
- The part contains regions of detail with dimensions of the order of micrometers.
- The part has tolerances in the micrometer range.

Parts fabricated by μIM are suitable for applications requiring low-cost and disposable components. Furthermore, the complexity of the design affects only slightly the processing costs of micro-molded parts. Once a mold insert has been manufactured, thousands of micro-parts can be produced with not big effort. Since micro-components need only small material quantities, the cost of raw material can be quite low.

Plastic products manufactured by μIM have made a successful entry into the market. The production capability, the disposability and the biocompatibility represent characteristics that make plastics as the best choice for a large number of products in the micro scale. The application of micro-molded products cover different fields such as micro-mechanics (micro switches, micro-pumps, micro-gears, micro-actuators), micro optics (micro/sub-micrometer gratings, fiber connectors, waveguides, micro-lenses), information storage and data carrier devices (CD, DVD, Bluray Discs, sensor discs), medical technology (hearing aid, components for minimal invasive surgery, microdispensers, microneedle arrays), microreactors (micro-mixers, microheat exchangers), biomedical applications (cell culturing, bioreactors, artificial skin,), microfluidic systems (DNA analysis, blood analysis). Some examples are shown in Figure 1. Examples of polymers adopted for such applications are: polylactide acid (PLA), polyglycolide acid (PGA), and poly(lactide-*co*-glycolide) acid (PLGA).

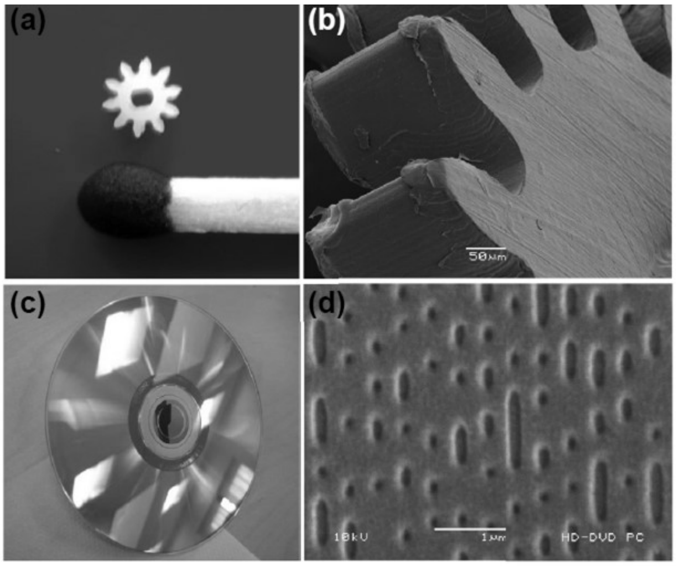

Figure 1. Examples of micro molded parts: (a) micro gear and (b) micro teeth, polymer: polyoxymethylene; macro-part with a sub-micro-structures region; (c) high density DVD disc; (d) detail view of sub-micro-features, polymer: polycarbonate.

An improvement of conventional molding and the following development of new ones are necessary because the requirement for micro scale products led to the limits of the conventional process.

Micro-injection molding, µIM, is also defined "precision injection molding", with the benefit of having wide experience in conventional injection molding, with standardized steps, a high level of automation and short cycle times.

The downscaling of the molded parts requires a special molding machine and equipment to conduct for example injection, ejection, shot volume control, process parameters control. Moreover, micro manufacturing is required to produce the micro cavity (Tosello, 2015).

The µIM process developed in the late 1980s modifying conventional machines, with clamp forces between 250 and 500 kN. In the conventional machines, the rotating screw in a barrel produce thermal and mechanical heating that makes the polymer homogeneously plasticized. Since the mass of the micro part is only a few percent of the whole processed mass, the production of micro components with these machines causes large amount of waste. Because of the large amount of melt compared to the volume injected, a degradation can take place and the control hydraulic of the metering is not accurate enough for the replication of micro parts. For this application, the electrical molding machine is preferred. Light clamp forces are needed for the small amount of injected polymer. Also, the dimension of the parts determines the size of the entire machine that can be smaller than that of conventional machines. Particular equipment was developed by Giboz et al., to reduce the amount of the waste and to limit the degradation of polymer (Giboz, Copponnex and Mélé, 2007).

In conventional injection molding (CIM), an injection cycle is characterized by these steps:

1. Plastification during the which, the rotating screw pushes the melt needed for the injection step. The pressure withdraws the screw. When enough polymer has built up screw stop rotating.
2. Injection, filling, and packing occur when the mold is closed, the screw moves forward during the injection. The melt fills the sprue, the runners, and the cavity during the filling. The screw moves forwards to push more polymer during the packing.
3. After the solidification the cooling step and ejection one occur, the mold opens and ejector pins eject the molded part (ejection).

A screw have in one single unit these operations:

1. Melting and homogenization;
2. Metering;
3. Injection.

When a conventional reciprocating screw of macro-machines is used to produce micro-parts problems like difficult control about the melt metering accuracy and a melt backflow can occur.

These issues have to be resolved by dividing the different operations of the screw at least in two different elements:

- A screw for the melting and homogenization
- A piston for the metering and injecting.

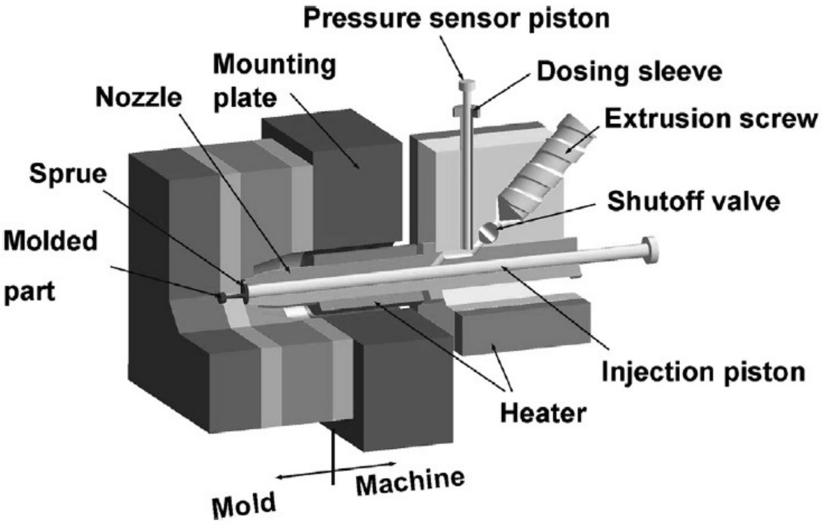

Figure 2. Unit of a micro injection molding machine.

The main difference between the new micro-molding machine design (schematized in Figure 2) and the conventional machines is that the separation of the melt plastification phase and the melt injection permits the use of an injection plunger of a few millimeters in diameter to control metering accuracy (Tosello, 2015).

To produce high-quality injection-molded micro parts the filling capabilities of the polymer into the cavity has to be studied and the effect of the process parameters should be known.

To investigate the filling behavior, different techniques can be used:

- Flow visualization, used to observe how the melt front advances in the cavity during the injection step.
- Short shots, that involve only a partial filling of the cavity.
- The length flow test, used to evaluate the filling capability of the molding system in terms of achievable flow length and aspect ratio.

In micro-molding of components with micro-features, the capability for the polymer melt to flow into the micro channels represents a fundamental factor for good moldings. For features with a depth of 10 to 100 μm, the cooling rate of the melt is so fast that the flow length can result very short when the mold temperature is the one usually adopted. It is not easy to force the melt to entirely fill the geometry if there is a high aspect ratio or the dimensions are in the micrometer scale. It is well known that the mold temperature and packing pressure represent the most important factors for successful micro-moldings (Yang and Young, 2004).

During the filling stage, when micro-molding, the polymer does not fill in the micro features. Therefore, the surfaces of the mold have to be maintained at a higher temperature to permit a complete filling. The ideal condition is to heat the mold over the no-flow temperature during the filling and packaging stages, and lower to the solidification temperature in the cooling step. Regulating the mold temperature without increasing much the cycle time and the energy consumption is not easy. Also, a direct heating and a cooling that involve all the volume of the mold is not economic because of the large mass of the mold.

Conclusion

The application of the micro-injection molding process covers different fields of applications. In fact, for a large number of products in the micro scale, the production capability, the disposability and the biocompatibility represent characteristics that make plastics as the best choice. However, processing components with micro-features is not easy because of the less capability for the polymer melt to flow into the micro channel. Local heating of the cavity surfaces represents the best solution to take on this issue. In the next chapter, there is an overview of the systems for the mold conditioning proposed in literature and the idea of the technique adopted in this work is presented. Some studies and simulations of the developed system will be also shown.

Chapter II. Study and development of a system for the rapid temperature control

Introduction

After a description of the methods studied in literature for the conditioning of the mold this chapter establishes the importance for the development of a new system to rapidly regulate the temperature of the cavity. A clear description of the system will be given and the simulations will be supported by experimental data.

State of the art

The control of the temperature of the mold is very important in injection molding and fundamental for micro parts. In order to permit a filling complete without an extremely high pressure with a big stress on the polymer, the temperature should be higher than solidification point during filling. After the filling, the temperature should rapidly decrease to obtain a solid polymeric part in short cycle times. Su et al (Su, Zhang and Gilchrist, 2016) reviewed the applications of different variotherm systems in µIM stating even though the technology to condition the mold, including many kinds of heating methods, has existed for many decades, it is still not a proven one for use with µIM because there are many heating methods, each has their own disadvantages. For example, the use of conformal cooling channels is a good choice, but is very expensive. Among all available rapid thermal technologies, there is high-frequency proximity effect induced heating, its principle is shown in Figure 3. Chen (Chen *et al.*, 2012) combined this technology with cooling water channels to reach dynamic mold temperature control. He applied the system on both plates of a mold and investigated the effect of various parameters such as different materias of the mold plates, inductor designs and depths of the inductor channels. The convective heating methods are widely used in industry, mainly based on the use of gas and liquids. Although, these heating systems are quite slow and do not have a high efficiency. In fact, since the oil has a low thermal conductivity and low boiling temperature, it takes more than several minutes to rise the temperature of 100°C. For this purpose, high temperature gas, steam and hot air are used as alternate convective media in variotherm systems. Recently, the method based on the steam heating has been used in industrial applications. Combination of hot and cold fluid for the temperature control in injection molding is schematized in Figure 4. Jeng et al (Jeng *et al.*, 2010) combined steam heating with cool water considering the same mold design to reach dynamic mold surface temperature and obtain a control. Their results showed that when the steam was used, the time to heat the mold plates can decrease from 18 s to 8 s with a heating rate of 9°C/s, and the water heating can reduced. Xie (Xie *et al.*, 2013) proposed a variotherm concept based on the combination of silicon wafer and a micro electric resistance heating structure and studied its efficiency by analysing the thermal graphics (Figure 4).

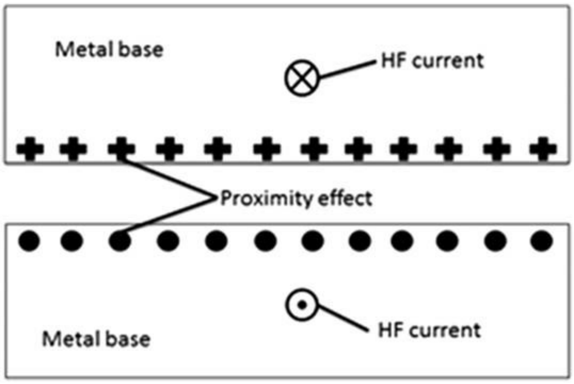

Figure 3. Principle of high frequency proximity heating (Su, Zhang and Gilchrist, 2016).

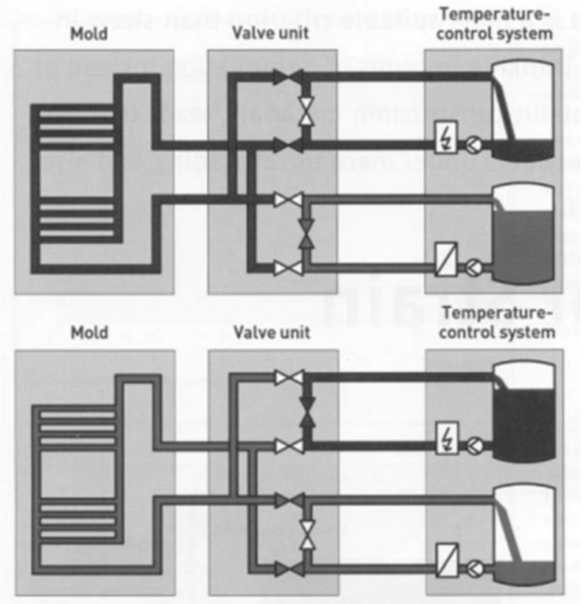

Figure 4. Schematic of the alterning temperature control system with hot and cold fluid (Xie et al., 2013).

Tang et al studied attempted to improve the precision of a temperature control based on the control system of micro injection molding machine. By using a gradual approximation control method based on an algorithm of gradual approximation, they obtained fast and accurate control of the temperature of the micro injection molding machine avoiding big overshoot typical of the traditional PID control. Their technique permitted to improve precision of the temperature control up to ± 0.5 °C (Tang *et al.*, 2013).

Gao et al (Gao *et al.*, 2017) adopted an infrared heating method to increase the mold temperature quickly and improve the quality of micro molded needle arrays (Figure 5). Their main results are shown in Figure 6. The experimental results revealed that the developed infrared heating system was highly efficient and permitted to obtain an uniform heating of the mold surfaces.

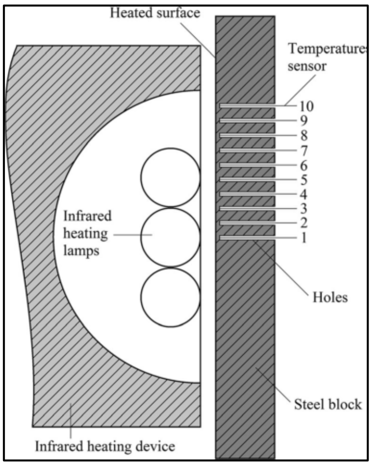

Figure 5. Representation of the system adopted for the infrared heating *(Gao* et al.*, 2017)*.

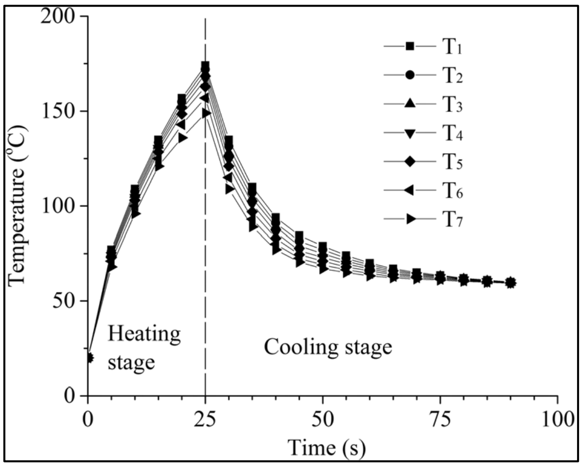

Figure 6. Temperature curves of hole 1 to hole 7 (Gao et al., 2017).

A silicon insert with a carbide bonded graphene coating was adopted by Xie (Xie *et al.*, 2017) to obtain rapid thermal cycling in injection molding. Chemical vapor deposition was used to coat the surface of the silicon cavity with continuous and dense carbon-bonded graphene coating. Working as a thin film resistance, their coating was able to increase the temperature of the mold cavity rapidly above the glass transition temperature of the polymer, with good results obtained also by using a low power source with a voltage of 120V. By applying a voltage of 240 V, the temperature reached by the coating in 10 seconds was 145.6°C. Zhang (Zhang, Zhou and Yi, 2017) developed a novel heater based on a graphene thin film that permitted rapid localized heating adopting electromagnetic induction. The authors used a graphene coating synthesized by chemical vapor deposition and cross linked into a 3D network by silicon-oxy carbide and Si-carbide covalent bonds on patterned Si molds. The nanoscale thin graphene coatings present many advantages, such as high electrical and thermal conductivity, that permit to raise the temperature above T_g in a few seconds, while the rest of the mold remains at a lower temperature.

A porous mold insert was studied and adopted by Crema et al (Crema, Sorgato and Lucchetta, 2017). To maximize the heat exchange, the porous mold (Figure 7) was optimized by means of numerical simulations studying the effect of thermal exchange between water and the cavity surface, without affecting the integrity of the mold. Compared to the common convective technologies, the performance of the optimized porous inserts was quite higher, showing a maximum heating rate of 7°C/s and a mean heating rate of 6°C/s (Figure 8).

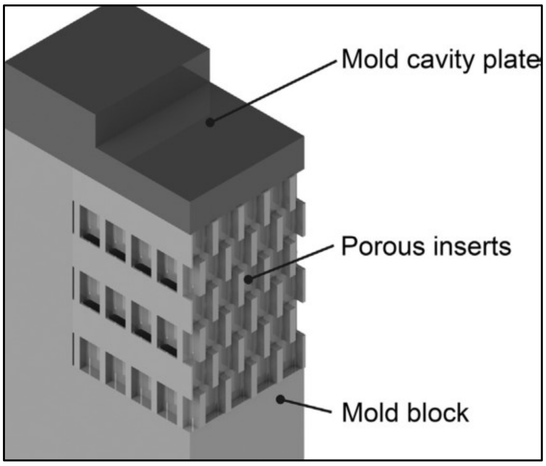

Figure 7. Solid domain considered in the thermal fluid dynamic simulations.

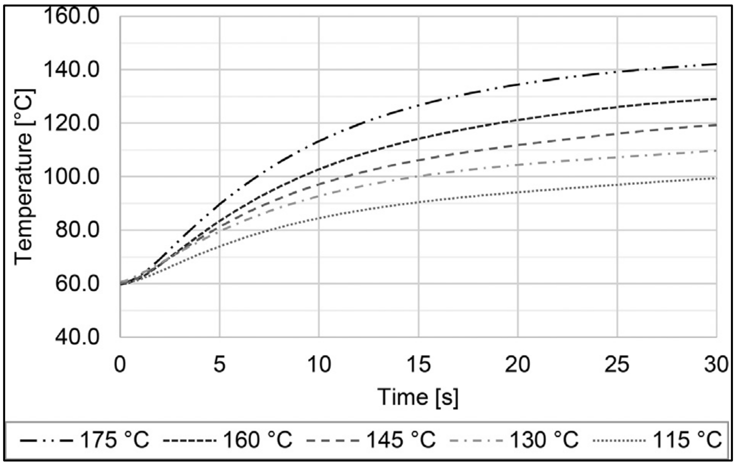

Figure 8. Heating profiles at different water temperature.

Injection molding with dynamic mold temperature control was developed by Zhao et al (Zhao *et al.*, 2017) to develop a thermo mechanical environment in which the mold stays at a high temperature and cooled down with a slow cooling rate. Their technique included the application of high temperature in the cavity that affected the orientation of the polymeric structures avoiding the formation of the skin-core structure that is induced from the hierarchical morphology distribution leading to a more homogeneous morphology along the thickness. For this purpose, the temperature of the mold cavity was high for enough time to allow molecular chains having a fast relaxation. The development of different microstructures played an important role on the enhancement of the mechanical performance (Fischer *et al.*, 2017).

Liparoti et al (S Liparoti *et al.*, 2019) adopted a technique based on the electrical heating to change the temperature of the cavity surfaces. The tool they used was a thin heating device located on the cavity surface and sandwiched between two insulating layers. They modulated the cavity surface temperature evolution during the injection molding experiments and simulated the process coupling the thermal transients of the polymer melt flowing in the cavity with the thermal transient of the multilayer heating devices.

Effect of vario-thermal system on parts were widely studied. For example, Li (Li *et al.*, 2017) verified that the volume fraction of the air kept in the metal surface microstructures after the filling decreases by increasing metal temperature because the melt show enhanced filling of the microstructures. Because of these aspects, the area of the mechanical connection between the polymer and the metal surface was increased, improving bonding strength. The effect of the application of temperature variations in injection molding on the flow length of different polymeric materials (Meister and Drummer, 2013), (Yao, Kimerling and Kim, 2006), on the final morphology of polymers (Zhao *et al.*, 2017), (Liu *et al.*, 2012), on the surface replication of parts (Speranza *et al.*, 2017), (Lucchetta, Fiorotto and Bariani, 2012), (Kim *et al.*, 2007) is also present in literature. Liu (Liu *et al.*, 2017) carried out a numerical investigation on polymer melt flow phenomenon in a variothermal mold cavity for microinjection molding.

Fischer et al produced microtensile bars by injection molding of two materials, one with a relatively high viscosity and another one with a relatively low crystallization kinetic. By varying the isothermal holding time during the dynamic tempered manufacturing phase different crystalline structure were created affecting the final mechanical and tribological properties. By increasing the isothermal holding time the crystalline structures in the core area became coarser and the crystallites appeared bigger (Fischer *et al.*, 2017).

While Harris (Harris and Lee, 2008) studied a way to improve mechanical performance of injection molded PLA, Srithep (Srithep, Nealey and Turng, 2013) and Vadori (Vadori, Mohanty and Misra, 2013) studied the effect of the temperature of the mold on the crystallinity and performance of PLA parts. No research was performed to study the effect of the application of rapid variations of temperature or the effect of the application of annealing step during the micro-injection molding.

The design strategy was based on a modular mold created by De Santis (De Santis and Pantani, 2016), in which inserts and layers can be easily assembled.

The injection molding machine

The machine adopted in this thesis is the injection-molding machine HAAKE Minijet II by Thermo Scientific. This machine is a mini-injection molding system that adopts a pneumatic piston to control the pressure during the molding. The amount of material the cylinder of the machine can contain is about 5 gr. Since there is not a rotating screw but a pneumatic piston, after inserting the material into the cylinder, a time of 5-10 minutes is necessary to melt the polymer. A 200 µm thick cavity, wide 4 mm and long 35 mm, is adopted by adding a steel slab to the mold specially made for the temperature control system (Figure 9). The molds for the HAAKE Minijet II present a truncated cone shape, with a diameter from 50 mm (at the gate side) to 35 mm over a length of about 90 mm.

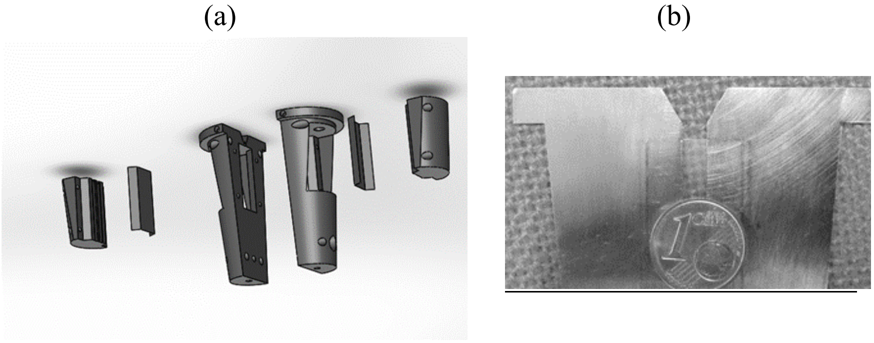

Figure 9. Representation of the geometry used in this work (a) mold and inserts, (b) cavity.

In addition to the experiments connected to the simulations presented in this chapter, this cavity will be adopted for the experiments performed in the chapters III, IV and V. In the chapter VI a different cavity will be adopted but the mold is the same.

The rapid temperature control system

To obtain a temperature control a resistive heating combined with temperature sensors will be used. The heater is attached behind the surface of the cavity whereas an insulation layer is located between the heaters and the rest of the mold. It is possible to facilitate the heat transfer towards the cavity and limit the dispersions to the rest of the mold. A schematic of the components is represented in the Figure 10. The temperature control is based on the use of very thin and flexible resistances as heating source and thermocouples that can be attached near the surface of the cavity. The electrical resistances are grids of constantan foil sealed in a polyimide film with a nominal resistance of 120 Ω. Each heating element is 3.8 mm wide, 5.7 mm long and 50 μm thick. Two heating elements, for each side of the mold, are used to cover a length of the whole cavity that is 11 mm. A thin wire thermocouple, (Type T, about 50 μm in diameter supplied by Omega Engineering Ltd.) between each resistance and the cavity surface is attached. The insulation layer is a PolyEtherSulfone (PES) film. The insulation has the fundamental role of lowering the heat loss towards the rest of the mold and permits a necessary conduction to allow a reasonable cooling rate.

A data acquisition board (DAQ NI-USB 6210 supplied by the National Instruments) allows transferring the temperature data to a computer where a dedicated software controls the values of each zone at 10 kHz. This system allows regulating the evolution of the local mold temperature switching the linked relays and thus imposing a given heating and cooling rate (in the limit of the maximum values determined by the heating power and the ballistic cooling without power supply). Each experiment in this work is carried out by using a power supply equal to 12 V.

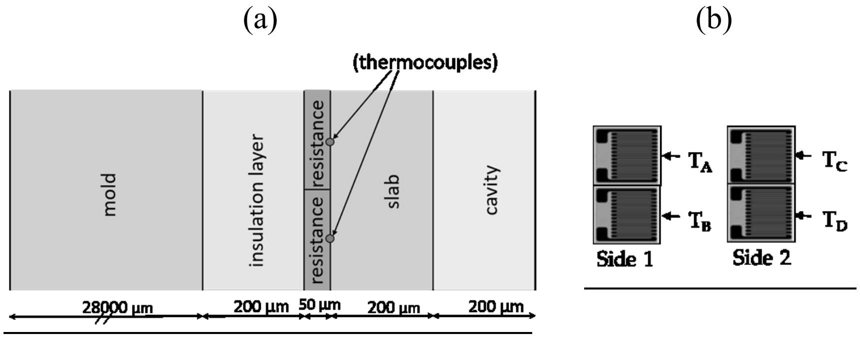

Figure 10. (a) Schematic of the heating assembly, (b) Representation of the heating elements.

Table 1. Thickness and physical properties of the layers.

	x, thickness [μm]	α [m^2/s]	k [W/m K]
steel mold	28000	8.0×10^{-6}	15
PES, **insulating layer**	200	1.5×10^{-7}	0.15
heating resistances	50	2.0×10^{-7}	0.37
steel slab	200	8.0×10^{-6}	15

Simulations of the temperature control system

In order to verify potentialities of the heating system several simulations were carried out. In the analysis the system was approximated as consisting in 4 different elements in perfect contact (as shown in Figure 10a, polymer in the cavity, steel slab, heating resistances, insulation layer, mold insert), each with their physical properties and dimensions reported in Table 1. Simulation were performed solving time-dependent heat transfer partial differential equations using FlexPDE, a finite element commercial software, for the domain shown in Figure 10a. In particular, the heat equation is a parabolic partial differential equation that describes the distribution of heat (or variation in temperature) in a given region over time. For a function T(x,y,t) of two spatial variables (x,y), in Cartesian coordinates, and the time variable t, the heat equation for each element i is represented by the Eq.1.

$$\frac{k_i}{\alpha_i}\frac{\partial T}{\partial t} = \nabla \times (k_i \nabla T) + G_i \qquad \text{(eq.1)}$$

with continuity of temperature T and heat flux, $k_i\frac{\partial T}{\partial x}$ at the interface between each element, while the physical properties of each element, thermal conductivity k_i and thermal diffusivity, α_i, are summarized in Table 1.

The temperature evolution is calculated with uniform initial temperature T_0 =27°C, a value close to the room temperature in the first case, T_0=60°C, in the second one selected to study the evolution of temperature in the case the mold is at a higher temperature than the room one and with Neumann boundary conditions at the boundaries (Eq.2, Eq.3, Eq.4).

$$BC1 \quad x=0 \quad -k_{steel}\,(\nabla T \times \widehat{n}) = k_{steel}\,\frac{\partial T}{\partial x} = h\,(T_0 - T) \qquad \text{(eq.2)}$$

$$BC2 \quad x=L \quad -k_{steel}\,(\nabla T \times \widehat{n}) = k_{steel}\,\frac{\partial T}{\partial x} = h\,(T_0 - T) \qquad \text{(eq.3)}$$

$$BC3,\ BC4 \quad y = \pm\frac{W}{2} \quad \frac{\partial T}{\partial y} = 0 \qquad \text{(eq.4)}$$

where the convective heat transfer coefficient for still air is assumed to be h = 5 W/m^2 K.

The thickness of each element is also reported in Table 1, so that the total length in x-direction, L, is the sum of all of them, while the length in y-direction, W, is 54400 µm for all the elements.

Finally, the internal heat generation, due to joule heating P, and the control function G_{hr} are given by the equation 5.

$$P = \frac{V^2}{R} \times \frac{1}{V_R} \qquad \text{(eq. 5)}$$

$$G_{hr}(t) = \begin{cases} 1 \; if \; T_w < T_{sp} \; and \; 0 \leq t \leq t_{hr} \\ 0 \; if \; T_w > T_{sp} \; or \; t > t_{hr} \end{cases} \qquad \text{(eq. 6)}$$

Where V, R and V_R are the applied voltage, the heating resistance and the volume of the heating resistance, respectively.

As reported in equation 6, a simple temperature protocol is implemented: during the first part, that lasts t_{hr}, the temperature of the surface of the cavity, T_w, after thermal transient from T_0, is kept at the set point temperature T_{sp} switching on and off the heating resistances. After t_{hr} , intended as the time to fill the cavity, the heating resistances are switched off performing a ballistic cooling of the mold, and in particular the cavity. Obviously more complicated temperature protocols could be designed and implemented too.

The principal parameters (time t_{hr}, the set point temperature T_{sp}) are changed in the simulations to explore the potentialities of the designed system. Power supply V was fixed to 12 V that corresponds to the maximum current bearable for the resistances.

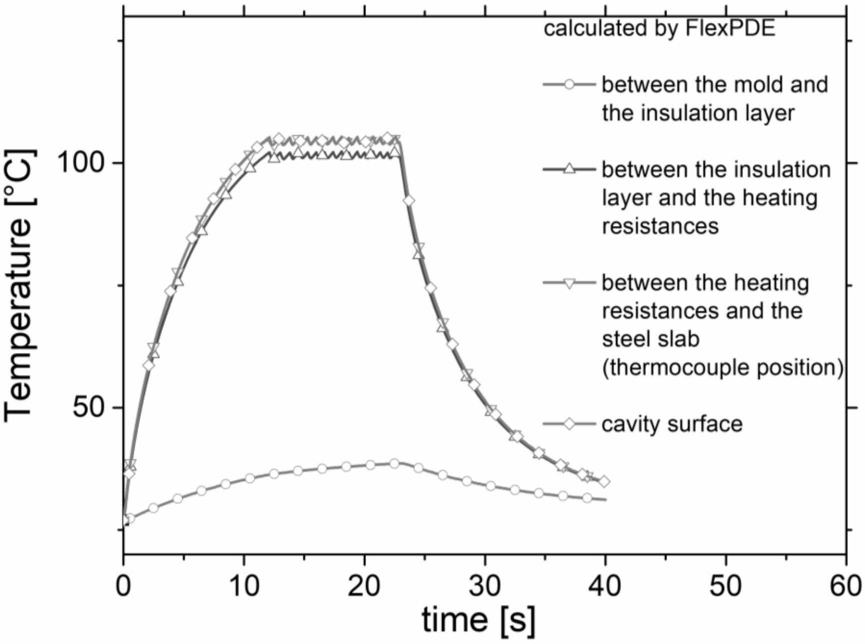

Figure 11. Temperature evolutions calculated by FlexPDE when one resistance in each zone is used.

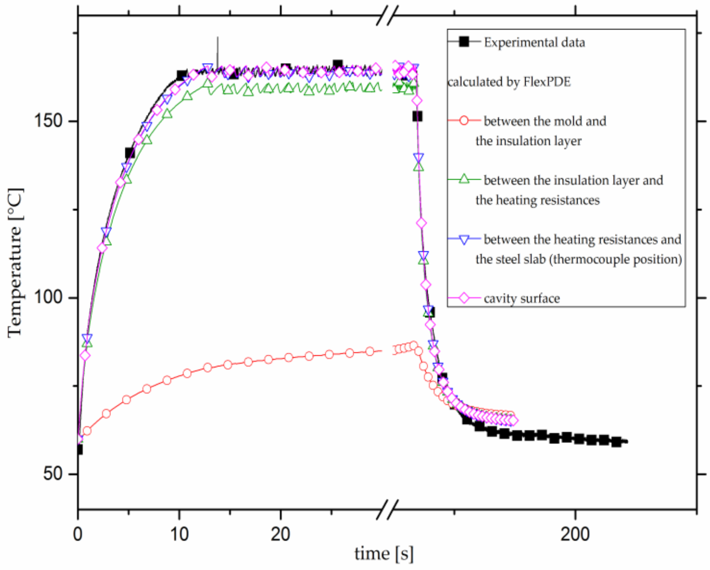

Figure 12. Temperature evolutions calculated by FlexPDE two resistances in each zone is used.

In the first case, the simulation code was used with time t_{hr} = 30 s, the set point temperature T_{sp} = 105 ◦C and the resulting temperatures in specific positions are shown in left plot in Figure 11. Obviously in the simulations these parameters could be easily changed, but without forgetting the thermal-mechanical properties of some of these elements (i.e. heating resistances can break exceeding a temperature value of 200 °C). In the second case, adding a supplementary layer of resistances in the scheme power density increases. By setting the initial temperature T_0 equal to 60°C a temperature of the cavity equal to 160 °C is reached in a few seconds (Figure 12). The experimental data obtained by acquiring thermocouples values are well described by the simulations.

Conclusions

The simulations carried out in this part of the thesis demonstrated that a 200 μm steel slab between the resistance and the cavity does not affect the heat transfer between the resistance and the cavity surface and it is possible to increase the temperature up to 160°C in a few seconds and cool down to the mold temperature in less than 10 seconds.

Chapter III. Effects of cavity temperature variations on filling and orientation properties of micro- injection molded PLA parts

Introduction

The rapid temperature control described in the chapter 2 is used to investigate the effects on the filling capabilities of a polylactid acid. The PLA was chosen because of the recent need of the market to substitute some oil-based polymers with biodegradable ones. In addition, it is very interesting experiment the thermal cavity variations because PLA has a relatively high viscosity. Optical and spectroscopy analysis will be used to assess the final morphology of the produced microparts.

State of the art

In injection molding, the final orientation of the molecular chains are affected by the shear induced by the process and the cavity temperature. In conventional injection molding, during the filling stage, the polymer, in contact with the mold wall at a temperature lower than the melt temperature, a layer of a solidified material instantaneously generates. This layer is known as "skin layer". The skin layer formation not only affects the flow cross section area but also causes the creation of a thermal insulating barrier for the molten polymer in the center, increasing the shear stress and decreasing the cooling rates respectively. If the material processed is a semi-crystalline polymer that is characterized by a half crystallization time compared with the time of the process, the shear can promote the flow-induced crystallization and the formation of lamellar structures highly oriented in the shear layer. During the filling, the polymer chains that have high molecular weight are stretched along the shear field direction and form the oriented structures. They can be microfibrils or shish structures characterized by an orientation parallel to the flow direction. They can form fibrous crystals that can act as nucleating threads for the lower molecular weight chain characterized by a time relaxation shorter during and after the application of the flow. When the lamellae grow on these oriented threads the result will be a shish-kebab structure. Because of the low thermal conductivity, the skin layer and the shear layer represent an insulation barrier and lead to a slower cooling in the core region where the oriented chains formed in filling stage can relax. In the core layer the crystallization acts in a quiescent-like condition generating a spherulitic morphology. The thermal gradients and the stress variations through the volume of the molding represent a thermomechanical environment that can strongly affect the morphological distribution in the molded part. In the case of a micropart, the higher shear rates and cooling rates due to micro scale cavity led the formation of oriented structures (Figure 13).

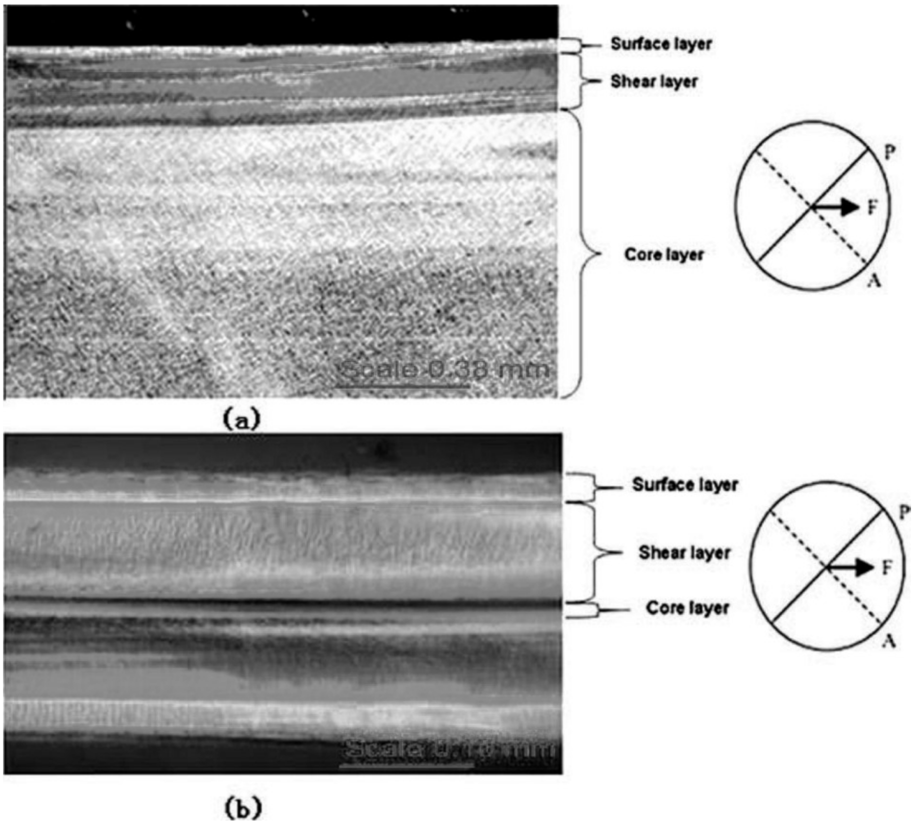

Figure 13. PLM micrographs of (a) macropart and (b) micropart.(Guo et al., 2012)

The amount of the oriented structures generated during microinjection molding is higher than that formed in conventional injection molding. Having a particular morphology, the microparts show physical properties different from those of the macroparts. The high level of orientation in the micropart can reflect good mechanical performance but in the same time can result in warpage because of the uneven shrinkage in the molding process (Guo *et al.*, 2012). This orientation, however, is affected also by the temperature of the mold. An increase of the cavity temperature enhances the flow ability and the replication of micro features and inevitably affects the final orientation. Jiang and coworkers verified the effect of the mold temperature on the mechanical properties of micro-injection molded polypropylene (Jiang *et al.*, 2015). Their investigation proved that the thickness of the shear layer decreases along the flow direction and the core layer thickness increases, verifying that the orientation decreases along the flow direction (Figure 14).

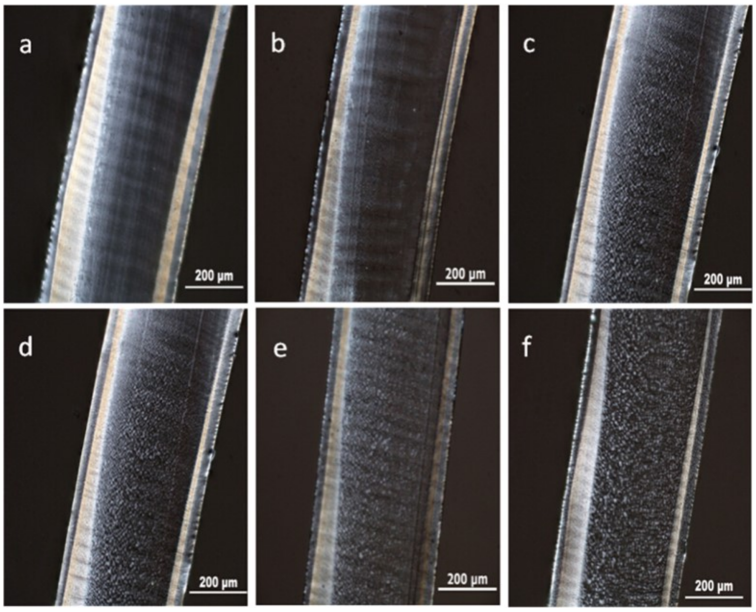

Figure 14. Images observed by the polarized optical microscope of the micro-injection molded isotactic polypropylene gear slices at different mold temperatures (a) 30°C (b) 40°C (c) 50 (d) 60°C, (e) 70°C, (f) 80°C *(Jiang* et al.*, 2015)*.

In the last decades, environmental and economic challenges led scientists and producers to substitute, in part, oil-based polymers with biodegradable ones. Poly(l,l-lactide) acid, hereafter called PLA, represents a leading candidate, it is a thermoplastic, high-strength, high-modulus polymer that can be made from annually renewable resources (e.g., corn, wheat, or rice). It is, also, recyclable and compostable (Drumright, Gruber and Henton, 2000) (Sawyer, 2003). Its production consumes carbon dioxide (Dorgan *et al.*, 2001). Another advantage of the PLA is its biocompatibility, especially with respect to biomedical applications, in fact, it does not produce toxic effects in local tissues (Farah, Anderson and Langer, 2016). Furthermore, the degradation products do not interfere with tissue healing. Even if PLA initial uses were limited for medical and dental applications due to its biocompatibility and biodegradability, recently, its usage has extended to packaging materials for food and consumer goods; applications in which the polymer product is typically discarded after use.

To allow the utilization in engineering sectors and in applications requiring higher added value, currently, many scientists focused their attention in the production of new grades of biopolymers characterized by improved characteristics such as processability, higher mechanical and thermal resistance, flame retardancy (FR), tailored electrical properties, long durability and stability (Murariu *et al.*, 2014). Nowadays, the market is turning to more “durable” biomaterials such as engineering components with microscale features or dimensions for automotive and electronics (Babu, O’Connor and Seeram, 2013), (Murariu *et al.*, 2014), (Auras, Harte and Selke, 2004), (Madhavan Nampoothiri, Nair and John, 2010), (Gupta, Revagade and Hilborn, 2007), (Drumright, Gruber and Henton, 2000), (Jamshidian *et al.*, 2010), (Raquez *et al.*, 2013). The concern for the use of this polymer to satisfy the demand of long-lasting bioplastics, in industry sectors such as electronics and automotive, with processing characteristics that satisfy those of existing polymers, is causing a rapid growth in PLA production global capacities.

PLA can be processed by microinjection molding but its relatively high viscosity and low crystallization rate limited its use and most of the literature research focused on the microinjection molding of PLA composites or blends (Zhao *et al.*, 2018).

The increasing interest on the PLA production and use in the market led to the consideration of this material to take part an investigation of the effects of the application of the system for PLA micropart production.

To understand processing behavior, knowledge of the rheological, thermal, and thermodynamic (pressure-volume-temperature [pvT]) properties of PLA is important (Kühnert *et al.*, 2018).

In the work of Zhao and coworkers (Zhao *et al.*, 2018) microinjection molding parts were compared with miniinjection molding parts. The size of the microinjection molded sample was 18 × 3 × 0.3 mm^3, and the one of mini-injection molded sample was of 78 × 10 × 4 mm^3. The injection speed adopted in microinjection molding was 600 mm/s that corresponded to a volumetric flow rate of 11781 mm^3/s. The mini-injection molding was pressure controlled at 500 bar by HAAKE Minijet with a volumetric flow rate estimated 3.0×10^3 mm^3/s. The analysis of the WAXD patterns of their samples reflected the crystallization structure and orientation modification, showing two strong circular spots, due to the high molecular orientation. A more intensive molecular chain orientation was detected by the diffraction patterns of microinjection moldings where more sharp arcs were present. The analysis conducted verified that the orientation degree increased from 0.54 to 0.86 after applying the extreme shear rate.

To monitor the structural changes due to mechanical deformation IR spectroscopy can be applied. Due to its low crystallization rate, PLA usually develops amorphous structure under common processing conditions. Several studies demonstrate the development of orientation and strain-induced crystallization during drawing of initially amorphous PLA in the rubbery state (Mulligan and Cakmak, 2005), (Wang *et al.*, 2014).

Lee et al. (Lee, Lee and Jin, 2001) adopted polarized Fourier transform infrared spectroscopy (FTIR) to study the orientation of solution cast semicrystalline PLA samples during drawing. They considered, however, only the orientation of the amorphous phase. Wong et al. (Wong, Stachurski and Venkatraman, 2008) combined the optical birefringence and the WAXD investigations to study the orientation of solution cast semicrystalline PLA during drawing in both crystalline and amorphous regions.

The spectra of the undrawn PLA samples prepared by Lee et al (Lee, Lee and Jin, 2001) showed the complete disappearance of the 920 cm^{-1} band that is assigned to the crystalline phase (Figure 15). The uniaxially stretched films exihibited strong dichroism for the parallel band at 920 cm^{-1} and the perpendicular one at 958 cm^{-1}. The first band is sensitive to the structure and the orientation, the second one is sensitive only to the orientation and is independent from the structural change from amorphous to crystalline state. They evaluated the average orientation of the samples by calculating the dichroic ratio of the 958 cm^{-1} band.

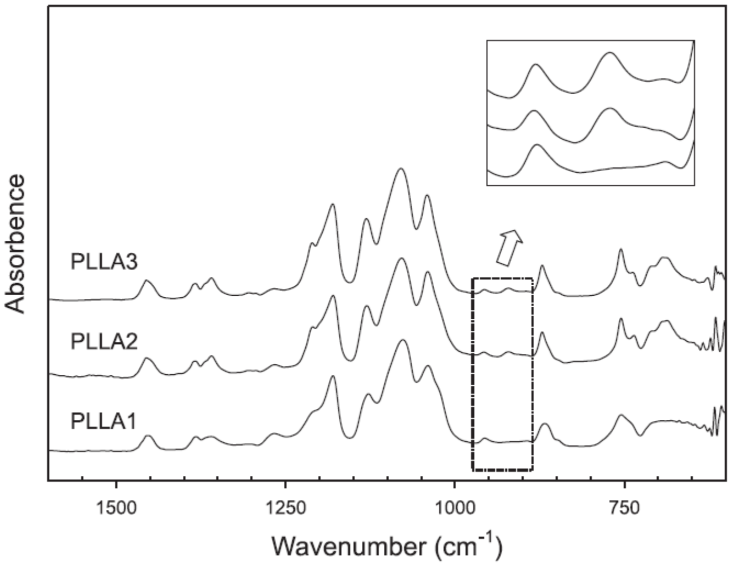

Figure 15. IR Spectra of undrawn PLA samples *(Lee, Lee and Jin, 2001)*.

Material and Methods

The PLA used in the experiments shown in this chapter is the biopolymer 3251D by NatureWorks. This polymer is designed for injection molding applications. It is characterized by a higher melt flow capability compared to other PLA grades with a MFR of 35g/10min at 190°C (2.16 kg). The PLA 3251D has a molecular weight of Mn=83 kDa, with the dispersity, Mw/Mn = 1.6, and d-isomer content= 1.4%. The glass transition temperature, Tg, measured by DSC is about 60°C. The melting temperature, Tm, measured as the peak of the melting endotherm during DSC heating ramp at 10°C min^{-1}, is about 170°C.

The producer recommends drying the polymer before processing to prevent viscosity degradation.

In all the experiments, the pellets of PLA were introduced in the injection molding cylinder for 5-10 minutes at 180°C for melting. Then, just before the injection, the mold surface system for the rapid temperature control is activated to reach the set temperature in less than 20 s, as shown in Figure 17. The investigated temperatures of the cavity surface are listed in Table 2. The melt polymer is injected in the cavity keeping a pressure of 100 bar for 3 s. Subsequently the temperature quickly decreases allowing the extraction of the solidified part. A schematic of the experimental protocol is shown in Figure 16.

Table 2. List of experiments.

Experiment	Temperature [°C]
A	25
B	120
C	140
D	150
E	160

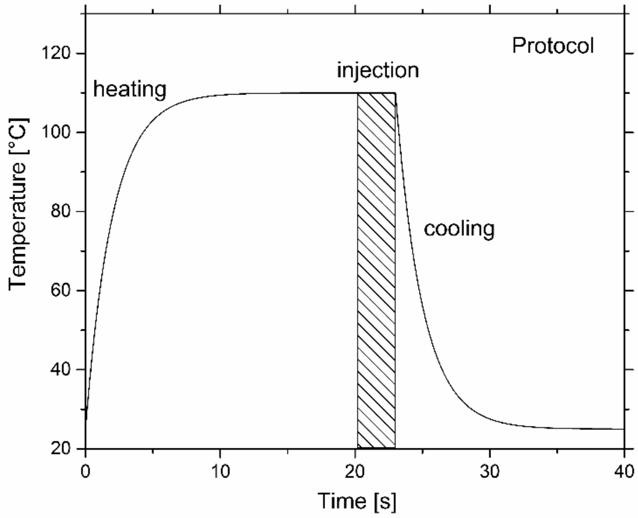

Figure 16. Experimental protocol: temperature of the cavity vs time.

The stereomicroscope LEICA MZ6 was used to observe each sample from the gate to the tip in polarized light.

IR spectra of the PLA microinjection molded parts at different temperatures of the cavity surfaces were collected at room temperature in transmission mode by means of the Perkin Elmer spectrometer in the mid-infrared range (4000÷400 cm^{-1}). The spectra were obtained by coadding 10 scans at 4 cm^{-1} resolution. For polarized IR measurement, the polarization direction of the incident radiation was adjusted parallel and perpendicular to the flow direction by a rotatable wire-grid polarizer on KRS-5-substrate.

A differential scanning calorimeter DSC 822e from Mettler Toledo was used for the evaluation of the final crystallinity of each sample. A piece of each sample, with a weight of less than 10 mg, was put into an aluminum pan and heated from 0°C to 200°C with a heating rate equal to 10°C/min. In order to prevent oxidative degradation at high temperatures, all the experiments were carried out at a nitrogen flow rate of 50 ml min^{-1}.

Results

The rapid temperature variations of the cavity surfaces affect the viscosity as well as the filling capability of the polymer melt. The temperature evolution of the tests "B" and "D" is shown in Figure 17, measured by one of the thermocouples between a heating element and the cavity surface. The cooling rate is also controlled by the system.

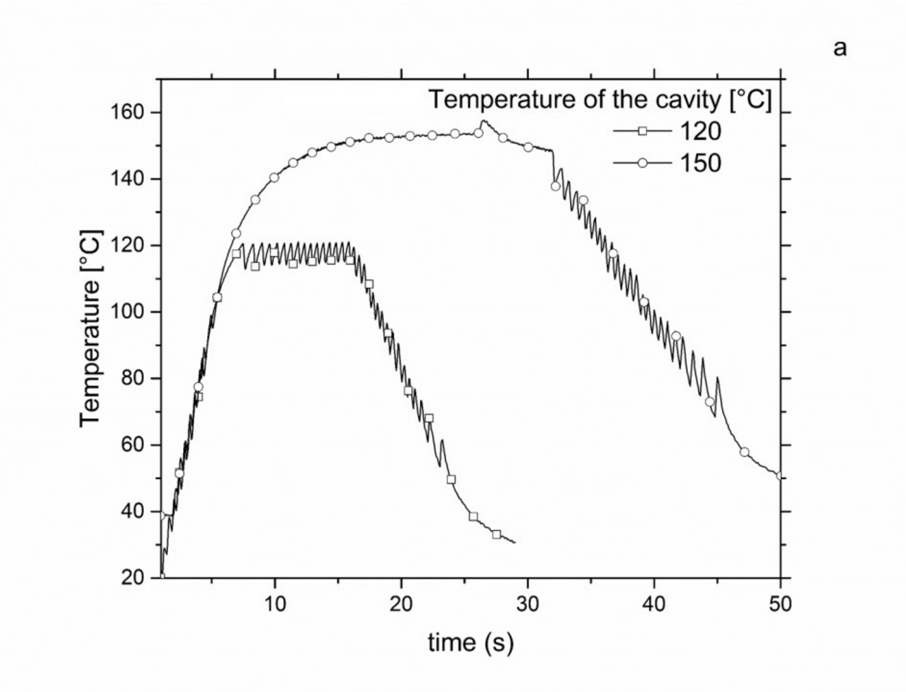

Figure 17. Temperature measurements during tests "B" and “D”.

The set temperature is reached in less than 20 s and after the injection, by switching off the power supply, a rapid ballistic cooling is obtained. If the heating system was not applied, the temperature of the entire mold was 25°C and as a consequence a length of less than 1 mm was reached by the part because the polymer immediately solidifies just after the gate. As the surfaces are heated up a greater length is achieved, and for each experiments, the lengths of the samples are listed in Table 2.

Table 3. Lengths of the parts.

Experiment	Length (mm)
A	0.8
B	2.1
C	4.2
D	8.0
E	8.7

The photographs of the parts taken with the stereomicroscope LEICA MZ6 between the crossed polarizers are shown in Figure 18. The microscope analysis highlighted in the part molded at 25°C, sample A, a strong birefringence with peculiar color patterns that is weaker on increasing the surface temperature in samples B, C, D, and E. In particular, when the temperature of the surfaces was 150°C or 160°C birefringence was not observed and the sample appeared completely transparent even rotating the polarizer.

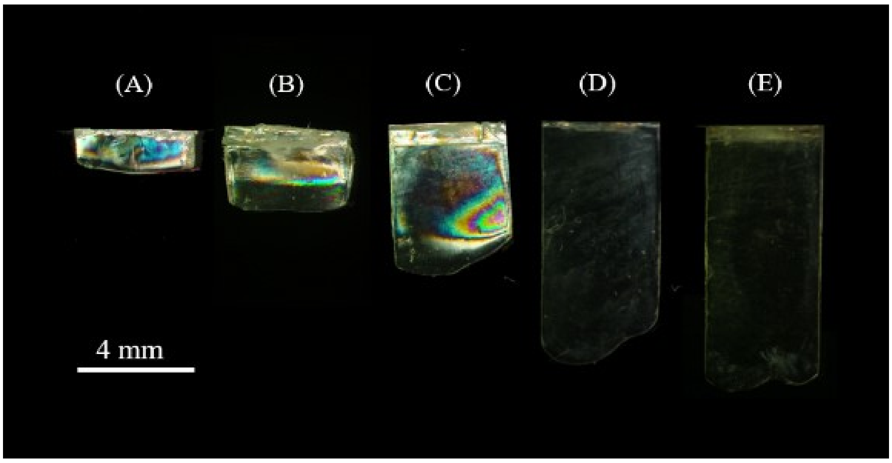

Figure 18. Photographs of the samples obtained with crossed polarizers.

The IR spectra collected in the mid-range (4000÷400 cm^{-1}) reproduced the characteristic peaks of the PLA (Figure 19). The analysis were carried out in the region after the gate for the samples “A”, “B” and “C” and considering two regions, one after the gate and one at the tip for the samples “D” and “E”. In the last case, the second acquisition overlays the first one showing no difference between different regions of the parts.

The infrared spectroscopy has the potential to quantify the molecular distributions in both the crystalline and amorphous regions. The bands 922 cm^{-1} and 956 cm^{-1} are both assigned to the coupling of the C-C backbone stretching with the CH_3 rocking mode, while 922 cm^{-1} is sensitive to the 10_3 helix conformation of the PLA crystals, 956 cm^{-1} is not dependent on the structural change from the amorphous to the crystalline phase.

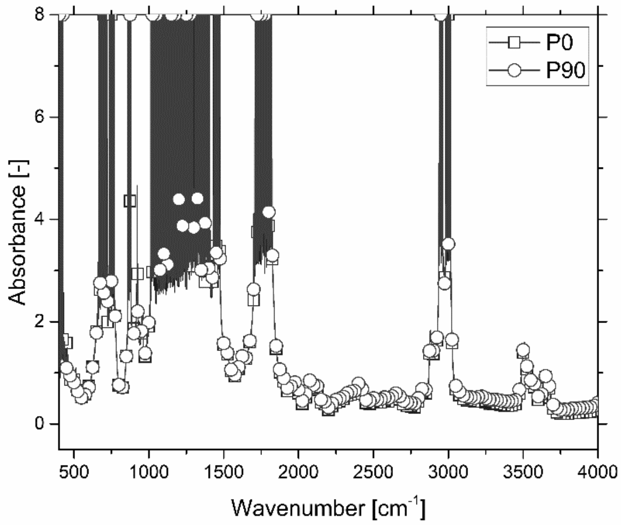

Figure 19. IR Spectra of the sample obtained with the protocol D. In p0 the polarizer is parallel, in p90 is orthogonal.

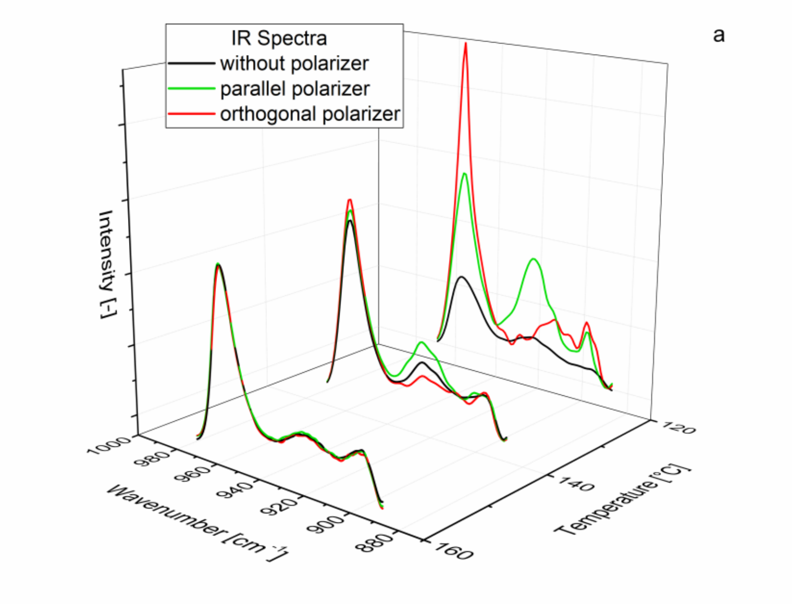

Figure 20. IR Spectra of the samples obtained with a cavity temperature of 120°C, 140°C and 160°C.

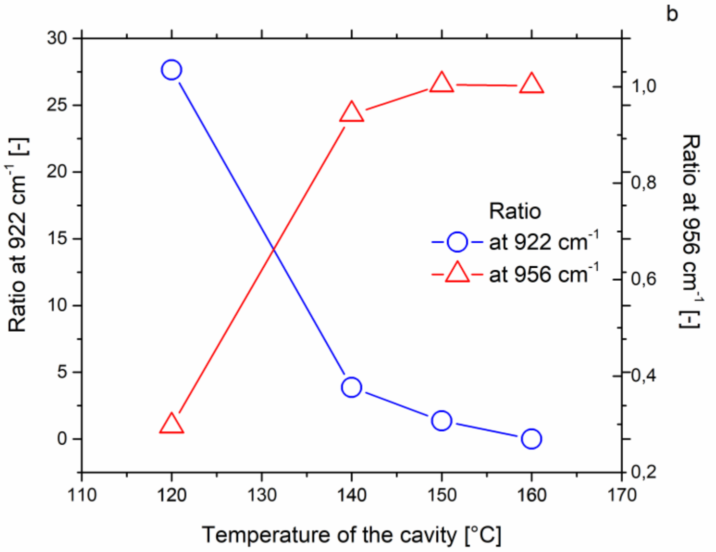

Figure 21. Height ratio evolutions.

The diagram in Figure 20 depicts the evolution of the spectra for the tests B, C and E in the region near the bands 922 cm^{-1} and 956 cm^{-1} taken with the parallel or orthogonal polarizer, and without the polarizer, depending on the surface temperature of each test. Furthermore, subsequent calorimetric analysis confirmed that all the samples are amorphous. This result is not surprising as PLA is a slow crystallizing polymer, if compared to the time, 3 s, that material stays at the set temperature. Even though the basic pattern is the similar, the analysis of the band at 922 cm^{-1} and 956 cm^{-1} highlighted that different values of the absorbances with the parallel and orthogonal polarizer are obtained, because this analysis is sensitive to the molecular structural details.

Wang and coworkers (Wang *et al.*, 2014) investigated the change of molecular orientation in PLA using the dichroic ratio defined as $D=A_{para}/A_{perp}$, the absorbances ratio with parallel and orthogonal polarizer of a desired absorption band. The degree of orientation for the amorphous phase is proportional to the dichroic ratio because the band at 956 cm^{-1} is a parallel band, whereas the relationship is opposite for the ordered phases because that at 918-923 cm^{-1} is a perpendicular band. The same spectrum, with the parallel and orthogonal polarizer, is obtained when the highest temperature of the cavity surface was adopted, as shown in Figure 21. No differences were found between the spectra taken with different positions of the polarizers whereas a sample in a colder surface exhibits differences between the experiment taken with a parallel polarizer and the one with an orthogonal polarizer. The differences were evaluated in terms of the heights ratio $H = A_{p0}/A_{p90}$ for both peaks 922 cm^{-1} and 956 cm^{-1} represented in Figure 10 with the temperature, A_{p0} is the height of the peak evaluated tracing a baseline between 900 cm^{-1} and 970 cm^{-1}. Whereas the ratio at 956 cm^{-1} increases with the temperature, the ratio at 922 cm^{-1} decreases.

Conclusions

In this chapter, the system to rapidly control the temperature of the cavity was used to produce PLA microinjection molded parts. In order to study the effect of the different thermal conditions of the cavity surfaces on the orientation of the parts, polarized microscope and infrared spectroscopy investigations were carried out. The optical observations identified the presence of birefringence decreasing with the increase of the temperature of the cavity, when the temperature was 150°C or higher the samples appeared completely transparent revealing the absence of orientations. The study of the IR spectra confirmed that all the samples produced were amorphous and the differences in height of the peaks obtained in parallel and orthogonal polarizer respect to the flow direction of the polymer in the cavity were attributed to amorphous orientation of the chains. The use of the control system allows designing the temperature evolutions of the surfaces in contact with the polymer and playing with its viscosity and the relaxation of the chains.

Chapter IV. Application of the system to locally control the properties of PLA microparts

Introduction

As described in the previous chapter, Poly-lactic acid (PLA) is at present the most promising and commercially available bio-based and biocompostable polymer. It is a semi-crystalline polymer, like many polymers, having chains that are oriented in both the highly organized crystalline phase and random amorphous phase.

The properties of PLA are relatively scarce, notably because of its low glass transition temperature, T_g, that is about 60 °C. It has a very low crystallization time. This leads to a large amorphous content in the polymer with traditional processing such as injection molding because it does not provide the time required for the PLA to crystallize to desired amount.

The aim of this chapter is adopting the technique to control the temperature of the cavity surfaces to influence the viscosity during the filling and the morphology after the solidification. In particular, in the part I of this chapter the protocols 2 and 3 were adopted to investigate the effect of annealing from the melt or the solid part. In the part II, the production of biphasic samples is studied. Both protocols presented in this part, protocol 4 and protocol 5 involve two steps in which the first one is similar and is represented by the injection in the cavity homogeneously heated up to 160°C and a second step that differs between the two protocols. After the cooling, in fact, the parts undertake a specific thermal treatment so that a crystallization can occur in a confined region without affecting the morphology of the region not involved in the treatment. The region interested can be the one closest to the gate (protocol 4) or the one closest to the tip (protocol 5). In this manner, biphasic parts with different level of crystallinity can be obtained. Morphological investigation are carried out to evaluate the crystallinity degree and the final orientation in both regions of each sample. The effect of the annealing from the melt and the solid microparts was also investigated in preliminary tests.

State of the art

The thermal conditioning strongly affect the crystalline structure of the PLA. The mobility of the chains depends on the amount of energy that is accessible to them. A higher temperature facilitate the movement of the chains into more desirable states. When the polymer is heated at a temperature between the glass transition temperature and the melting temperature for a relatively long time, the chains have the energy to move even if they are not in the molten state. This condition is called annealing and facilitate the polymer chains crystallization. The crystallinity degree depends on the temperature and the time of the annealing. It is well known that the crystallites, compared to the amorphous regions, have a much more rigid structure and less free volume for the chains to move into. On the other hand, chains in the amorphous phase have more mobility. The amorphous phase relaxation, however, decreases the enthalpy over time becasue the chains arrange themselves in a lower energy state (Cai *et al.*, 1996).

A higher crystallinity can influence positively the performances of the polymer. A lower amorphous content limit the relaxation process that is not desired for the PLA that is a brittle polymer. Increasing the crystallinity the chemical and thermal resistance of the PLA can improve (Gamez-Perez *et al.*, 2011). For this reason, the study of the crystallization kinetics of PLA was of relevant importance (Pantani *et al.*, 2010). The crystallization can also influence the compostability of PLA because the crystalline regions are more resistant to degradation than the amorphous ones.

Sometimes crystallization is undesired because it can led to properties that are not suitable for a particular application (Auras *et al.*, 2011). Furthermore, obtaining a highly amorphous polymer can increase some mechanical properties, namely elongation and impact strength.

Although an increase of the crystallinity improve the thermal resistance of PLA. To determine the short term heat resistance the heat deflection temperature (HDT) is usually evaluated. It indicates the temperature at which a standard test bar deflects a specified distance under a load. Harris et al showed that the heat deflection temperature increases more than 30 °C after amorphous samples are fully crystallized (Harris and Lee, 2008). The Vicat penetration temperature, that is the temperature at which a flat-ended needle of 1 mm^2 circular cross section penetrates a thermoplastic specimen to a depth of 1 mm under a specified load using a selected uniform rate of temperature rise, increases more than 100 °C, as reported by Perego et al, after a full crystallization of amorphous PLA. Their samples also showed an increase in flexural modulus and strength by 25% and increased impact resistance (Perego, Cella and Bastioli, 1996).

In order to understand how to maintain the PLA transparency or maximize the biodegradability of the PLA, it is important to study how the crystallization can be limited. Li et al (Li and McCarthy, 1999) produced films of PLA by compression molding annealed, after a rapid cooling, at 105°C for 0, 1, 2, 3, and 60 min and measured the weight loss. Their results showed that, below a crystallinity of 26%, the polymer had actually the same enzymatic degradability, in fact the great amount of chains is amorphous and accessible for enzymatic attack. Above that crystallinity content, however, the degradation rate decreases and the degradation rate can be reduced by more than 7 times for highly crystalline PLA compared to the amorphous samples. Finnis et al (Finniss, Agarwal and Gupta, 2016) studied a way to increase the hydrolytic stability of the PLA so that it can be used in more durable applications such as automotive components or equipment housing. Their compression molded samples and pellets were annealed at 80 °C for 48 hours the crystallinity increases to 30–35% for both pellets and molded samples. The weight change of the molded parts was monitored as a function of time and pH. While for the annealed samples, even after 6 weeks of immersion, the loss in weight is negligible, the unannealed samples show about 15% mass loss when the pH is 10, in the last three weeks of immersion.

Furthermore, the PLA crystallization improve the barrier properties. The PLA films of Duan et al. (Duan and Thomas, 2014) were annealed from 10 minutes to 24 hours at 75, 100, and 125 °C. For the annealing at 125 °C, large spherulites develop fast with shorter times of impingement, while at 100 °C a bigger amount of nuclei is activated and grows at a lower rate. Using the Avrami equation (eq. 7) the space filling (ξ) can be calculated:

$$\xi_g = 1 - e^{\left[\frac{-4\pi}{3} N G^3 (t - t_o)^3\right]} \qquad \text{(eq.7)}$$

where:

N: Nucleation density
G: Growth rate
t_0: time at which nuclei appear

Eq. 7 evaluates the space filling in isothermal crystallization, for which nuclei appear at t_0 and where the growth rate is constant for $t > t_0$. If the space filling is equal to 1 the spherulites fill the whole volume of the sample. The analysis proved that the crystallization of the PLA influences positively the barrier properties, decreasing the oxygen permeability, but not linearly with the decrease of amorphous portion. Other factors control the barrier properties of PLA. Crystallinity decreases the diffusivity and unexpectedly increases the solubility. Since increasing crystallinity the total permeability decreases, the observed reduction of the diffusivity with crystalline degree is dominating over the increase of solubility with crystallinity.

These aspects stress the importance of PLA crystallization not only from a fundamental point of view but also for obvious market development considerations.

The slow crystallization kinetics of the PLA makes the material unable to crystallize at the cooling rates involved in normal processing conditions. The overall crystallization kinetics is composed of two independent phenomena: crystal nucleation and subsequent crystal growth.

In quiescent, isothermal conditions, the growth rate, G, of PLA is essentially spherical. This is confirmed when the evolution of crystallinity under quiescent conditions is analyzed by Avrami's model (eq. 8), which generalizes eq. 7.

$$\xi(T,t) = 1 - exp[-(k_a(T)\ t)^{n_a}] \qquad \text{(eq.8)}$$

in which ξ is the relative crystallinity degree, k_a is the Avrami costant and na is the Avrami exponent, this latter takes a value close to 3 (describing predetermined, spherical growth) independently on the molecular weight and on the D-Lactide content (Pantani *et al.*, 2010).

The maximum growth rate for PLA spherulites is reported as about 30 micron/min (Iannace and Nicolais, 1997) at 110-120°C.

Sanchez and coworkers (Salmerón Sánchez *et al.*, 2007) used HPer DSC measurements to study the effect of the cooling rate on the nucleation kinetics of a PLA. They found that the cooling rate regulates the number of nuclei that form in the glass state. A high numbers of nuclei is found when the material is cooled at low rates in comparison to parts cooled at higher rates and faster cold crystallization kinetics. The optical observation revealed a high number of spherulites to the large amount of nuclei that grow simultaneously as shown in Figure 22. The effect of different numbers of nuclei is detected by DSC with the different enthalpies of melting. For longer time, when cold the crystallization is complete, neither the shape of the heating DSC curves nor the morphology by Optical Microscopy and AFM of the PLA samples seemed to depend on the number of nuclei generated during the cooling. They explained the phenomenon by the generation of nucleii during the annealing in a number that these cancel the initial nuclei difference due to the different cooling rates.

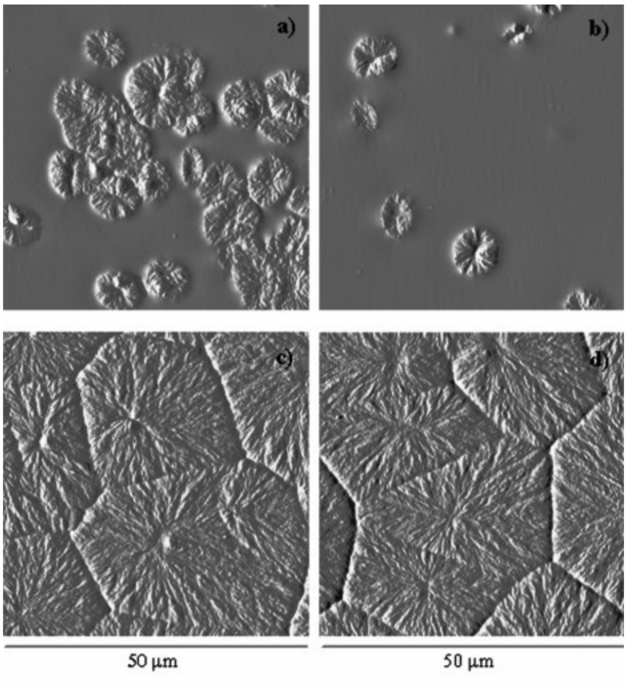

Figure 22. AFM amplitude images showing the spherulitic morphology after crystallizing at 110 °C for (a-b) 5 min, (c-d) 60 min. The samples were cooled at (a,c) 10 °C/min and (b,d) 90 °C/min from the melt into the glass before the isothermal cold crystallization process (Salmerón Sánchez et al., 2007).

While the quiescent crystallization of PLA has been broadly studied, the achieved understanding is not directly transferred to the polymer engineering of PLA, because quiescent crystallization studies describe PLA behavior in the absence of melt flow and orientation.

Flow induced crystallization is a broad term that describes the crystallization of polymers during and after they have been subject to shear flow (Ma *et al.*, 2014). Historically, most experimental investigations of FIC have focused on olefin-based polymers, and models which describe FIC behavior are almost exclusively derived from these flexible polymers. Considering the fast cooling rates involved in injection molding, PLA should not crystallize at all if just the quiescent crystallization kinetics are considered. It is important to note that for PLA grades with significant amount of D-lactide, injection molded parts are reported to be amorphous (Pantani and Sorrentino, 2013), and only special molding protocols can provide crystalline samples (Harris and Lee, 2008),(De Santis, Volpe and Pantani, 2017). This suggests that the enhancement effect on crystallization due to flow could be not enough to compensate the high cooling rates.

Only recently scientists focused their attention on the FIC of PLA (Bojda and Piorkowska, 2016), (Li *et al.*, 2019). Some developed techniques to mimic the effect of the flow. Monnier and coworkers (Monnier *et al.*, 2017) built a homemade device to pull a fiber through a molten PLA at a constant linear velocity of 10 mm/s for 1 s. The resulting shear rate at the interface between the fiber and the melt was estimated to be close to 1000 s^{-1}. They observed the effect of the application of the flow by pulling the fiber at different temperatures and then by applying a crystallization step at 130 °C. Their study proved that at 150 °C, the critical relaxation time was much larger than the time required to quench the sample to a suitable crystallization temperature, resulting in the formation of highly oriented cylindrical structures, which were embedded in an amorphous PLA matrix.

The team of Iqbal (Iqbal *et al.*, 2019) focused their attention on the flow induced crystallization of a PLLA and tried to validate the concept of the specific work of flow w, which the melt needs to allow shear induced formation of crystal nuclei. The equation 9 can be used to calculate the specific work of flow:

$$w = \int_0^{t_s} \eta \times \dot{\gamma}^2 \, dt \qquad \text{(eq.9)}$$

where $\dot{\gamma}$ is the shear rate, t_s the time and η is the viscosity, which depends on $\dot{\gamma}$ and t_s. They adopted plate-plate rheometer experiments with a gap of 250 µm and imposed to the PLA samples rotational shear at rates between 0 and 10 s^{-1} for variable time between 0 and 900 seconds. After the rheological experiments they cutted 10 microns slices from the discs to observe the morphologies. They concluded that the critical work for shear-induced formation of crystal nuclei in PLLA is approximately 20 to 50 kPa (Figure 23).

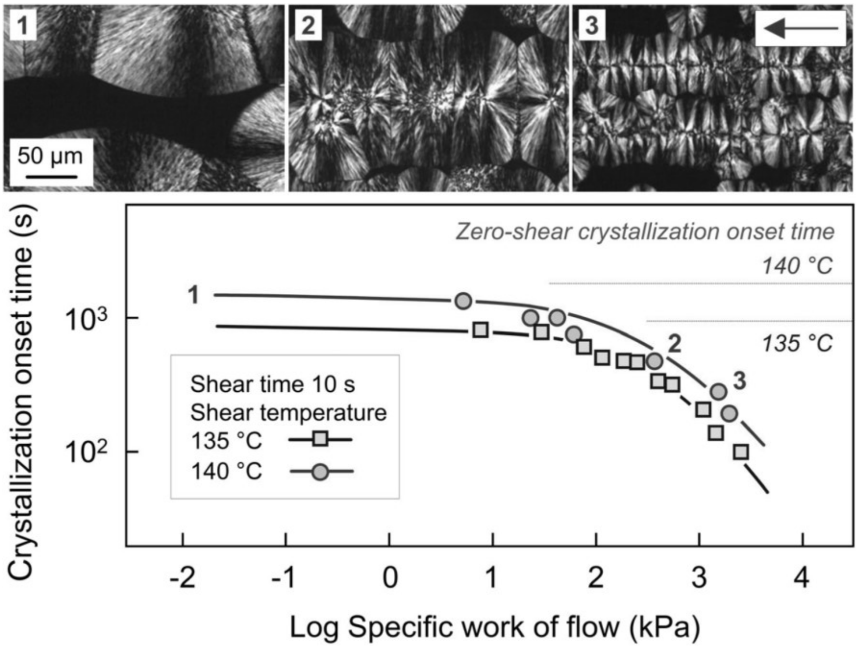

Figure 23. Onset-time of crystallization of poly (L-lactic acid) as a function of the specific work of flow. Shearing of the melt before crystallization was performed at 135 °C (squares) and 140 °C (circles) for a period of 10 seconds. The zero-shear crystallization onset time is shown with the dashed lines in the top right part of the graph. The top images serve for qualitative discussion of the number of nuclei forming at different shear conditions at 140°C, as indicated with the Arabic numbers at the corresponding data set (circles/curve) in the below plot (Iqbal et al., 2019).

Material characterization

The material used in this part is the PLA 3251D, the same adopted for the experiments described in the previous chapter. In order to study the effect of the process on the morphology of this polymer, viscoelastic and crystallization studies were performed on the pellet.

Viscosity measurements were obtained by a Haake Mars II rheometer at 120°C, 140°C, 160°C and 180°C.

The data were described by the Cross Model (Figure 24) as described in the eq. 10 adopting the parameters listed in the Table 4:

$$\eta = \frac{\eta_0}{\left(\frac{1+\eta_0\dot{\gamma}}{\tau}\right)^{(1-n)}} \qquad \text{(eq.10)}$$

Where η_0 is calculated from the equation 11:

$$\eta_0 = \eta^* e^{\frac{-A_1\left(T-T_{ref}\right)}{(A_2+T-T_{ref})}} \qquad \text{(eq.11)}$$

Table 4. Parameters used in the Cross description.

A1	6.58874
A2	104.0767
Tref	160
tau*	3.65E+05
n	0.253772
eta*	1315.747

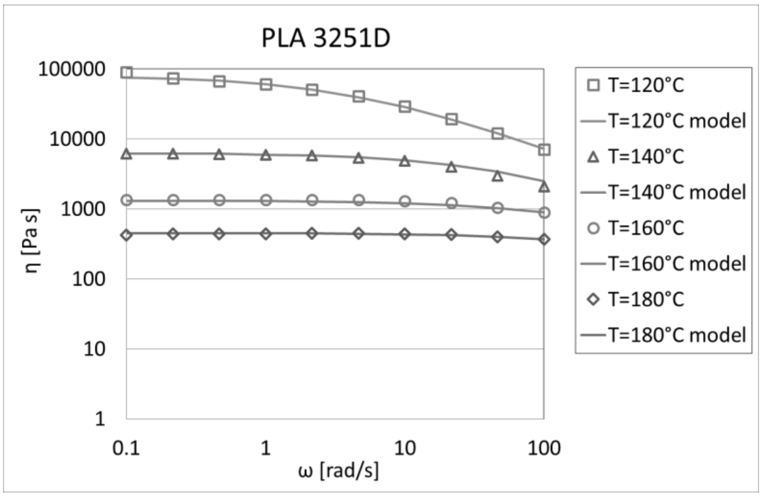

Figure 24. Viscosity measurements and model description.

A mastercurve for the moduli G’ and G’’ was determined and represented in the Figure 25.

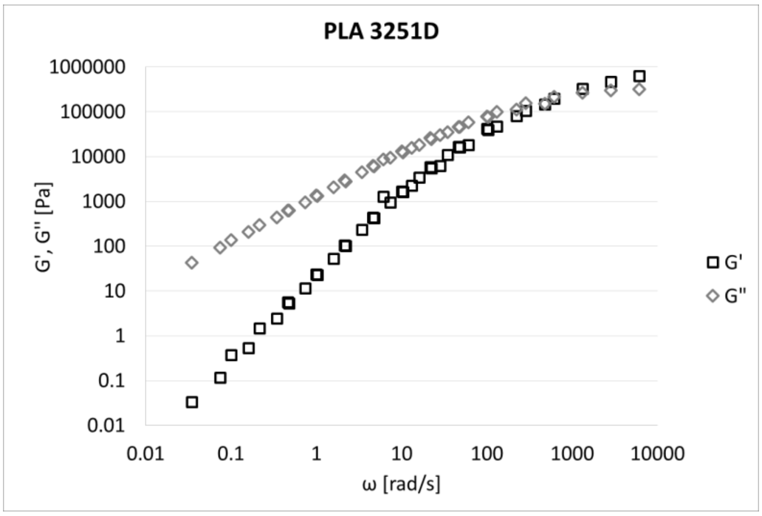

Figure 25. G’ and G’’ mastercurves.

The viscoelastic model described by Pantani and coworkers (Pantani, Speranza and Titomanlio, 2012) was adopted to model the evolution of molecular orientation during the process.

G’ and G’’ were used to calculate the relaxation time according to Laun’s rule (eq. 12).

$$\lambda(T,\dot{\gamma}) = \frac{G'(T,\omega)}{\omega G''(T,\omega)}\left[1+\left(\frac{G'(T,\omega)}{G''(T,\omega)}\right)^2\right]^{0.2}\Bigg|_{\omega=\dot{\gamma}} \qquad \text{(eq.12)}$$

In order to describe the dependence of the relaxation time upon the internal structural parameter, Δ, considered as a measure of the elongation of the system, it was was evaluated by a combination of the invariants of the conformation tensor. Δ is calculated by the equation 13.

$$\Delta = \sqrt{\left({A_{11}}^2 + 4\,{A_{12}}^2\right)} \qquad \text{(eq.13)}$$

Where:

$$\overline{\overline{A_{11}}} = 2\,\lambda^2\dot{\gamma}^2 \qquad \text{(eq.14)}$$

$$\overline{\overline{A_{12}}} = \lambda\dot{\gamma} \qquad \text{(eq.15)}$$

The following equation has been adopted for the determination of the relaxation time:

$$\lambda = \frac{\lambda_0}{\left[1+(a\Delta)^b\right]^c} \qquad \text{(eq.16)}$$

Where the parameters adopted are listed in Table 5.

Table 5. Parameters used in the relaxation time description.

λ_0	1.63E-02
a	2.64E+00
b	1.43479
c	0.747844

The Figure 26 represents the evolution of the relaxation time.

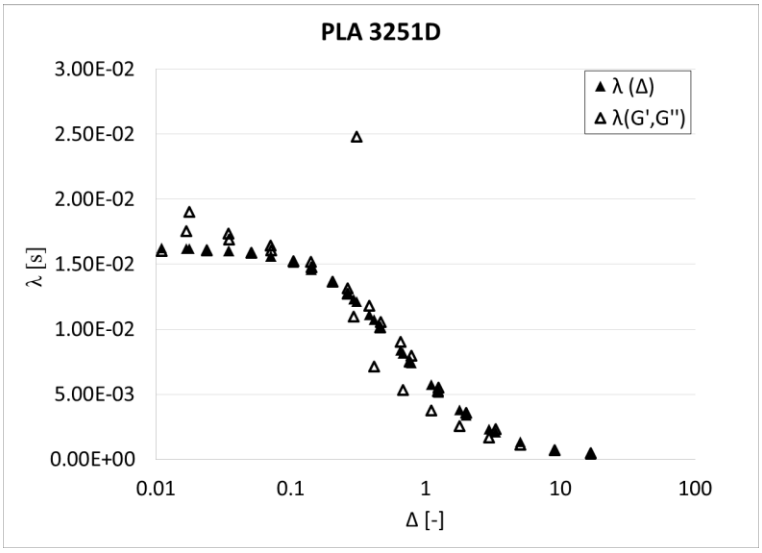

Figure 26. Relaxation time evolution.

Crystallization kinetics

The crystallization kinetics of the PLA 3251D was studied by means of calorimetric analysis. A differential scanning calorimeter DSC 822e from Mettler Toledo was used for the characterization of the thermal behavior of PLA 3251D. The pellets with a weight of less than 10 mg were put into an aluminum pan and hermetically sealed. In order to prevent oxidative degradation at high temperatures all the experiments were carried out at a flow rate of 50 ml min^{-1} of nitrogen. The crystallization kinetics was investigated in isothermal conditions starting from the melt after holding the sample at 200 °C for 5 min in order to erase the effect of previous thermomechanical history. The glass transition temperature, T_g, measured by DSC is about 60 °C. The melting temperature, T_m, measured as the peak of the melting endotherm during DSC heating ramp at 10 °C min^{-1}, is about 170 °C.

To study melt isothermal crystallization, the sample was cooled from 200°C directly to isothermal test temperature (crystallization temperature), with a cooling rate of 10 K min-1. As a result, the specific heat flow evolutions were obtained at different isothermal temperatures. The specific heat flow evolutions were obtained are shown in Figure 27. This investigation pointed out that the narrowest crystallization peak is at 105 °C: the shortest time is required at this temperature for the complete crystallization.

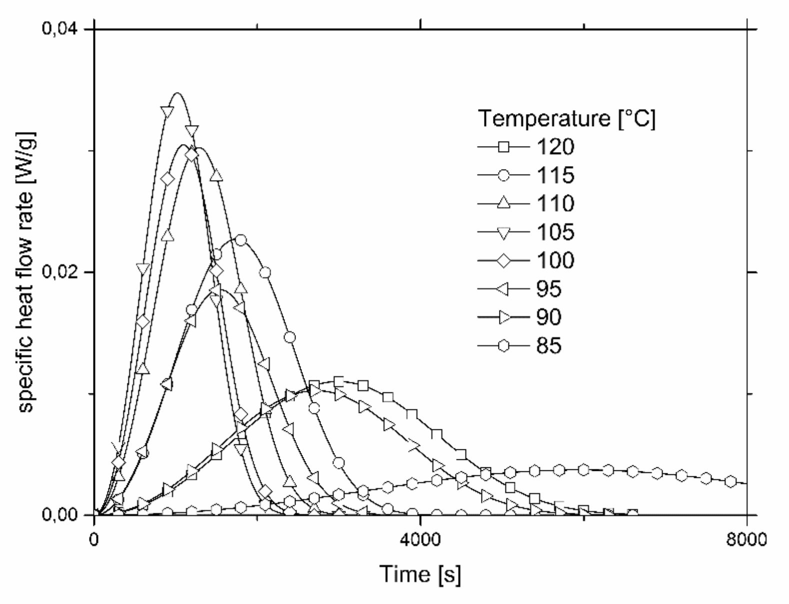

Figure 27. Specific heat flow evolutions.

The calorimetric analysis were coupled with the solidification study of the material performed by means of a hot stage. To deepen the crystallization study, the number of nucleii and the growth rate of the spherulites at different isothermal conditions were evaluated by our research group.
The experimental number of nuclei was well described by the equation 12 and the evolution with the temperature is shown in Figure 28.

$$N(T) = \frac{A}{1 + B \cdot e^{C \cdot (T - T^*)}} \qquad \text{(eq.12)}$$

With the parameters shown in Table 6:

Table 6. Parameters adopted in the eq. 12.

A(μm^{-3})	7.02E-06
B (-)	3.94E+16
C (°C^{-1})	-0.34
T* (°C)	218.75

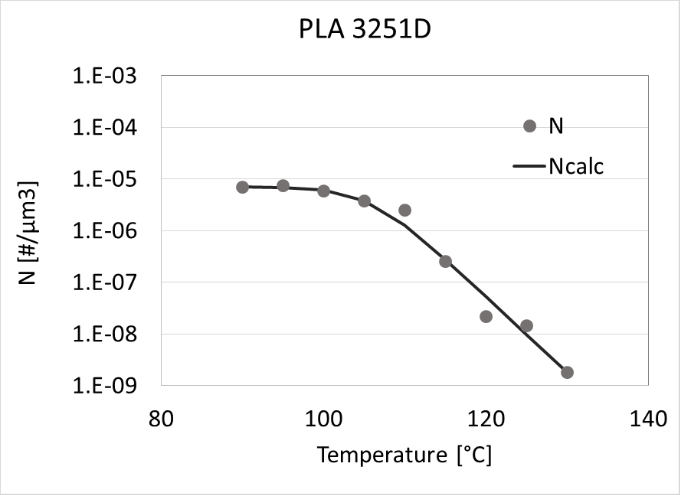

Figure 28. Nucleation density at different temperatures.

On the other hand, the growth rate can be described by the equation 13 and two possibilities have been considered. The data, in fact, can be modelled by a unique curve (G model in the Figure 29) or by considering two curves G low for the α’ phase and G high for the α phase with the same law but different parameters for high or low temperatures.

$$G(T) = A * e^{\left(\frac{-B}{T-C+30}-\frac{D(T+E+546)}{2(T+273)^2(E-T)}\right)} \qquad \text{(eq.13)}$$

Table 7. Parameters used in the growth rate description.

	One curve	α’	α
A (Micron/s)	8.37E+03	2.76E+05	1.17E+04
B (K)	6.72E+02	4.30E+02	8.70E+02
C (°C)	36.5255322	71.6827783	38.43771761
D (Micron/s)	2.14E+05	2.46E+05	1.25E+05
E (°C)	222.234563	183.891511	196.853259

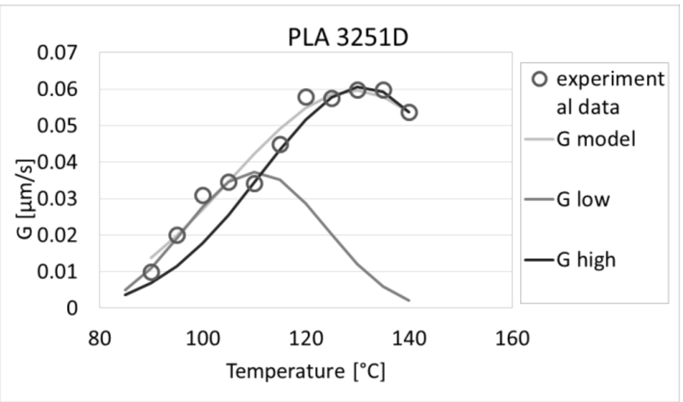

Figure 29. Growth rate with temperature.

The semi-crystallization time, i.e. the time necessary for half crystallization of the material $t_{1/2}$, was evaluated from isothermal DSC experiments from the melt and compared with the one obtained from the nucleation density and growth rate evolutions. As shown in Figure 30 there is a good reproducibility of the crystallization behavior detected by two different techniques.

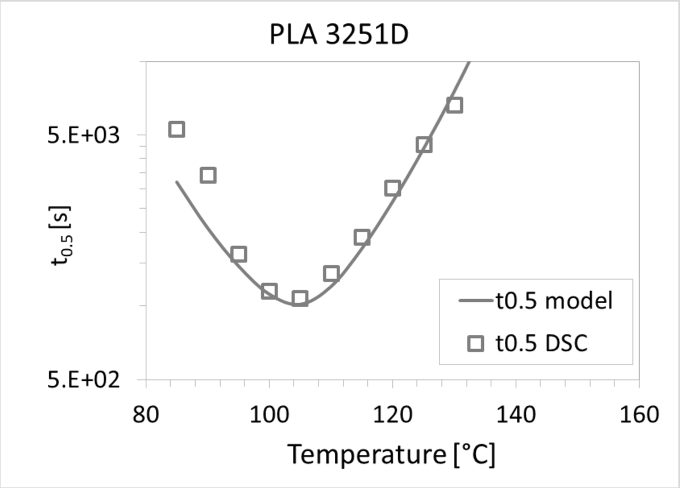

Figure 30. Semi-crystallization time with temperature.

The shortest semi-crystallization, at the temperature of 105 °C, is about 1000 s.

Part I. Influence the final morphology.

Protocols

Investigations on the crystallization from the melt and the solid microparts were considered. In particular two different protocols were adopted, in the case of "*protocol 2*", after the injection step, the cavity surface was cooled to a lower temperature, $T_{isotherm}$=105 °C, for the set isothermal time. After this isothermal step, the power supply of heating elements was automatically switched off and the temperature of the cavity is lowered under T_g for part extraction.

In the case of "*protocol 3*", after the injection step, the cavity surface was immediately cooled under T_g. Subsequently, the cavity surface is heated again to $T_{isotherm}$=105 °C, for the set isothermal time, and then cooled again for the part extraction.

The effect of time of the isothermal step, for both the "*protocol 2*" and the "*protocol 3*", is explored with times of 10 s, 100 s and 1000 s.

Results

Temperature measurements

Figures 31 and 32 represent the temperature measurements.

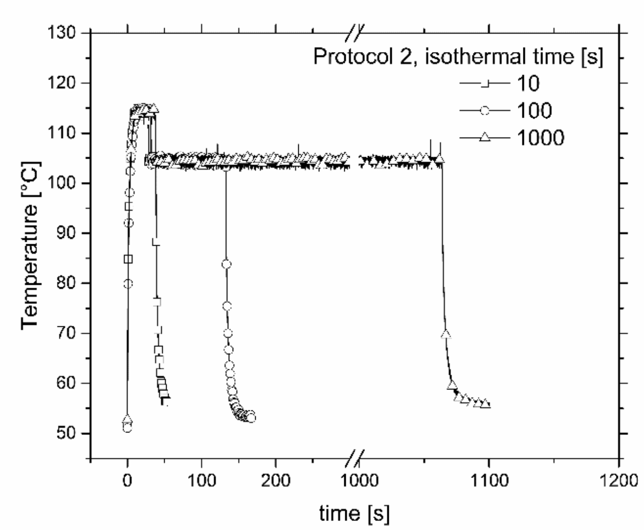

Figure 31 Temperature evolutions Protocol 2.

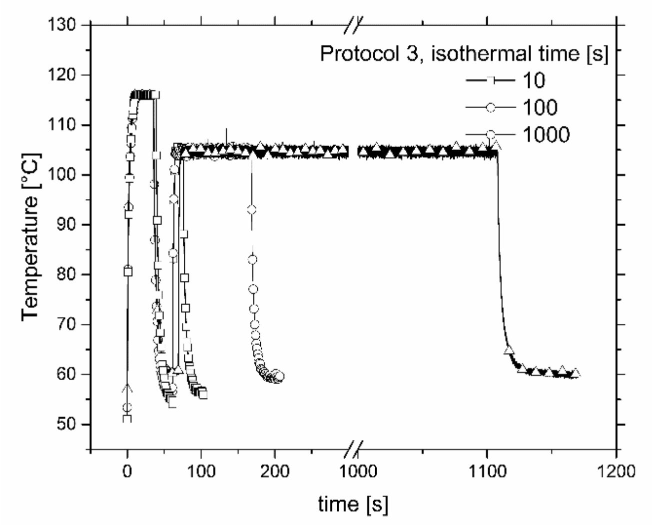

Figure 32. Temperature evolutions Protocol 3.

Polarized Optical Microscopy Images

The different thermal histories affect the opacity of the injected parts as shown in Figure 33, the samples under 1000 s are completely opaque.

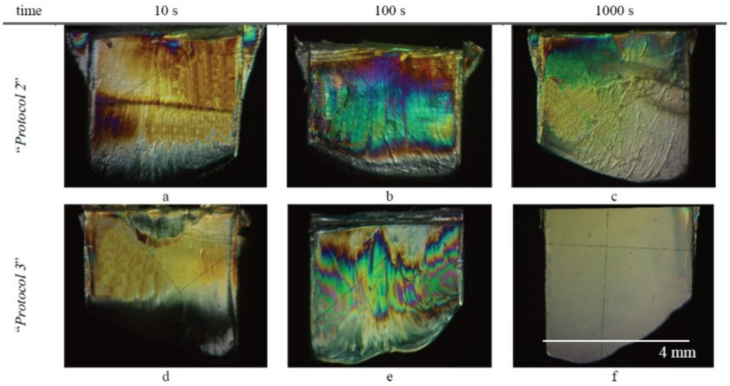

Figure 33. Polarized Optical Observations.

X-Ray Diffraction

To get further information of crystallization, the crystalline nature of the injected samples was checked by X-ray diffraction. Figures 34 and 35 reveal the X-ray diffraction profiles of PLA and injected parts. The pellet and the samples kept at 105 °C for 1000 s presented two peaks at 16.7° and 19.0° that are characteristic peaks of crystalline PLA which represent (200)/(110) and

(203) reflections of stable α-crystals (Xiao *et al.*, 2010). The parts obtained after a permanence of 100 s present a lower peak at 16.7°. Vice versa, patterns of samples kept at 105 °C for only 10 s did not present any peak, resulting amorphous. Furthermore, the peaks of the samples obtained from "protocol 3" are slightly higher than the corresponding one, with the same isothermal time, obtained with "protocol 2".

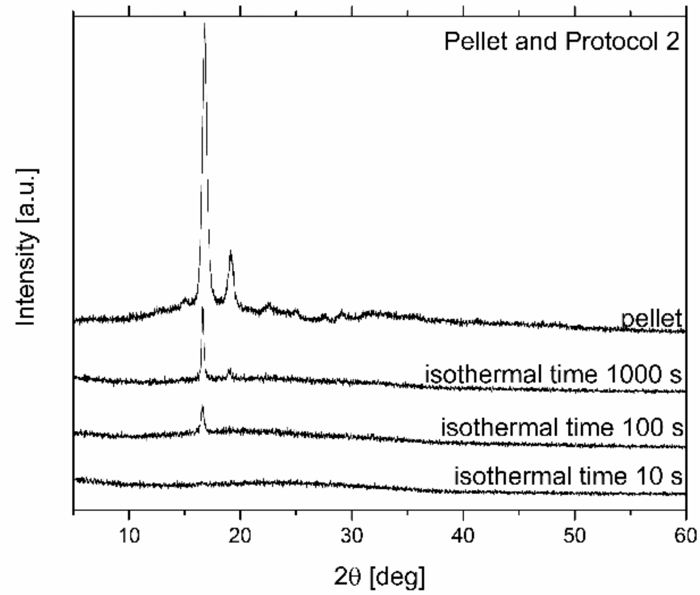

Figure 34. X-ray diffraction profiles of PLA and injected parts produced by the Protocol 2.

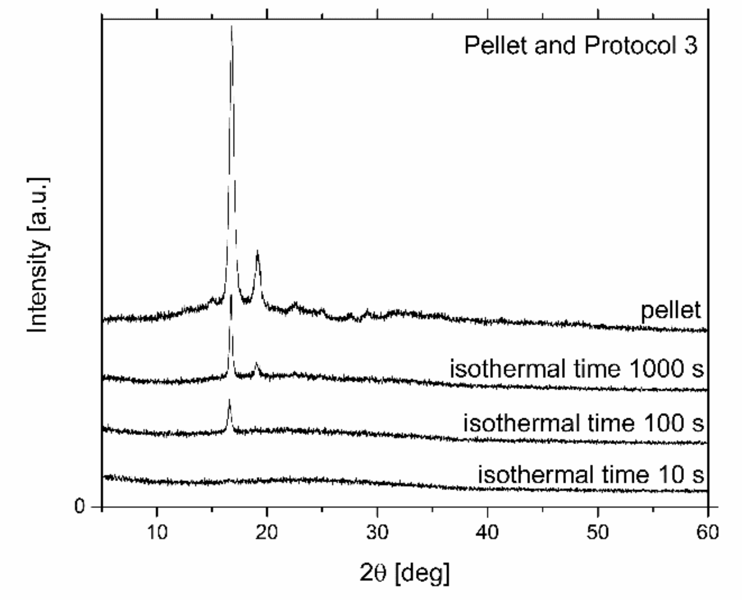

Figure 35. X-ray diffraction profiles of PLA and injected parts produced by the Protocol 3.

Calorimetric Analysis

Mimicking the same thermal history experienced by the samples in "protocol 2" and "protocol 3", the calorimetric analysis was performed on a piece of pellet of the neat PLA.

In particular, the effect of the isothermal time at 105 °C is analyzed in the subsequent heating up to 200 °C. The differences in the specific heat flow released during the melting of the samples are quite evident, as shown in Figures 36 and 37, corresponding in the previous crystallization of the sample. The analysis confirms that the length of the isothermal step promotes the crystallization, in particular for the "protocol 3" with the annealing of the solid part (De Santis, Pantani and Titomanlio, 2011).

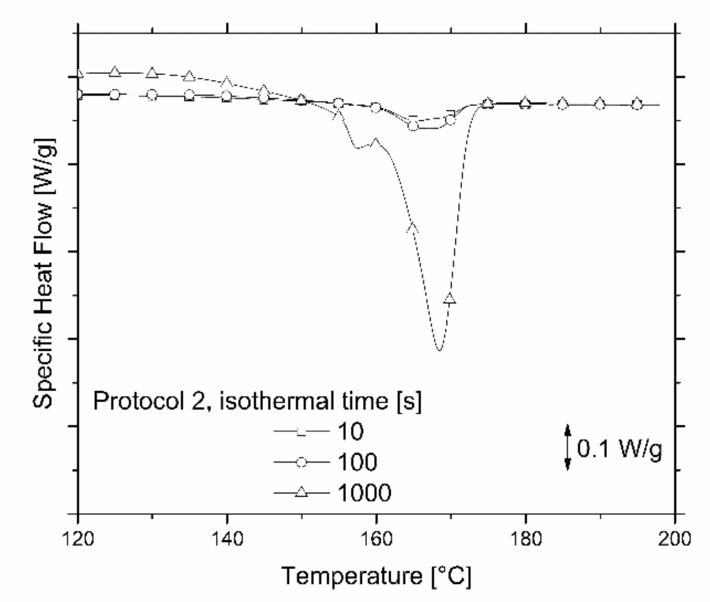

Figure 36. Heat Flow curves Protocol 2.

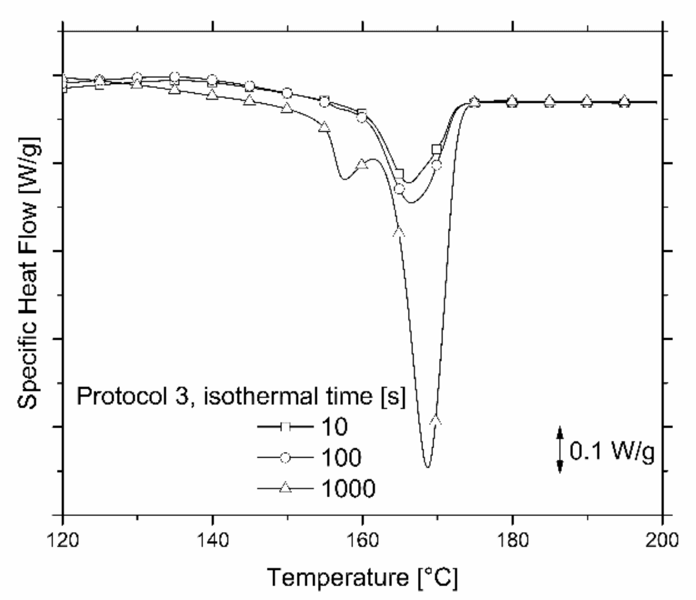

Figure 37. Heat Flow curves Protocol 3.

Conclusions

This analysis demonstrates that the system can tune the morphology of semi-crystalline thermoplastic materials. Microscopy, X-ray diffraction analysis and calorimetry demonstrate that the application of an annealing step, after the injection, affects the morphology of the samples indicating an enhancement of the mechanism of the crystallization on a resin that has a slow crystallization kinetics. Furthermore, the crystallization is higher when the annealing is performed on the solid part, this could be due to a formation of a number of point nuclei higher in the case the polymer is solidified and then heated again.

Part II. Local control of the morphology.

Method

The Labview code was rewritten to control differently two zones of the cavity. The micro-injection molded bars were obtained by applying the process parameters shown in Table 7 and the experimental protocols are shown in Figure 38. For each experiment, two steps were considered. In the first one, the cavity surfaces were heated up to 160°C to permit the complete filling of the microcavity. When the temperature was reached, the polymer is injected applying a pressure of 100 bar for a time of 5 s, 10 s, 20 s. These different values of permanence at 160°C inside the cavity were chosen on the base of the relaxation spectrum analysis, previously described according to which the polymer at this temperature requires a time of 8 s to lose its orientation. After this time at 160°C, the power supply are switched off and because of the ballistic cooling the polymer injected solidifies. In the second step, the temperature control is used to heat only one of the two zones of the cavity (zone 1 or zone 2 of the Figure 39). Half sample experiences an isotherm at 105°C for 250 s, 500 s and 1000 s. For the protocol 4 the zone under annealing is the one after the gate position (zone 1), for the protocol 5 the other zone at the tip (zone 2).

Table 8. Injection Molding set parameters.

Melting temperature	180°C
Injection pressure	100 bar
Mold temperature	60°C
Surface cavity temperature	160°C

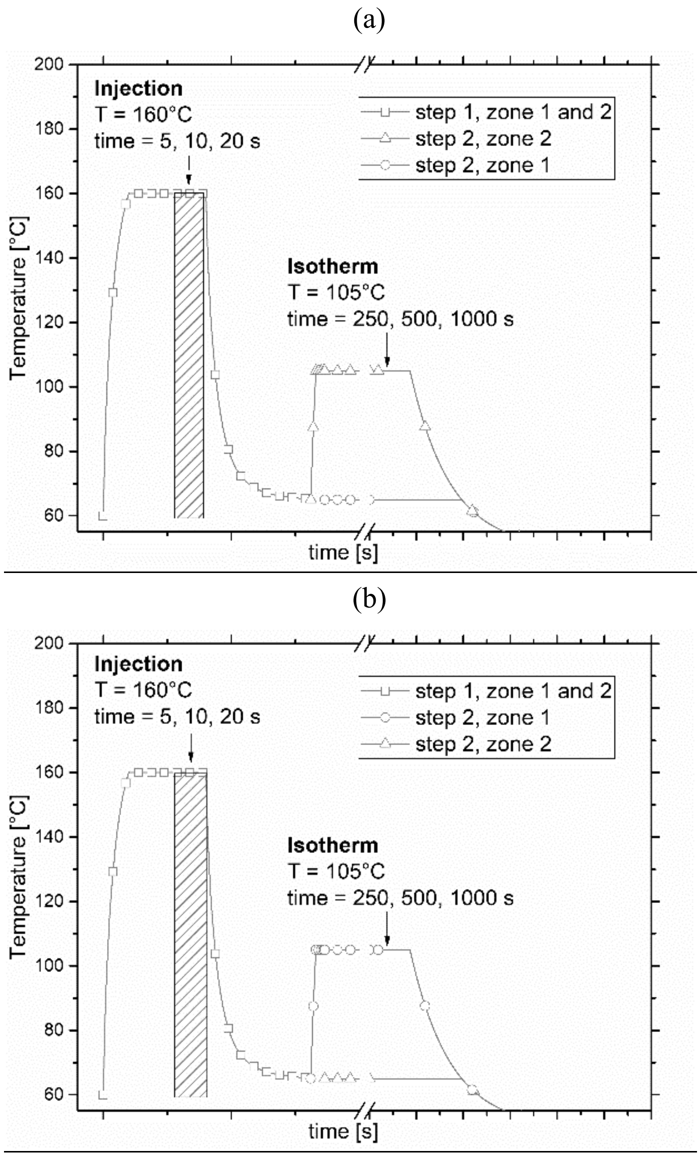

Figure 38. Set time and temperature for (a) Protocol 4 and (b) Protocol 5.

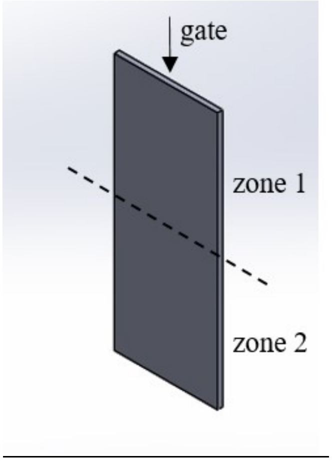

Figure 39. Schematic of the sample

For shortness, the experiments will be named as described in the Table 9.

Table 9. List of the experiments.

Annealing time		**Permanence at 160°C**		
		5 s	**10 s**	**20 s**
1000 s	gate	AG5	AG10	AG20
	tip	AT5	AT10	AT20
500 s	gate	BG5	BG10	BG20
	tip	BT5	BT10	BT20
250 s	gate	CG5	CG10	CG20
	tip	CT5	CT10	CT20

Results

Temperature acquisitions

The rapid temperature control was used to rise the temperature of the cavity up to 160 °C, as that temperature was reached, the injection process was activated and the polymer filled the cavity. The temperature of the cavity was set equal to 160 °C for 5 s, 10 s, 20 s. The Figures from 40 to 45 show the evolution of the temperature for the experiments performed with 20 s of permanence at 160 °C.

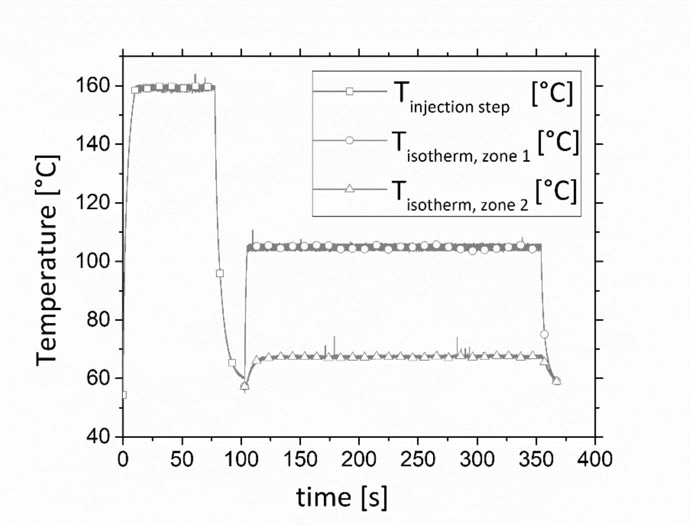

Figure 40. Temperature evolution with an annealing step =250 s in the zone 1.

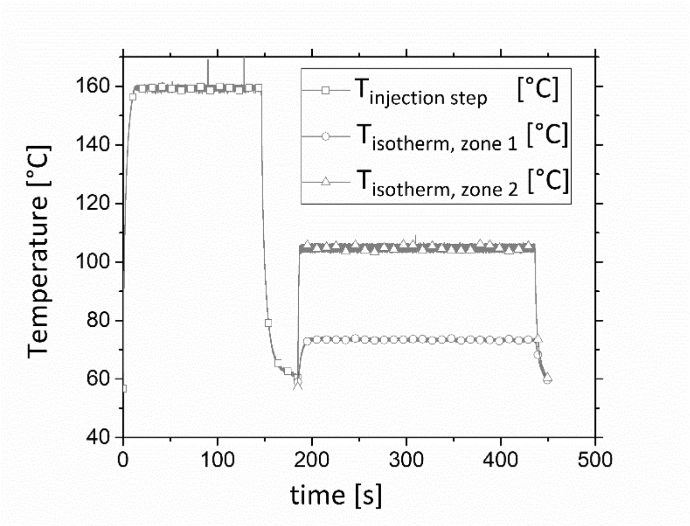

Figure 41. Temperature evolution with an annealing step =250 s in the zone 2.

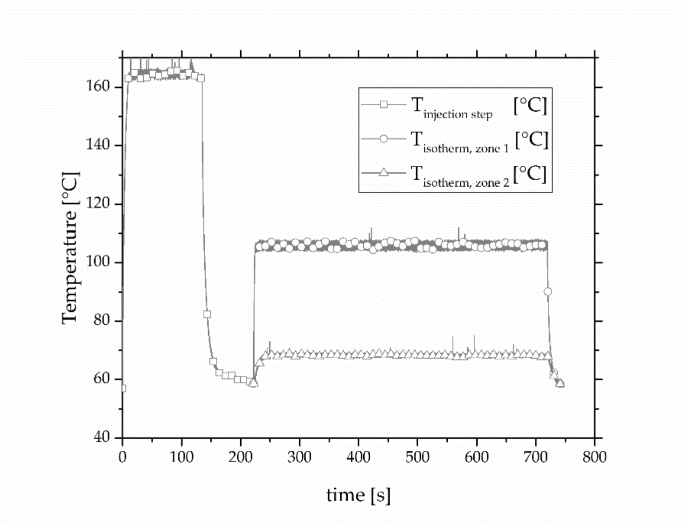

Figure 42. Temperature evolution with an annealing step =500s in the zone 1.

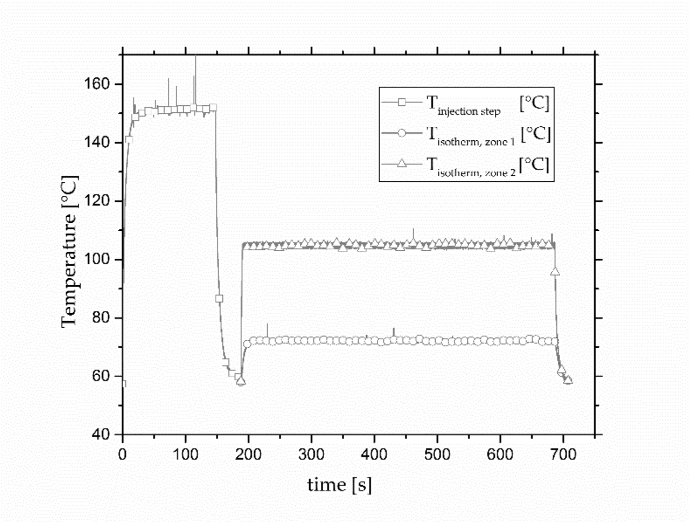

Figure 43. Temperature evolution with an annealing step =500s in the zone 2.

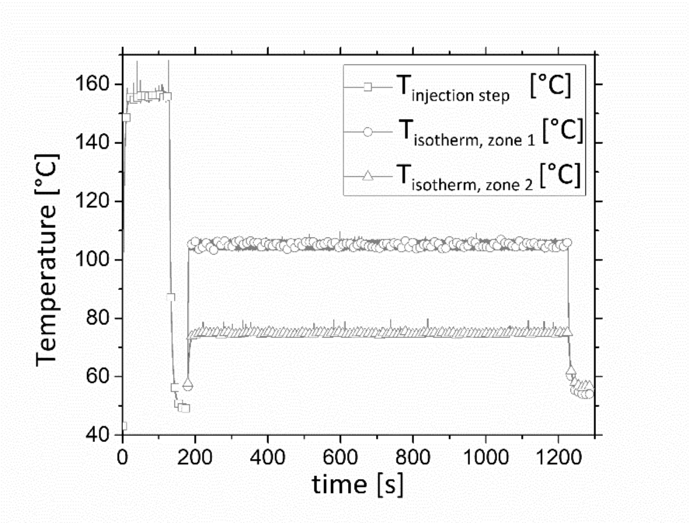

Figure 44. Temperature evolution with an annealing step =1000s in the zone 1.

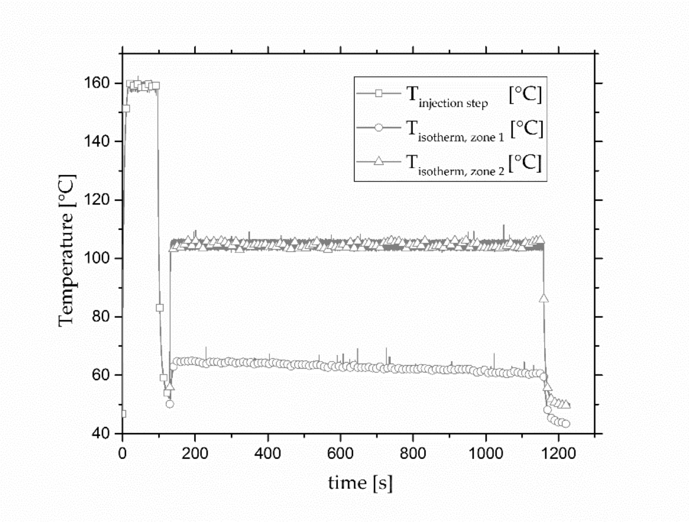

Figure 45. Temperature evolution with an annealing step =1000s in the zone 2.

The experiments carried out with different time of permanence at 160°C experienced the similar thermal histories. The temperature evolutions accurately reproduced the set values. As shown in the Figures 40-45, the measurements show different time at 160°C because this time include also the time of activation of the heaters before the injection step. While the cavity is empty, through the labview code the heaters are powered continuously up to the set temperature equal to 160 °C and then by a control “on-off” the system maintains lowest possible the difference between the data acquired and the set values. The measurements are acquired with a frequency of 10 ÷11 ms. The injection is manually activated after the pellets have been in the cylinder at 180°C for 10 min to make them completely melt and avoid the degradation that can occur with longer time at high temperature. The permanence at 160°C inside the cavity is timed and manually the heating is deactivated by using the button called cooling that regulate the temperature on the base of the values given in the cells *isotherm gate* and *isotherm tip* in the front panel in labview (Figure 46). As the temperature reaches the one of the rest of the mold that is 60°C the button *stop* is clicked on and the data are automatically saved in txt file.

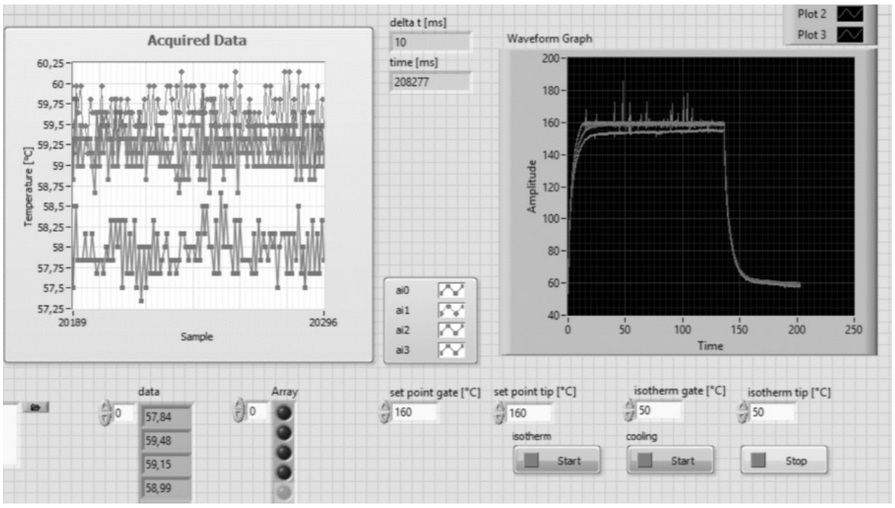

delta t [ms] 10

time [ms] 208277

data 0
57,84
59,48
59,15
58,99

set point gate [°C] 160

set point tip [°C] 160

isotherm gate [°C] 50

isotherm tip [°C] 50

Figure 46. Front Panel of the Labview code.

After the filling step, by using the same labview code, the annealing is carried out in one zone of the cavity. If the zone annealed is the zone after the gate, in the cell *set point gate* the value 105 is set and in the *set point tip* is 60, the opposite if the annealing is at the tip.

After the annealing, the heaters are switched off and the mold is opened to get the sample.

Polarized Optical Microscopy

Optical observations include the analysis of the massive samples to highlight the different opacity and a deepest analysis of the slices to observe the morphology along the thickness.

Massive samples

The samples obtained were observed by using the microscope Leica MZ6 and the images, with crossed polarizers, of some parts are shown in Figures 47 ÷ 52.

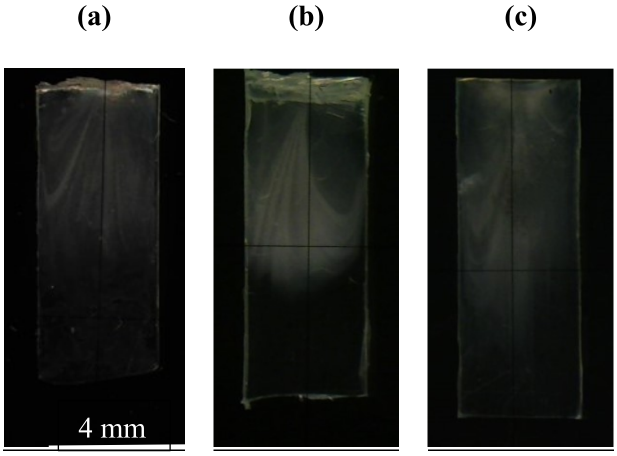

Figure 47. Samples with an annealing of 250 s in zone 1 after a permanence at 160°C of (a) 5 s, (b)10 s and (c) 20 s.

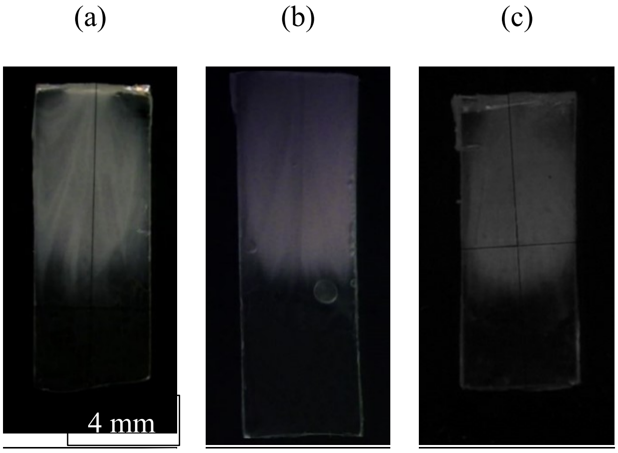

Figure 48. Samples with an annealing of 500 s in zone 1 after a permanence at 160°C of (a) 5 s, (b) 10 s and (c) 20 s

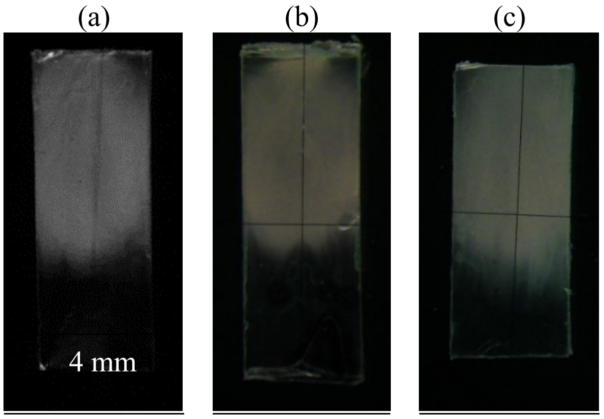

Figure 49. Samples with an annealing of 1000 s in zone 1 after a permanence at 160°C of (a) 5 s, (b) 10 s and (c) 20 s.

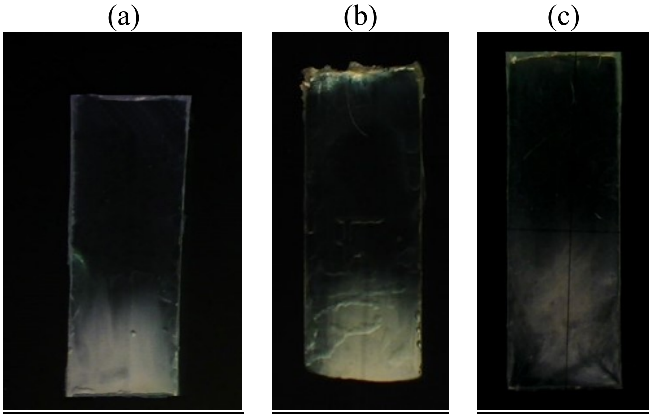

Figure 50. Samples with an annealing of 250 s in zone 2 after a permanence at 160°C of (a) 5 s, (b) 10 s and (c) 20 s

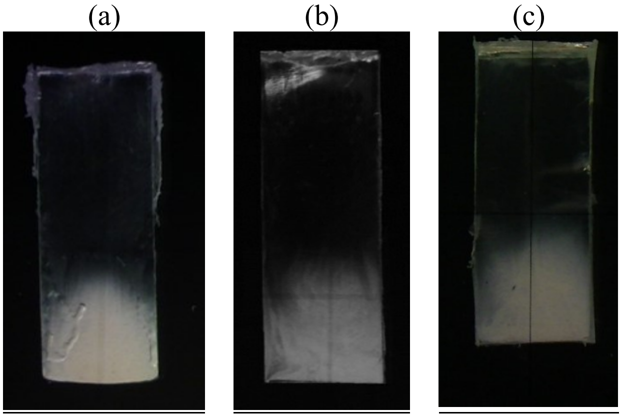

Figure 51. Samples with an annealing of 500 s in zone 2 after a permanence at 160°C of (a) 5 s, (b) 10 s and (c) 20 s.

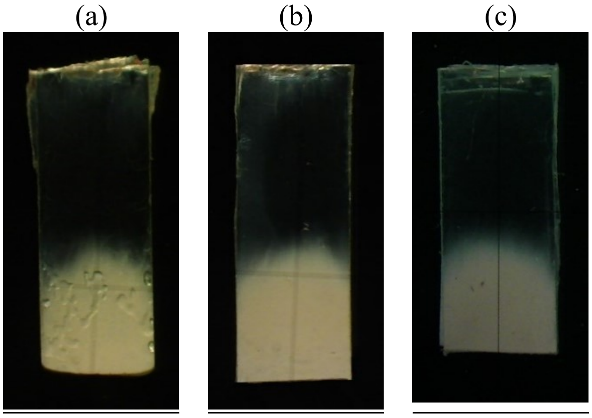

Figure 52. Samples with an annealing of 1000 s in zone 2 after a permanence at 160°C of (a) 5 s, (b) 10 s and (c) 20 s.

Slices

Some of the parts were imbedded in a mixture of an epoxy resin and a hardener to shape a parallelepiped piece that can be easily cut by microtome. Slices 15 μm thick were obtained from the gate to the tip along the entire thickness of the samples that is 200 μm. PLA is known to form spherulitic morphology after zero or low shear deformation, to experience enhanced nucleation and isotropic growth after experiencing moderate flow, and to exhibit cylindrites and shish kebab structures after strong shearing in the melt.

The Figures 53, 54 and 55 represent images captured at the Olympus BX51 microscope, in polarized optical light, by means of 20x lens and a blue filter.

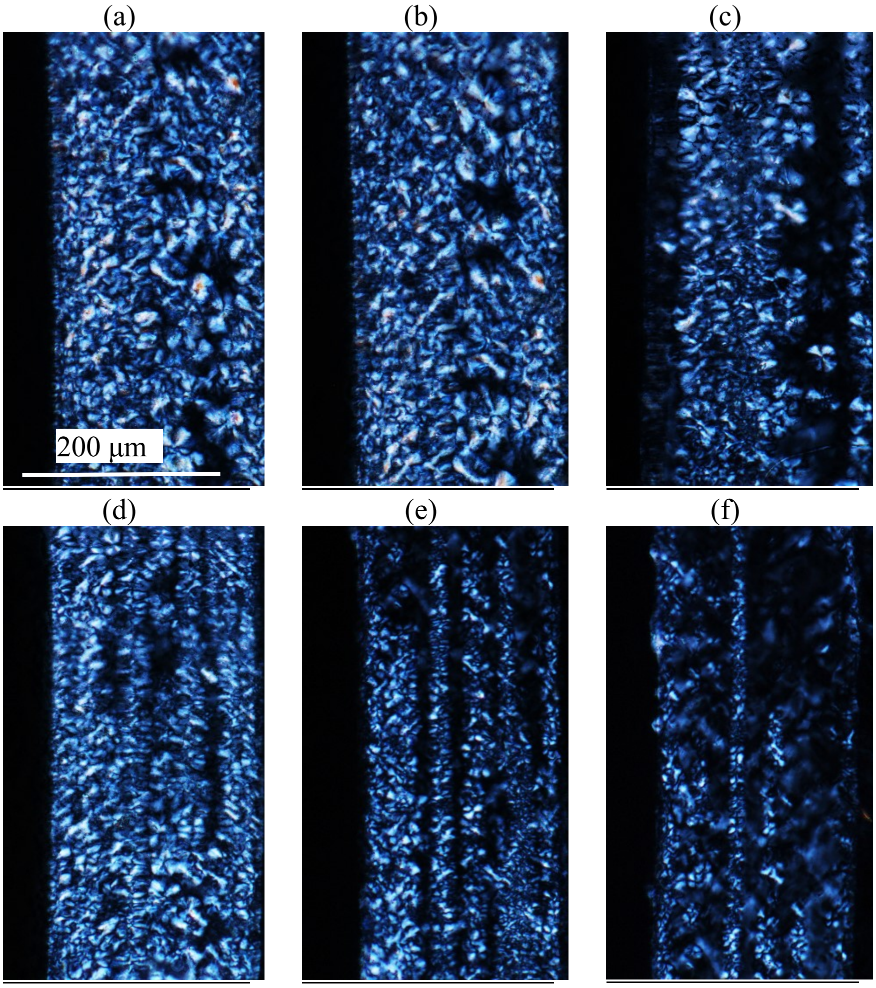

Figure 53. Polarized Optical Microscopy images from the gate to the center of the sample BG5.

The images a, b, c, d of the Figure 53 are taken in the zone 1, after the gate, that is the area annealed for 500 s. They show a predominant filling of the space by crystalline structures that are clearly spherulitic. The images e and f are taken in the center of the sample: a lower number of spherulites is visible, they are smaller in diameter and most of them seem to be arranged in sequence. This part is in the middle of the sample, between the area heated during the annealing and the subsequent that is at a lower temperature and where no crystalline structure are visible because the sample appear completely transparent.

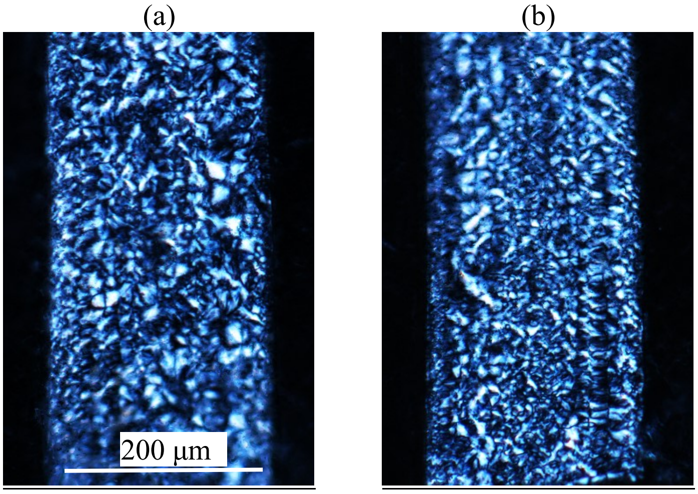

Figure 54. Polarized Optical Microscopy images from the gate to the center of the sample BG20.

The images of the sample BG20 (Figure 54) confirm that the annealing of 500 s produces a high amount of crystalline structures, also in this case spherulites.

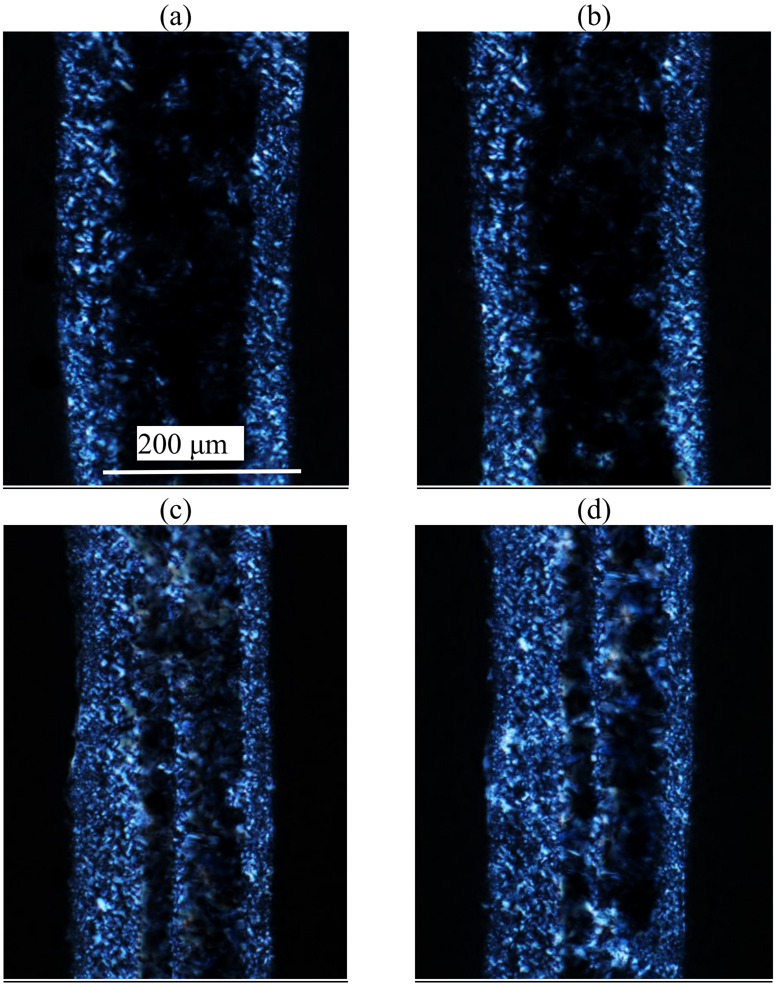

Figure 55. Polarized Optical Microscopy images from the center to the tip of the sample CT10.

By decreasing the time of the annealing (250 s) the birefringence is lower and, as shown in the Figure 55, most of the crystalline structures are near the surface of the cavity.

Calorimetric Analysis

The differential scanning calorimeter DSC 822e from Mettler Toledo was used to evaluate the crystalline content of each zone of the biphasic samples by heating the sample at 10 °C min^{-1} from 0 °C up to 200 °C, holding at 200 °C for 5 minutes and cooling down 0°C. The protocol is depicted in the Figure 56.

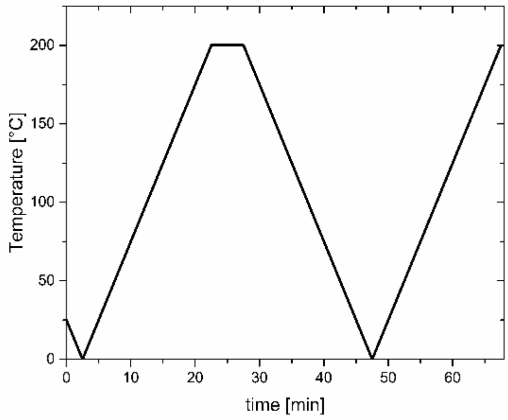

Figure 56. Experimental protocol for the DSC analysis.

From the analysis of the specific heat flow released from the samples during the crystallization and the heating process (Figures 57-58), the crystalline degree was calculated by considering 93 (J/g) (Farah, Anderson and Langer, 2016) the melting enthalpy of very crystallized PLA.

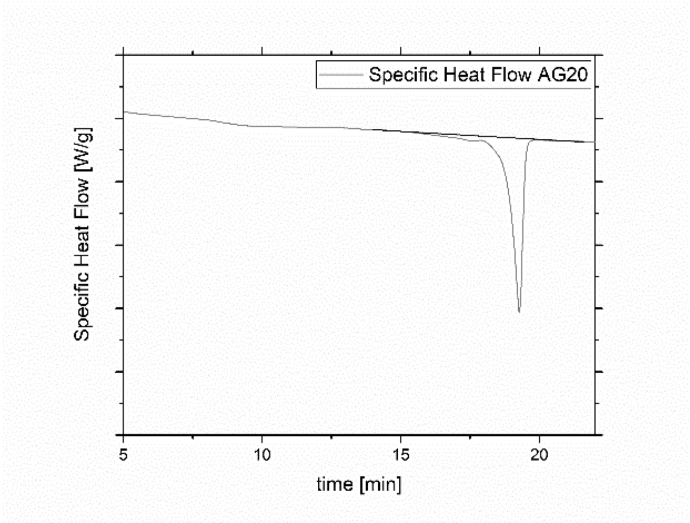

Figure 57. Specific heat flow released from the sample AG20.

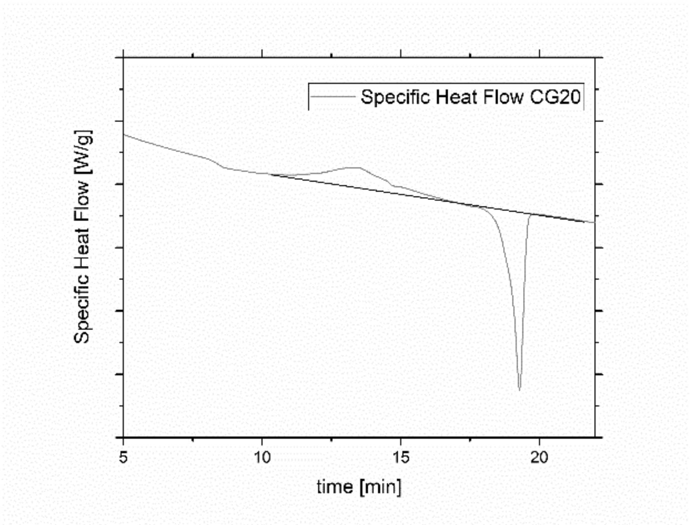

Figure 58. Specific heat flow released from the sample CG20.

The DSC analysis proved that for an isothermal time equal to 250 s a relative crystalline degree of 17% was present in the opaque zone whereas when the isothermal time was 1000 s the relative crystalline degree rises up to 90%. The transparent zone was also checked by DSC but a negligible value for the crystalline content was found. The data were described by the Avrami model (eq.7) and the parameters used are listed in the Table 10.

The half crystallization time was found equal to 445 s s that is lower than 1000 s in quiescent conditions.

Table 10. Parameters obtained by the Avrami description.

k [s]	0.0015
n	2.7

The Figure 59 shows the evolution of the relative crystalline content with the isothermal time.

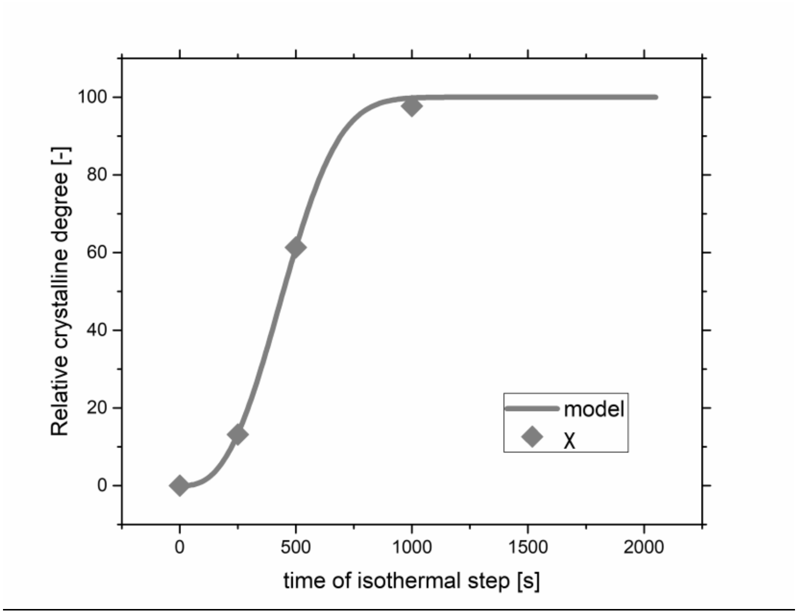

Figure 59. Relative crystalline degree evolution with the annealing time.

Spectroscopic Analysis

IR spectra were collected in absorbance mode by means of Perkin Elmer Spectrum 100 spectrometer in the mid-infrared range (4000÷400 cm^{-1}) to check, without a polarizer, the presence of any crystalline peak, with a polarizer parallel and orthogonal, the presence of dichroism in the same zone. Figure 60 is an example of IR acquisitions and Figures 61-72 represent the IR spectra acquired from all the samples.

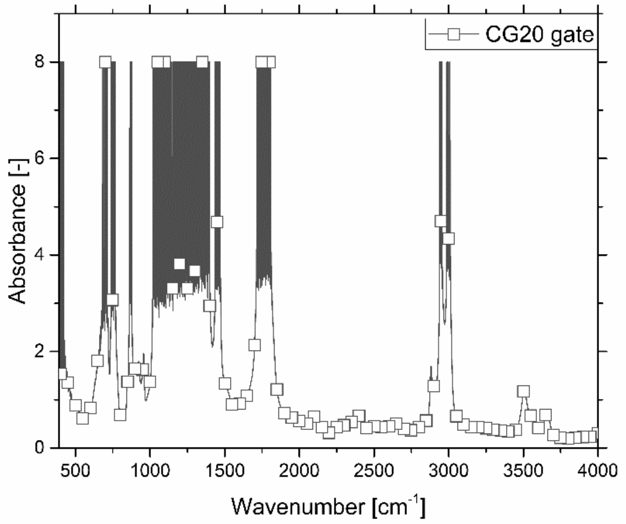

Figure 60. Complete IR spectra of the sample CG20.

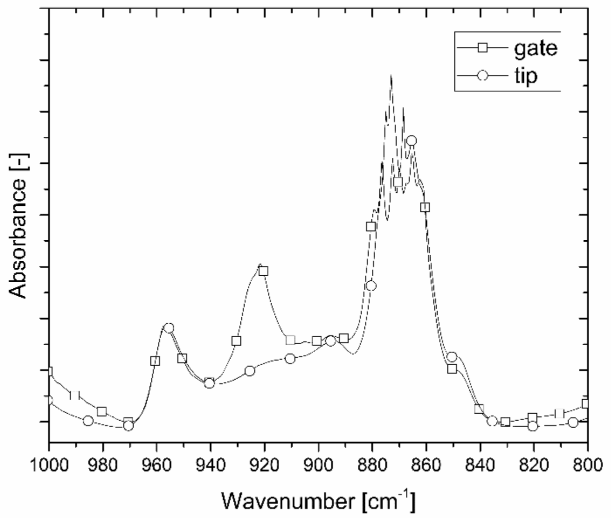

Figure 61. IR Spectra of the sample cg5 in the zone 1 after the gate and the zone 2 at the tip.

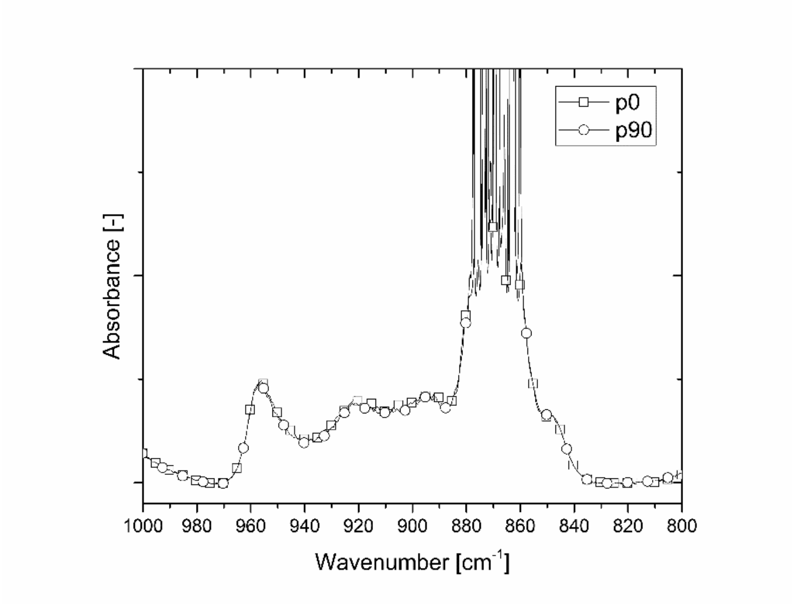

Figure 62. IR Spectra of the sample cg5 after the gate with the polarizer parallel p0 and perpendicular p90.

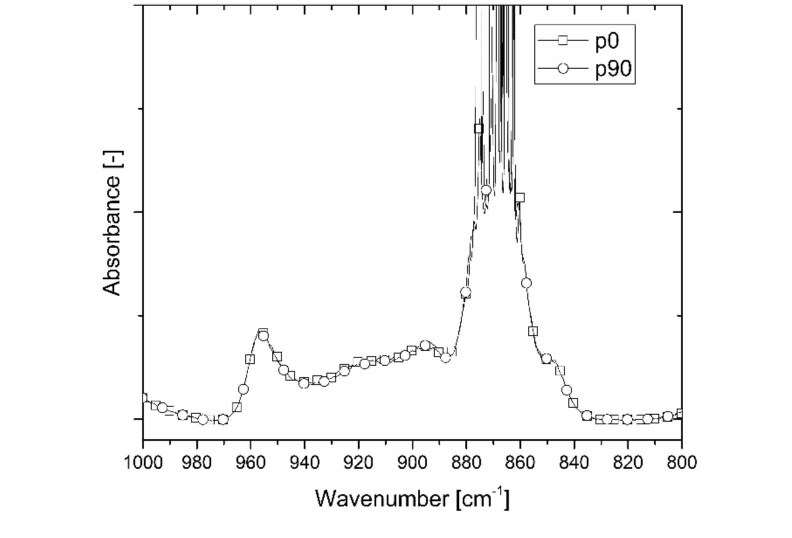

Figure 63. IR Spectra of the sample cg5 at the tip with the polarizer parallel p0 and perpendicular p90.

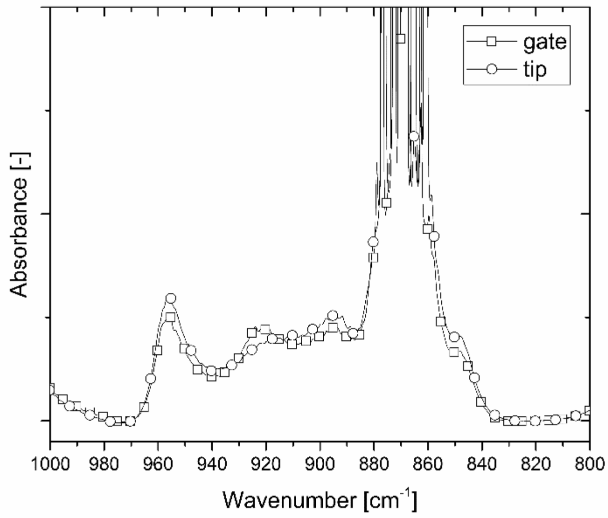

Figure 64. IR Spectra of the sample cg20 in the zone 1 after the gate and the zone 2 at the tip.

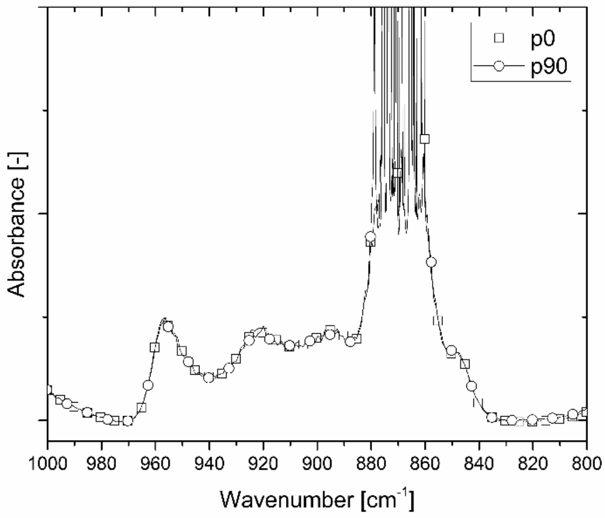

Figure 65. IR Spectra of the sample cg20 after the gate with the polarizer parallel p0 and perpendicular p90.

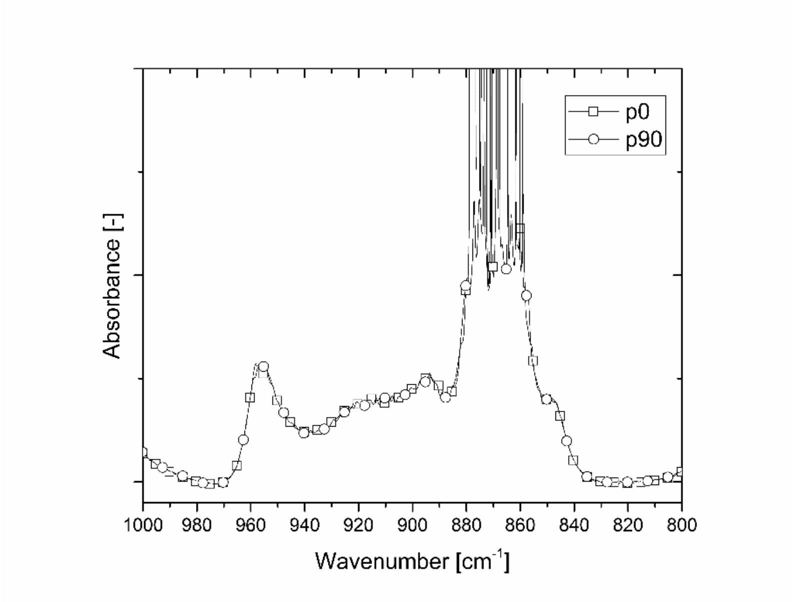

Figure 66. IR Spectra of the sample cg20 at the tip with the polarizer parallel p0 and perpendicular p90.

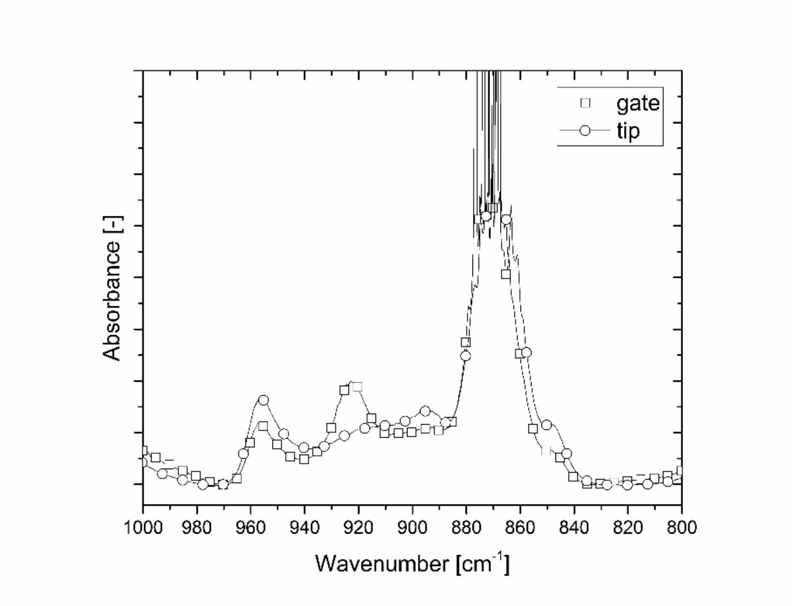

Figure 67. IR Spectra of the sample ag5 in the zone 1 after the gate and the zone 2 at the tip.

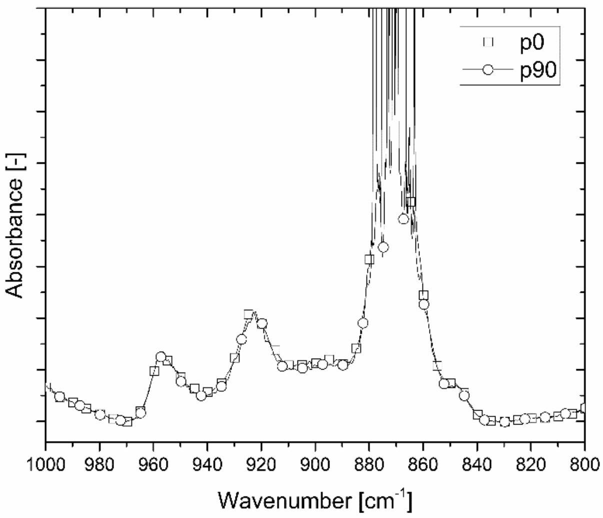

Figure 68. IR Spectra of the sample ag5 after the gate with the polarizer parallel p0 and perpendicular p90.

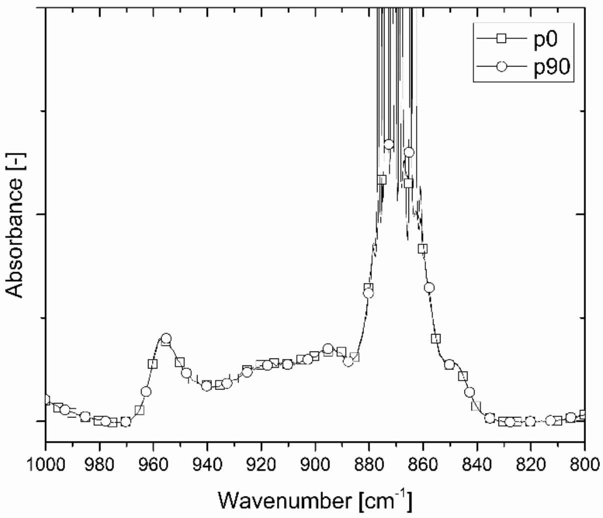

Figure 69. IR Spectra of the sample ag5 at the tip with the polarizer parallel p0 and perpendicular p90.

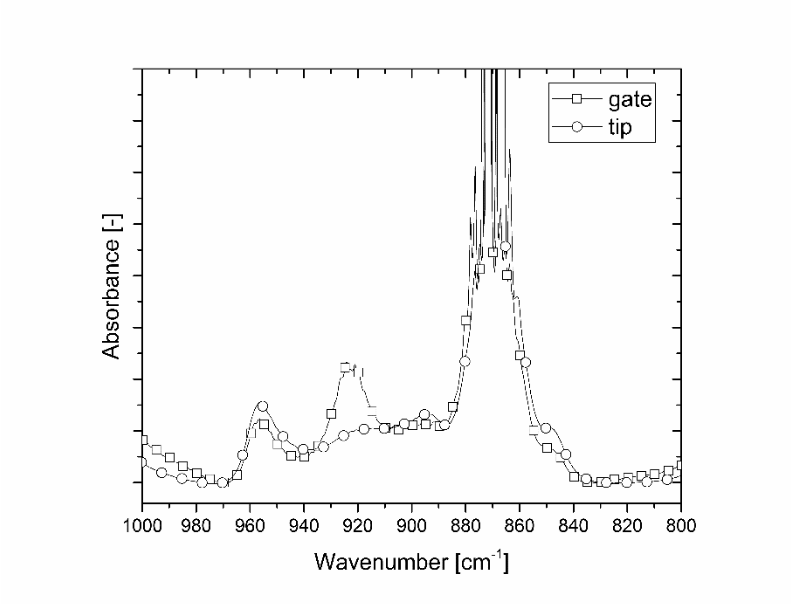

Figure 70. IR Spectra of the sample ag20 in the zone 1 after the gate and the zone 2 at the tip.

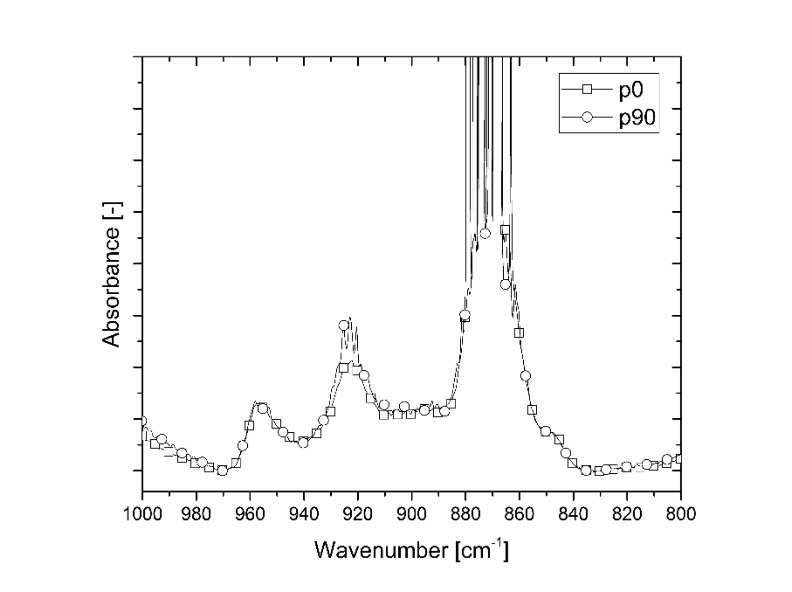

Figure 71. IR Spectra of the sample ag20 after the gate with the polarizer parallel p0 and perpendicular p90.

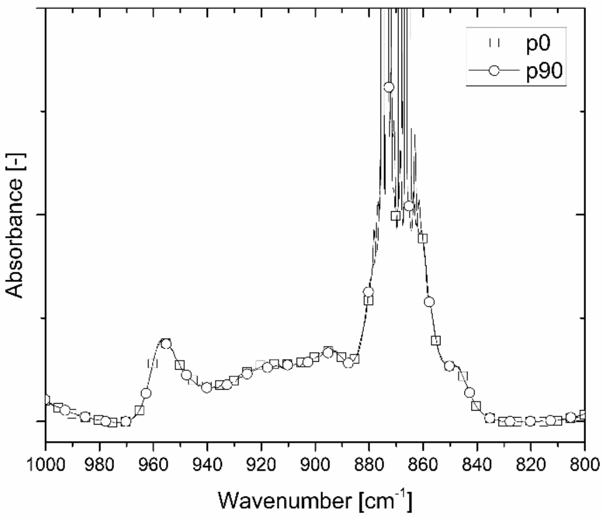

Figure 72. IR Spectra of the sample ag20 at the tip with the polarizer parallel p0 and perpendicular p90.

In all the samples produced, no dichroism was found. As shown in Figures 61-72, the opaque zone always exhibits a peak at 920 cm^{-1} that is a characteristic peak of the PLA crystals. This peak is not present in the transparent zone of the same sample and it is higher in the regions that experienced a longer time at 105°C. Spectra were collected also by means of a Bruker Vertex spectrometer that has a polarizer integrated controlled by the software, also in this case no difference was found between the measurements taken parallel and orthogonal to the flow direction.

Diffractometric Analysis

Single crystal X-ray diffraction measurements (XRD) were performed by the Brucker D8 Quest diffractometer for the patterns shown in Figure 73 and the WAXS-diffractometer Seifert ID 3000 for the patterns in Figures 74-76. The analysis have been conducted in the transparent and the opaque zone of the biphasic samples.

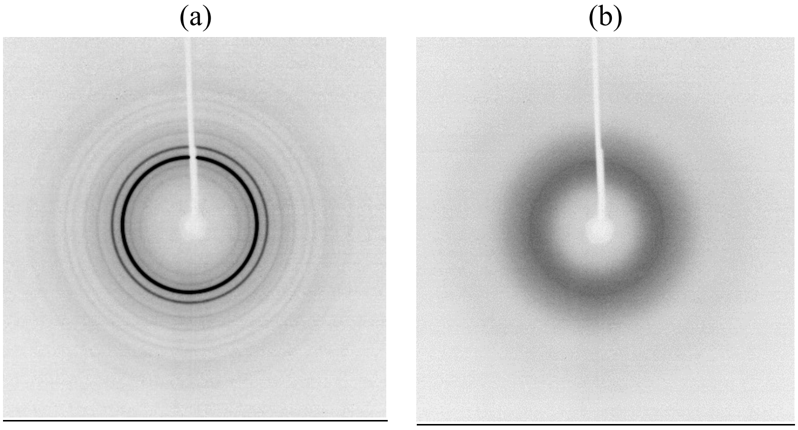

Figure 73. X-ray pattern of sample AG20 in the zone (a) opaque, (b) transparent.

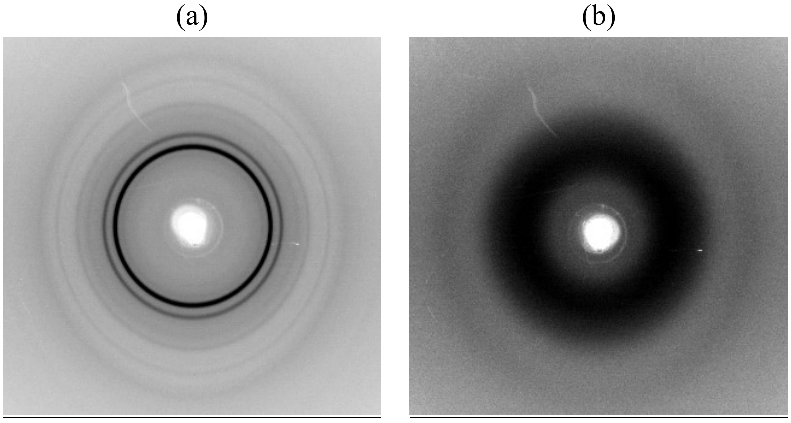

Figure 74. X-ray pattern of sample AG5 in the zone (a) opaque, (b) transparent.

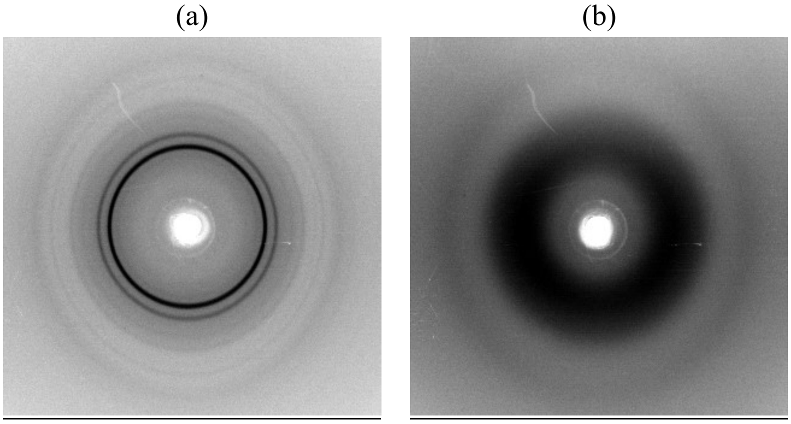

Figure 75. X-ray pattern of sample BT5 in the zone (a) opaque, (b) transparent.

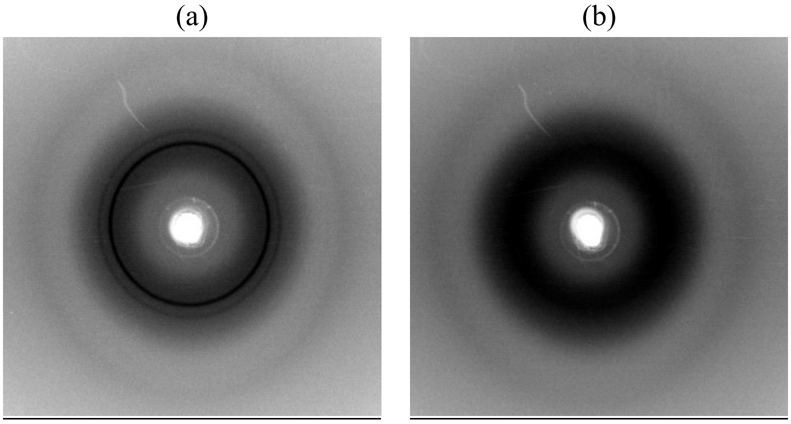

Figure 76. X-ray pattern of sample BT5 in the zone (a) opaque, (b) transparent.

As shown in the Figures 73-76, while the opaque zone was characterized by clear Debye Scherrer Rings, the transparent one did not show concentric circles. The analysis of the spectra confirmed the results obtained by the calorimetric analysis. In fact, an absolute crystalline degree equal to 32% was present in the opaque zone of the sample AG20 whereas the content in the transparent zone was less than 1%.

Dynamic Mechanical Analysis

The dynamic mechanical properties of the samples were tested using a Perkin Elmer DMA 8000 dynamic mechanical analyser. The testing was performed in tensile mode at a frequency of 1 Hz and a heating rate of 5°C/min. The biphasic samples were cut in the middle and each part was test separately by using the same technique. They were heated from 20 °C to 180°C. The distance between the clamps is 2.25 mm, the width is the same of the sample that is 4 mm and the thickness is the mean of the values measured by calipers along the width.

Under an oscillatory load the elastic modulus E' and viscous modulus E'' of the sample are measured as a function of temperature as the polymer is deformed. The storage modulus gives an indication of the stiffness.

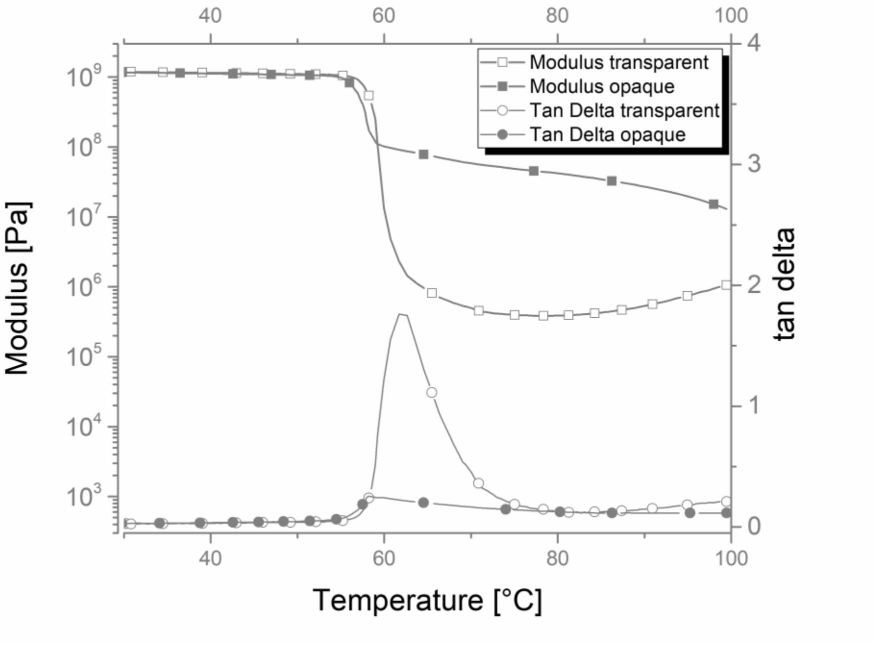

Figure 77. Dynamic mechanical properties.

As represented in the Figure 77, both parts of the samples, the transparent and the opaque, behave like a glass at low temperatures with a high modulus and like a rubber at higher temperatures with a low modulus. By scanning the temperature during a DMA test the glass transition, can be observed at a temperature of about 60°C. After the T_g, the dynamic mechanical analysis carried out on the opaque and the transparent part highlighted the enhancement of the modulus when the part has the highest crystallinity degree: the modulus decreases of an amount of three orders of magnitude for the transparent zone while the modulus of the crystalline zone is only one order of magnitude lower.

Surface Roughness Measurements

To check the roughness changes of the biphasic sample surface a confocal laser microscope Lext by Olympus was used. The confocal laser scanning microscopy capturs multiple two-dimensional images to reconstruct the three dimensional structures (Figure 78).

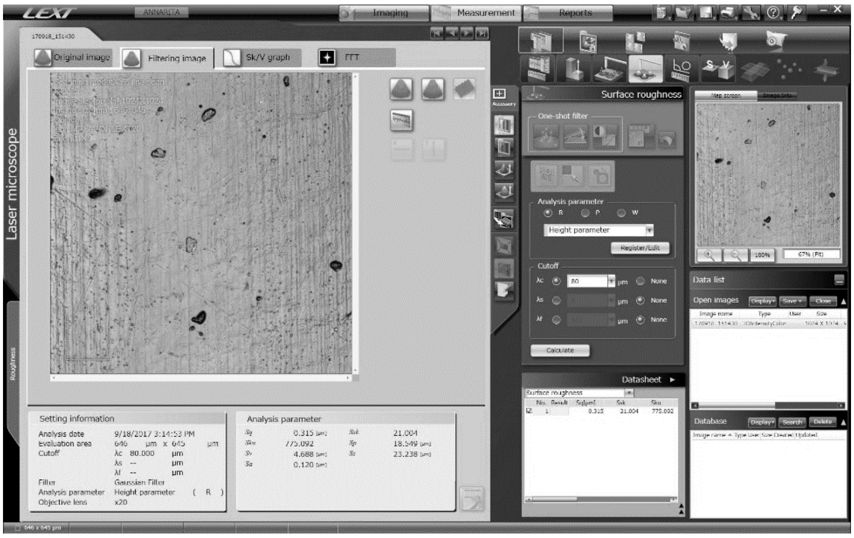

Setting information

Analysis date	9/18/2017 3:14:53 PM
Evaluation area	646 µm x 645 µm
Cutoff	λc 80.000 µm λs -- µm λf -- µm
Filter	Gaussian Filter
Analysis parameter	Height parameter (R)
Objective lens	x20

Analysis parameter

Sq	0.315 [µm]	Ssk	21.004
Sku	775.092	Sp	18.549 [µm]
Sv	4.688 [µm]	Sz	23.238 [µm]
Sa	0.120 [µm]		

Figure 78. Surface mapping of the area close to the gate of the micro-injection molded part.

The parameter R_a, the arithmetical mean height indicating the average of the absolute value along the sampling length, was measured from the gate to the tip of a biphasic sample with an opaque zone after the gate and a transparent one at the tip. The data are shown in the Figure 79.

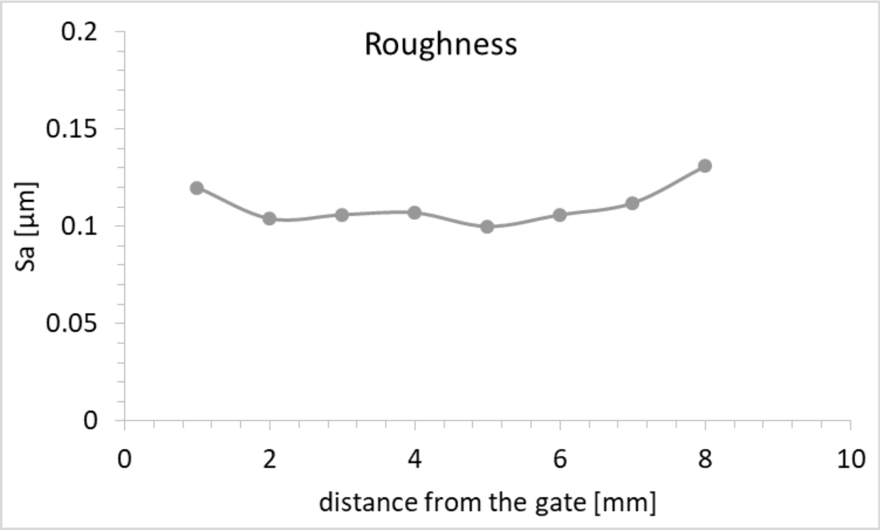

Figure 79. Evolution of the roughness from the gate to the tip.

The analysis highlighted that thermal treatment of 1000 s on the solid part, after the injection in the cavity, at a temperature lower than the melt temperature does not affect the final surface quality.

Conclusions

The investigations performed on the PLA micro-injection molded parts confirms that the system for the temperature control of the cavity is an excellent strategy not only to affect the filling behavior during the injection step of the polymer, but also to tune the final properties of the parts by controlling the amount of crystallinity. The parts were injected by applying the same pressure when the cavity surfaces were at 160°C. The polymer, after the filling, remains at 160°C for different time up to 20 s. Longer is the time of permanence at high temperature and lower are expected to be the orientations of the polymer chains. However, a significant decrease of the half crystallization time was evaluated by the crystallinity measurements showing that some precursors generate during the injection and the time considered in the experiments carried out up to now is not sufficient to eliminate the mechanical history. This phenomenon is known as Flow Induced Crystallization, FIC. In the flow induced crystallization the nucleation density increases, the crystallization kinetics is accelerated and the resulting microstructure is oriented or anisotropic. To explain the thermodynamics which drive FIC phenomena the entropy-reduction model (ERM), is perhaps the most widely-accepted model. During melt flow, some fraction of the longest chains become oriented and stretch in the melt. This orientation leads to an entropy reduction, which lowers the energy barrier for FIC according to equation 5. The energy barrier for FIC is expressed in terms of the quiescent nucleation energy barrier (ΔG_q) and the degree of entropy reduction by shear (ΔS_f);

$$\Delta \mathrm{G}_f = \Delta \mathrm{G}_q + T_s \Delta S_f \quad (\Delta S_f < 0) \qquad \text{(eq.5)}$$

Both the reptation time and the Rouse time of the polymer are important characteristics that dictate the amount of flow required to induce FIC.

Three resulting microstructure regimes can be identified that stem from the competition of shear flow and polymer relaxation in the FIC process.

- The first regime occurs if the shear rate does not exceed the reciprocal of the relaxation time. In this case no noticeable FIC effects are observed.
- The second regime requires increasing the strength of the shear flow such that the shear rate exceeds the reciprocal of the relaxation time but does not exceed the reciprocal of the polymer Rouse time. This regime yields enhanced point-like nuclei and accelerated crystallization kinetics, but the morphology remains isotropic.

- If the shear rate exceeds the reciprocal of the polymer Rouse time then these long chains extend during flow, and ultimately form the anisotropic shish-kebab structures indicative of the third regime.

The phenomenon experienced by the polymer in the experiments carried out in this Chapter, may belong to the second regime because the effect of the flow is noticeable and the morphology is essentially isotropic.

Chapter V. Micromolded Polylactid Acid with Selective Degradation Rate

Introduction

The objective of this part of the thesis is verifying the possibility to modulate the rate of degradation in the same part, in time and at different rates. The method is represented by the same technique described in the previous chapter that is able to influence locally the morphology of the samples. Biphasic samples (half amorphous and the other half crystalline) were obtained by micro-injection molding and the degradation process was monitored by means of hydrolysis tests.

State of the art

The degradation of biopolymers is the result of two mechanisms: the chemical hydrolysis and the water and oligomer diffusion. In order to estimate the effects of one of the two mechanisms, the hydrolytic degradation kinetics in the chemical regime, the study can be performed in solution (Gamez-Perez *et al.*, 2011), (de Jong *et al.*, 2001), (Zhang *et al.*, 1994). Different studies have been reported in the literature suggesting Arrhenius-dependent kinetics (Tsuji, 2003), (Weir *et al.*, 2004), (Speranza, De Meo and Pantani, 2014). Many papers concerned the hydrolysis of PLA, studying the elements that can affect the mechanism of chain scission like the molecular weight, the temperature and the chain stereo-configuration, (Gorrasi and Pantani, 2017), (Drumright, Gruber and Henton, 2000), (Lostocco and Huang, 1998). It has been demonstrated that hydrolysis of PLA is auto-catalytically accelerated through their carboxyl end groups (Hocking *et al.*, 1995), (Li, Garreau and Vert, 1990), and that the pH of the degrading medium determines the kinetics solution (de Jong *et al.*, 2001). The mechanism of hydrolysis is still under investigation, in fact, some authors verified that the scission of the chains occurs randomly also in acid (Shih, 1995) or in basic conditions (Belbella *et al.*, 1996). The process of chain scission compared to the end scission determines a substantial reduction of the physical properties (Gleadall *et al.*, 2014) rather than end scission. Also, the effect of the stereochemical composition is not fully understood (Gorrasi and Pantani, 2013).

The control of the biodegradation rate is interesting for the application in many sectors (Ha and Xanthos, 2010). There are several techniques that can be used to modify the rate of biodegradation. Examples are developments of blends, copolymers and use of particular fillers (Arias *et al.*, 2014), (Stloukal *et al.*, 2015), (Valentina *et al.*, 2018).

Literature research reveals that the morphology itself of the PLA can affect its degradation. Since the possibility for the water molecules to enter inside the rigid crystalline regions is extremely limited, the crystalline portion of PLA parts show higher resistance to the hydrolysis respect to amorphous regions. When different crystallinity levels are present in the part, the hydrolysis proceeds breaking the chains in the amorphous regions, therefore, removing the oligomers and monomers that are soluble in water, only intact crystalline regions remain (Tsuji, 2010). Others (Pantani and Sorrentino, 2013) demonstrated, also, that the initial morphology of PLA parts strongly affects the degradation, in particular the swelling and flake off processes. Completely amorphous PLA showed considerably higher degradation than semicrystalline PLA under similar conditions of hydrolytic degradation (Fukushima, Feijoo and Yang, 2013). The results indicated that the level of hydrolysis obtained for amorphous PLLA matrix is relevant and can be attributed to the easier hydrolytic attack of ester bonds that occurs in crystalline polymers.

Material

The material adopted in this part is a commercial PLA from Natureworks (4032D), with a D-enantiomer content of approximately 2%. The molecular weight distribution was characterized by chromatography: Mn 119,000 g/mol and Mw 207,000 g/mol. The reason for which this grade of PLA was chosen is the availability of degradation studies on this polymer conducted by our group that allows a critical analysis of the results.

Rheology

The viscosity measurements carried out with a Haake Mars Rheometer have been described by a Cross Model and are represented in the Figure 80.

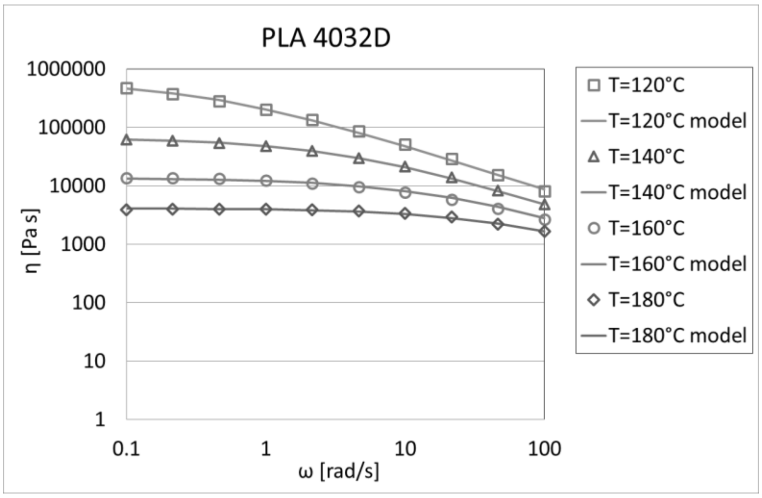

Figure 80. Rheology of PLA 4032D.

In order to evaluate the relaxation behavior, as described in the previous chapter, a mastercurve from G' and G'' was depicted (Figure 81).

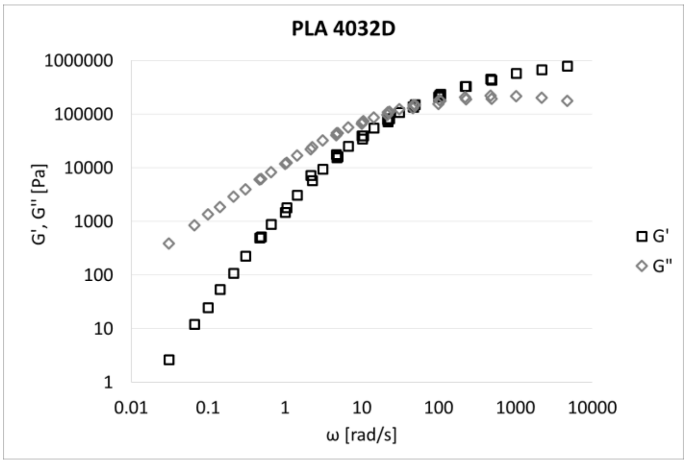

Figure 81. G' and G'' mastercurve.

The Figure 82 represents the evolution of the relaxation time with the molecular stretch.

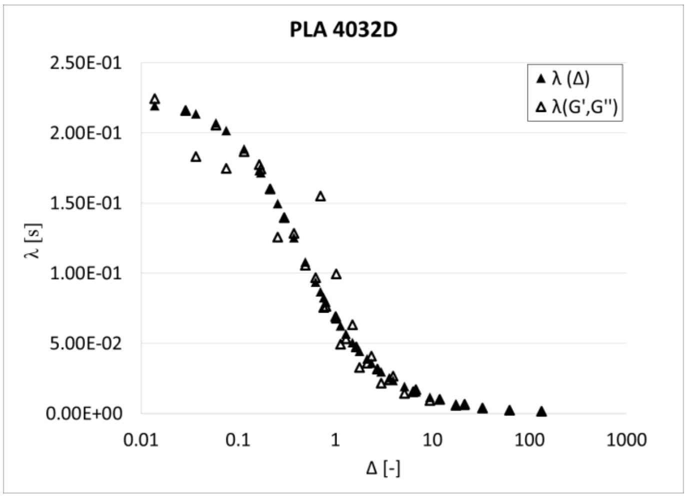

Figure 82. Relaxation time of PLA 4032D.

Crystallization kinetics

The crystallization kinetics was determined by means of optical and calorimetric analysis, in the same way of the PLA 3251D discussed in the previous chapter. Therefore, the growth rate and the nucleation density have been used to predict the half crystallization time calculated from calorimetric analysis conducted in isothermal conditions and at different temperature values.

The comparison between the DSC results and the crystallization predictions based on the growth rate and nucleation density measurements show that the results are similar and also in this case it is possible to describe the crystallization behavior by considering one or the combination of two curves, one for the α’ phase at low temperatures and the α phase at high temperatures.

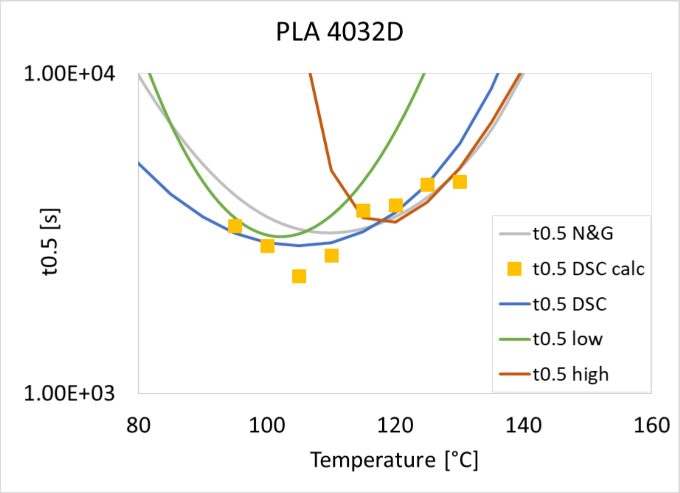

Figure 83. Half crystallization time evolution for the PLA 4032D.

Samples Preparation

PLA bars were produced by adopting the same protocol shown before. In particular, the process involved these steps: after the cavity surfaces were heated up to 160°C the molten PLA was injected into the thin the cavity (injection step), the material was cooled by switching off the resistances from about 160 °C to about 50 °C in 15 s (cooling step). Then only one zone of the solid injected sample was kept at 105°C for 500 s (annealing step). Due to the very slow crystallization kinetics of this grade of PLA, the region of the injection-molded samples that did not experience the annealing step resulted to be fully amorphous. The region that was kept at 105 °C resulted crystalline. Two protocols were used to produce the samples for the degradation study. In the first, Protocol 4, after the filling and cooling steps, the region under annealing is the one after the gate. In the second, Protocol 5, the region under annealing is the tip of the sample.

Hydrolysis

The degradation of the PLA parts was investigated by means of hydrolysis tests. Each part was immersed into distilled water with a pH value of about 6.5. The tests were performed at 58°C, the temperature adopted for biodegradation tests according to ASTM D6002-96, ASTM 5338-98 that give the same indications of the ISO 14855. The ratio between the amount of water

[ml] and the mass of the dried sample [g] was set at 800. In order to keep a constant temperature of 58°C during the hydrolysis test, a thermostatic bath with lid was used. After every 24 h of hydrolysis, the water of each sample was analysed by using a Crison pH-meter at 25°C. After the analysis of the pH, the liquid was replaced by the same amount of fresh distilled water, in particular, by using a syringe the glass vessel was emptied. The syringe was equipped with a needle having a diameter of 0.2 mm. At pre-established times, the samples, in their vessels, were dried in vacuum conditions at 60°C for about 3 h and then weighed. After these operations, one of the samples was kept dry for further analysis. At the end, the several vessels were put again into the thermostatic bath. The samples, for the whole of the hydrolysis test, never left their vessels, in order to avoid undesirable losses of the hydrolyzed material. The hydrolysis of all samples was carried out for about 60 days. After 60 days, since the samples became fragments with a very small mass an accurate analysis was not possible anymore.

Optical Observations

All the samples were observed and photographed under polarized light. As shown in the Figure 84 there was a clear difference between the two regions of the sample: the amorphous region was transparent whereas the crystalline one appeared opaque.

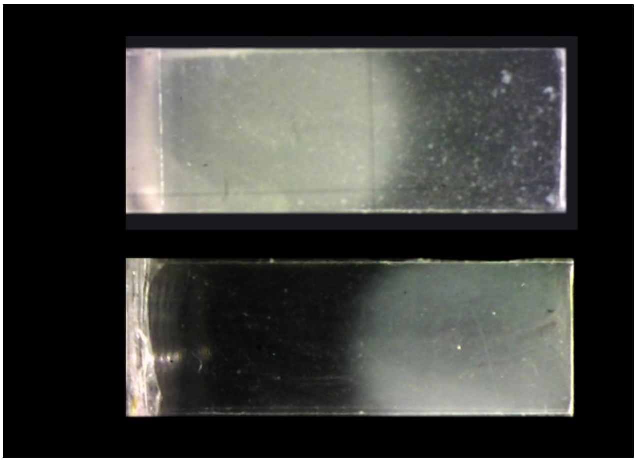

Figure 84. Biphasic samples, on the top the one produced by Protocol 4 and bottom by Protocol 5.

Analyzing the images of the samples under hydrolysis it is evident that the crystalline zone of the sample remained unchanged for a time of 12 days (Figure 85).

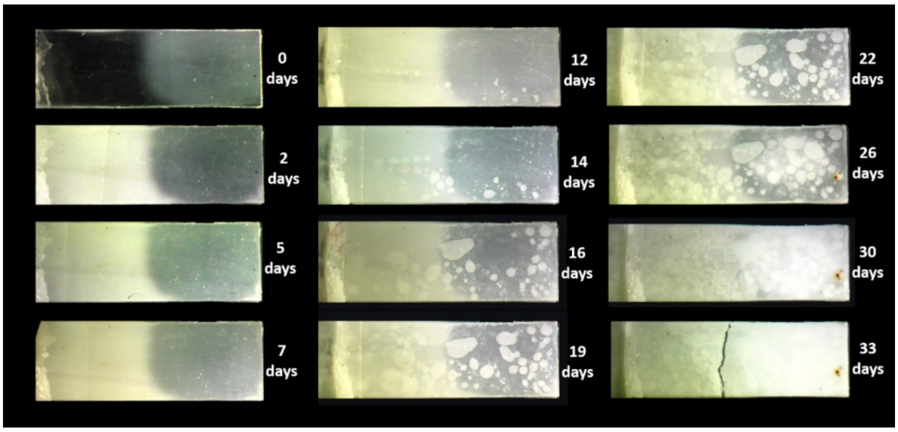

Figure 85. Images of hydrolyzed samples of micro-injected biphasic PLA sample (amorphous gate, crystalline tip)

The appearance of the amorphous zone changed after the second day turning from transparent to opaque. The same phenomenon was already observed in the PLA (Pantani and Sorrentino, 2013). This could be due to the micro-fractures due to the water moving away from the sample during the drying phase. Obviously, the crystalline zone had a lower water permeability at least for the first 25 days of hydrolysis. From 30 days there were no differences between the two different morphologies. The degradation tests confirmed that crystalline regions had a slightly better resistance to hydrolysis.

Calorimetric Analysis

From the results of the DSC analysis, before the hydrolysis (samples 0 days) reported in Figure 86 and Figure 87, it is evident that there was a difference between the phases: there were crystallization and melting peaks for the amorphous phase and there was only a melting peak for the crystalline phase. The Glass Transition Temperature T_g and the Melting Temperature T_m exhibited the same values for both phases. T_g and T_m, also, are very similar to those observed in the pellet indicating no degradation had occurred in the manufacturing process, neither in the crystallization step.

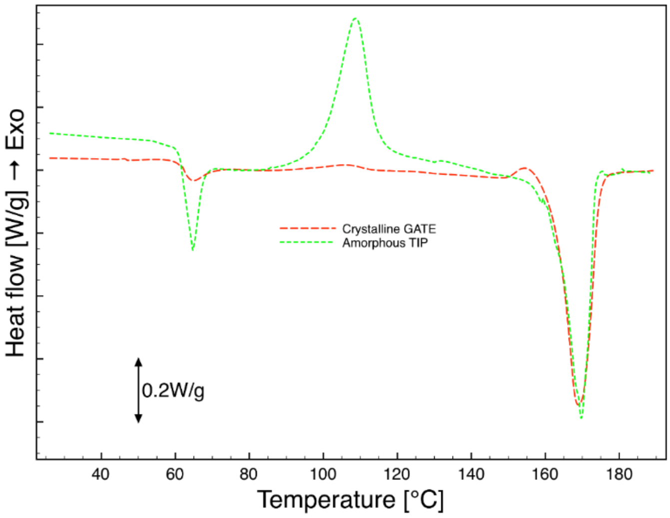

Figure 86. DSC analysis of micro-injected biphasic PLA sample (amorphous tip, crystalline gate), first scan

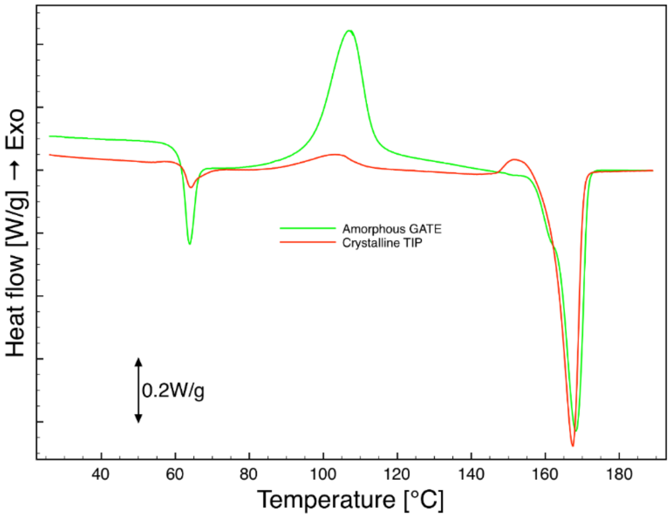

Figure 87. DSC analysis of micro-injected biphasic PLA sample (amorphous gate, crystalline tip), first scan

The degree of crystallization calculated from the analysis of the thermograms is negligible for the amorphous region in all the samples, whereas for the crystalline phase, in the case of both protocols adopted, 4 and 5, the values were between 30% and 35% (Table 11). In all the biphasic samples, the crystallization degree reached in the annealing step was then maximum achievable for this grade of PLA.

Table 11. Crystalline degree of the biphasic samples before the hydrolysis.

Protocol	Region detected	Xc [%]
a	gate	30
a	tip	negligible
b	gate	negligible
b	tip	35

During hydrolysis a small piece from each region of the sample was analyzed by calorimetry with the same protocol used for the sample 0 days. The results are reported in Figure 88. As expected, an increase in the crystallinity degree was observed. This result could be ascribed to two possible phenomena: crystallization of the amorphous parts and erosion of the amorphous parts.

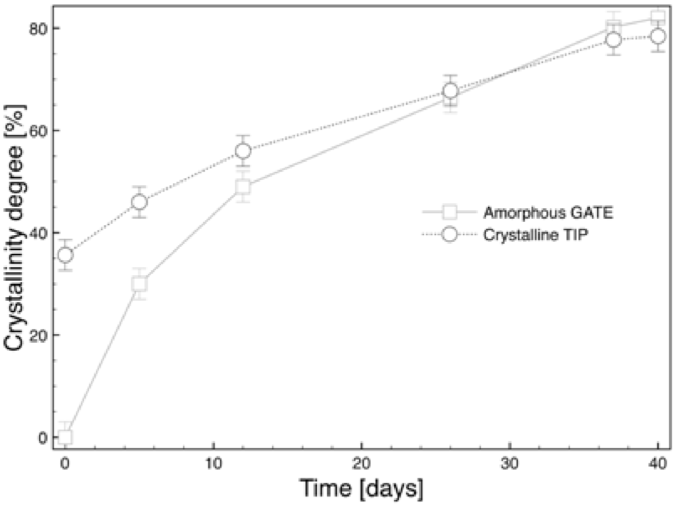

Figure 88. Evolution of degree of crystallinity during hydrolysis of micro-injected biphasic PLA sample (amorphous gate, crystalline tip).

As the hydrolysis proceeds the crystallization is more fast in the amorphous region than in the crystalline one. The difference in crystallization rate probably indicates a slower degradation of the crystalline zone with respect to the amorphous one. After 25 days of hydrolysis, however, no significant difference can be observed between the values of the Xc of the two morphologies.

Mechanical tests

Penetration mechanical tests were carried out to evaluate the breaking force of the samples as hydrolysis proceeds. The dynamic mechanical measurements were performed by using the DMA 8000 Perkin Elmer (Waltham, MA, USA). A tip with a diameter of 150 μm was used, with a maximum force of 7 N and a load rate of 0.2 N/min. The operating scheme of the apparatus is shown in Figure 89.

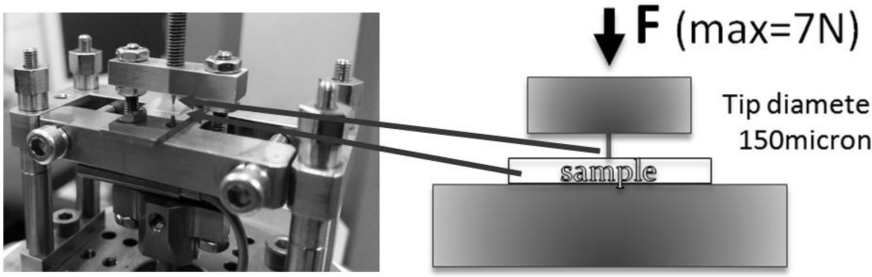

Figure 89. Assembly for penetration test and Scheme of the test.

The sample was placed under the tip with an increasing force up to the maximum allowed value of 7 N (the instrumental limit). DMA returned the values of the force and the displacement of the tip.

The resistance to the penetration was evaluated with the time of the hydrolysis. In each region of the sample, the mechanical test gave the force applied and the corresponding displacements (Figure 90). The maximum force applied was 7 N.

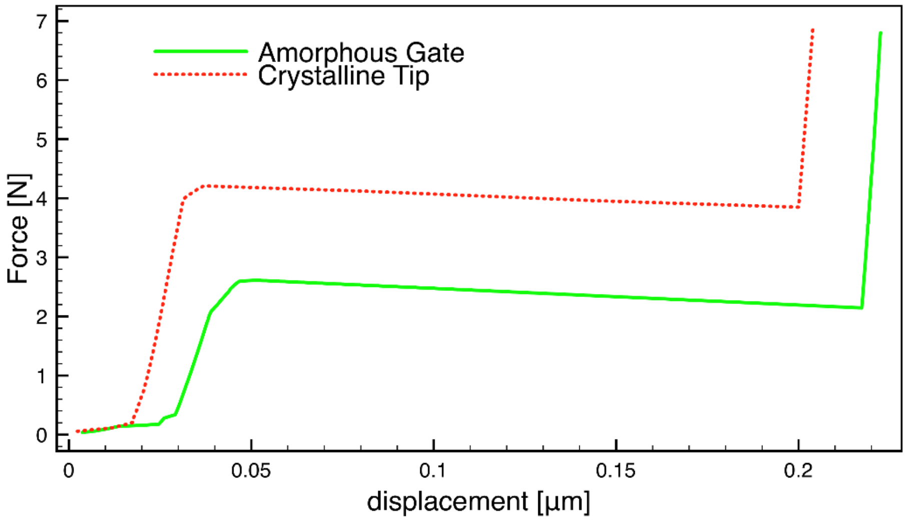

Figure 90. Evolution of the Force with the displacement.

Observing the Figure 91, it is evident that up to 12 days, no fracture was detected in either phase. After 19 days, the sample did not withstand the force applied and broke. As the hydrolysis proceeds a decreasing mechanical stresses was needed to break the sample. For the crystalline phase the force at break is slightly higher than the one noticed in the amorphous phase.

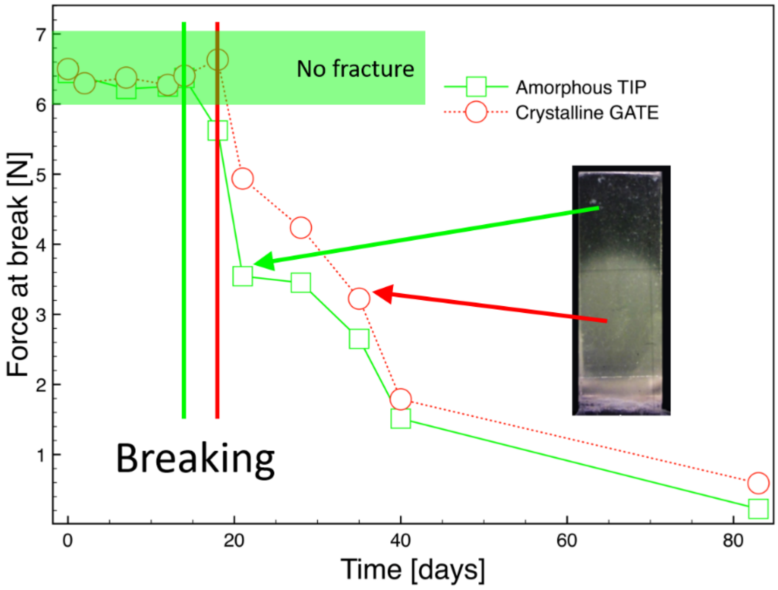

Figure 91. Evolution of force at break during hydrolysis of micro-injected biphasic PLA sample (amorphous tip, crystalline gate).

Conclusions

The system to control the temperature of the cavity permitted to decrease the viscosity of the polymer and affect the final morphology in a confined region of the sample by imposing an annealing in only one of the two regions of the parts. In the case of the PLA 4032D, a degradation study was carried out in order to determine the effect of the morphology on the hydrolysis process. By analyzing the mechanical tests, from the eighteenth day, the amorphous zone of the parts showed higher fragibility than the crystalline revealing that the crystalline regions present a slightly better resistance to the hydrolysis.

Chapter VI. Effect of dynamic thermal variations on the morphology and the weld line in iPP microparts

Introduction

In this chapter the innovative system for the rapid temperature control, developed and previously tested using a modular mold created for the Haake Minijet Injection Molding System to produce 200 micron thin bars with modulated morphology, will be adapted for the development of a new geometry. The study includes the design of a new insert, that is characterized by a rectangular shape cavity with two symmetrical gates and the final part is obtained by forcing the melt into the channels and enter into the cavity in which two melt front meet in the center line. In order to investigate the polypropylene flow filling, the insert is adopted for short shots experiments of an isotactic polypropylene. The flow behavior is then simulated by Moldflow studies and compared with the solidification behavior of the polypropylene thin parts. In the second part of the chapter, the effect of the application of the system to control the temperature locally on the weld line formation along the thickness of the sample is investigated. The reason for which a different polymer was adopted in this part is to verify the potentiality of the system. The weld line is crucial for the final properties of the part, especially, due to the premature solidification that can occur. Most of the literature research focused on the effect of several process parameters on the weld line appearance but no interest has been put into the analysis of the weld line along the thickness of very thin parts. In this chapter, experiments of polypropylene microinjection molding with different cavity temperature will be shown. A morphological analysis along the thickness is conducted to clarify the final mechanical properties exhibited by the microparts.

State of the art

Weld lines form when two separate melt fronts join during injection molding. They often occur because of multiple gating, obstacles and variable part thickness. The weld lines reduce the strength of injection-molded parts. The reasons could be found in the incomplete molecular entanglement, formation of V notches at the surface, presence of micro voids at the weld interface and the different orientation of fibers at the weld.

Even though the complete elimination of weld lines is not always successful, their appearance and mechanical performance can be minimized.

In micro injection molding process, there are also many factors related to the mechanical properties of weld line, but literature works are quite limited in this aspect.

Tjader et al used different grades of polypropylene and polyethylene with different MWD and correlated mechanical behavior to material properties, and also to the weld line morphology. An increase in molar mass gave a more visible weld line whereas a broader molecular weight distribution enhanced the molecular diffusion. In general, the weld line formation affects the mechanical properties because in that region the polymer does not present a plastic deformation zone at the crack. However, they did not find a significant effect on the tensile strength but the elongation behavior was very sensitive to the weld line for any grade of polymer used. (Tjader, Seppala and Jaaskelainen, 1998).

The factors that can affect the weld line are the processing parameters. Some authors verified that for a polypropylene part, the melt temperature was the most influential factor, followed by packing time, injection velocity, and mold temperature. Other parameters such as packing pressure showed little influence on the weld-line strength (Wu and Liang, 2005). To reduce the weld line, the ultrasonic oscillation was found to be able to reinforce the weld line strength in micro injection (Xie, Ziegmann and Jiang, 2009).

Others used the high-frequency induction heating to heat the mold before injecting a polycarbonate and verified that the mold temperature can effectively decrease the weld depth (Wu and Liang, 2005). Bociąga et al compared the behavior of two polypropylene materials, one pure and another filled with 20% of talc. They verified that the addition of the filler reduced by about 50% the mechanical properties because the talc particles resulted oriented parallel to the front flow, like the macromolecules. Although, the addition of a foaming agent did not improve the resulting tensile strenght (Bociąga *et al.*, 2019). Others produced nanocomposites usign polypropylene, carbon nanofibers and TiO2 nanoparticles (Xie *et al.*, 2010). In this case, they found that the addition of fillers had a negative effect on the tensile strength and elongation, but the E modulus of micro weld lines increased.

It is well known that the morphology is affected by the type of injection. If two injection point are considered, the skin layer decreases with increasing the mold temperature and in proximity of the weld line the skin layer almost disappears. Wenig et al verified that the core of the samples presented alfa crystallites and the skin beta modification which amount increases by increasing the molecular weight and reaches values of 11%. However, near the weld lines no beta crystals were detected because the formation of beta strongly depends on the orientation beyond the mold temperature.(Wenig and Stolzenberger, 1996).

Geometry

The new insert is customized for the modular mold already used for the control system and shown in Figure 92.

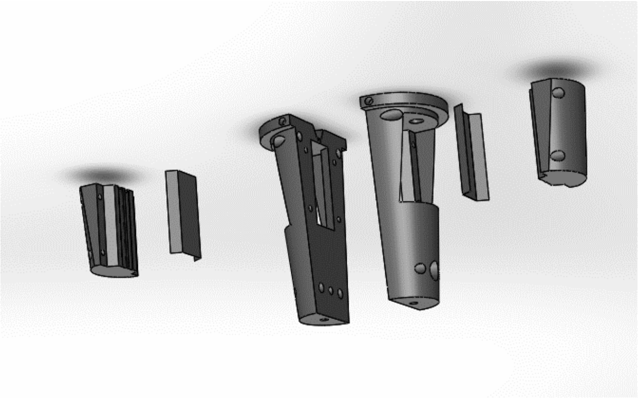

Figure 92. Modular mold for the rapid temperature control.

In particular, one of the two half is considered for the manufacturing of the cavity with two gates and the channels.

To permit the use of the fastening blocks (blue in Figure 92) a plate with a thickness of 1.5 mm is chosen for the new insert.

The material chosen for the insert is the steel C18.

The proper fabrication method and the corners geometry were chosen in accordance with the manufacturer's instructions. In particular, the micromilling technique was chosen and corners rounded 0.2 mm were the constraints for the tools available. The milling is a subtractive manufacturing process that uses rotating cutting tools to remove material from a starting stock piece, commonly referred to as the workpiece. The basic milling system, or mill, consists of a worktable for positioning the workpiece, a cutting tool (most commonly an endmill), and an overhead spindle for securing and rotating the cutting tool.

A cavity 3 mm wide and 6 mm long with a thickness of 200 micron is located in the center of the insert and rectangular shape channels wide 2 mm and deep 1 mm were symmetrically designed.

The drawing of the cavity and the channels is reported in Figure 93.

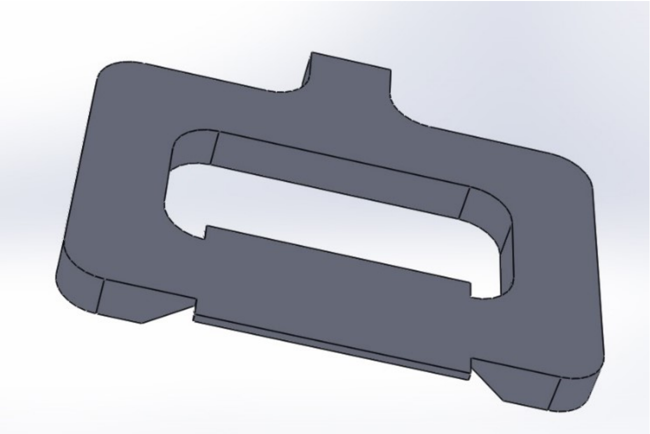

Figure 93. Cavity and channels drawing.

The back of the insert is also manufactured to include the seat for the heater, the thermocouple, the insulation layers and the wires. The area of the heaters is 6 mm x 5 mm, the hot joint of the thermocouple is less than 0.1 mm and the wires used to connect the heaters to the external power supply have a diameter of 0.4 mm.

The 2D drawings are shown in the Figure 94.

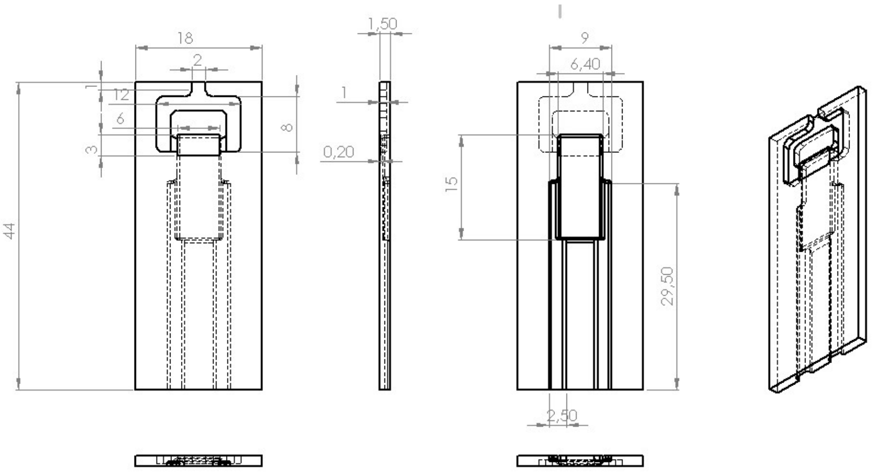

Figure 94. Insert drawing.

The assembly of the new insert in one half and the plate in the other half of the mold represent the cavity used in the work (Figure 95).

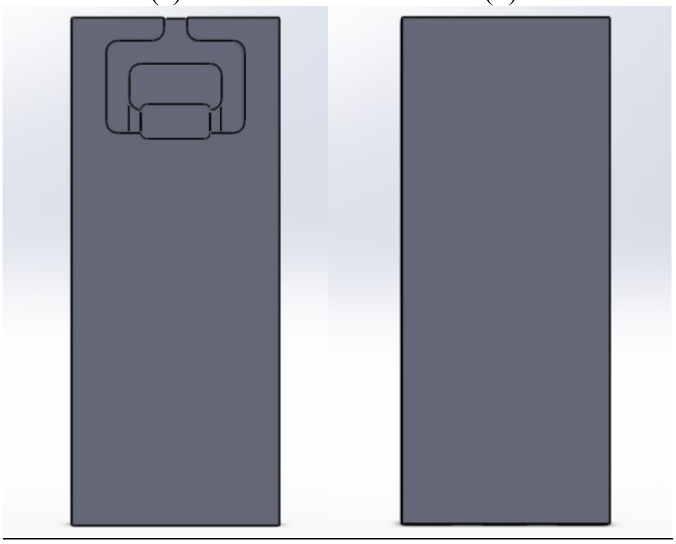
(a) (b)

Figure 95. Assembly of the two slabs.

Material

The material used in this part of the thesis is the isotactic polypropylene T30G by Montell (now LyondellBasell). Mw ¼ 376,000, Mw/Mn ¼ 6.7, tacticity ¼ 87.6%mmmm). This material is the same as the one adopted by Titomanlio and co-workers (Coccorullo, Pantani and Titomanlio, 2003), (Pantani *et al.*, 2005) to analyze effects of flow rate and mold temperature on morphology distribution of injected samples and the effects of pressure on crystallization (Pantani *et al.*, 2005), (Pantani *et al.*, 2007), (Pantani, Speranza and Titomanlio, 2017), (Sara Liparoti *et al.*, 2019).

This material was previously carefully characterized in terms of quiescent nucleation density, spherulitic growth rate and rheological properties (Figure 96).

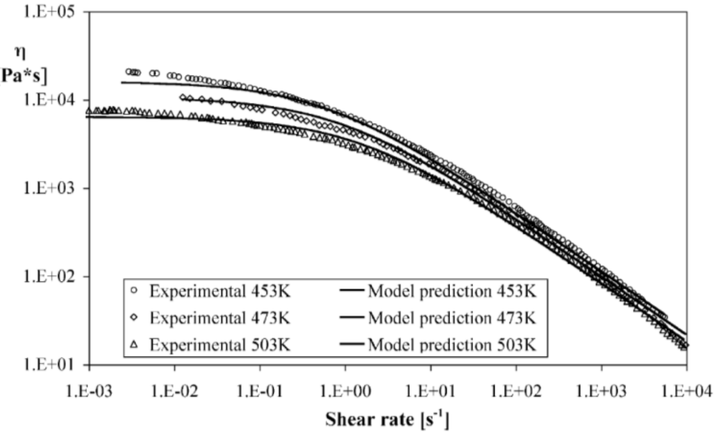

Figure 96. Experimental data of melt viscosity of iPP T30G (Pantani et al., 2005).

Being a non-Newtonian and viscoelastic fluid all parameters depend on temperature, pressure, crystallinity that are all function of time. Compressibility cannot be neglected because the flow during the packing and holding steps is characterized by density changes due to pressure, temperature, and crystallinity evolution.

Isotactic polypropylene (iPP) has several crystal modifications. Depending on the crystallization conditions and molecular characteristics, different packing geometries of the PP helices lead to four well-known crystal structures: monoclinic (α), trigonal (β), triclinic (γ), and smectic (δ) form. (Jones, Aizlewood and Beckett, 1964). Among them, the most important and widely occurring is the α -form structure. The morphology of injection-molded iPP is represented by a skin–core structure (Liu *et al.*, 2012). The thickness of microparts is reduced sometimes to a few hundredths microns that determine processing features of micro-injection molding different from conventional injection molding (higher injection pressure and speed, higher melt and mold temperature). In theory, the shear thinning effect decreases the polymer viscosity allowing a higher length of filling in the microcavity but the rheological behavior of flow in micro-cavities is different from the one described by conventional laws (Giboz, Copponnex and Mélé, 2007). In the microchannels the wall-slip effect can occur and viscosity increases (Whiteside *et al.*, 2004).

Pantani and coauthors (Pantani *et al.*, 2005) studied the relationship between the observed microstructure and processing conditions in the isotactic polypropylene. They proposed a strategy to predict morphology distribution in the final samples. For this purpose a complete analysis of crystallization kinetics, in processing conditions characterized by high cooling rates and high pressures, strong and complex flow fields, is necessary. They show that the heterogeneous nucleation of iPP parts is satisfactorily described by a nucleation density, which is a decreasing function of temperature.

The morphology determined in the melt by effect of flow strongly affect the kinetics and morphology of crystallization. The possibility to identify a parameter to describe the effect of flow on the crystallization kinetics and morphology evolution during crystallization, is a challenging task (Pantani, Balzano and Peters, 2012).

Literature works indicate that there is a critical shear rate that determines the crystallization kinetics from a slightly oriented melt a much more oriented crystalline phase. At higher value of critical shear rate crystallization changes from spherulitic to fibrillar. A formulation of a criterion in terms of critical values of both a molecular stretch parameter and the mechanical work was adopted by Liparoti and coworkers (Sara Liparoti *et al.*, 2019), starting from a critical amount of mechanical work to describe morphology evolution in injection molding. Even if their model does not include the existence of intermediate transitional layers between the highly oriented and the spherulitic layers they succeed in the description of the morphology developed along the molding cross sections, 1.5 mm thick, in terms of position of the shear and the core layers.

Experiments

Part I. Analysis of the filling of the double gate cavity

The insert described in the previous paragraph has been used for short shots experiments of the polypropylene. A short shot is the incomplete filling of a mold cavity that results in the production of an incomplete part and can be useful to describe the fluidity of the polymer.

For each experiment, the temperature of the melt, the temperature of the mold and the injection time was fixed and the values are shown in the Table 12.

Table 12. Process parameters.

Melt Temperature (°C)	230
Mold Temperature (°C)	35
Injection Time (s)	3

The effect of the application of different values of the injection pressure was investigated. In particular, the values used are listed in the Table 13.

Table 13. Pressure values for short shots.

P (bar)	10	30	50	70	90	110	130	150

The samples produced will be analyzed in terms of filled length of the channels and the cavity.

Results

The Table 14 shows the pictures of the samples produced by changing the injection pressure.

Table 14. Short shots samples.

P=10 bar	P=30 bar
	
P=50 bar	P=70 bar
	
P=90 bar	P=110 bar
	
P=130 bar	P=150 bar
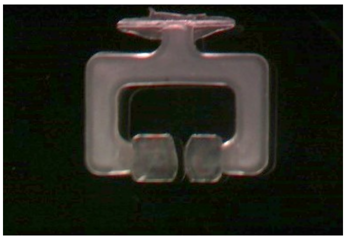	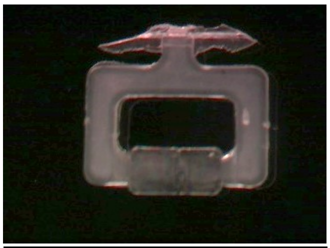

Because of the geometry of the channel, the melt injected splits in two directions and reaches the cavity by the two gates designed symmetrically.

The length obtained for each condition is reported in Table 15.

Table 15. Filling measurements.

Injection Pressure (bar)	Filling percentage left side	Filling percentage right side
10	35	32
30	51	51
50	51	51
70	89	83
90	95	95
110	97	97
130	99	98
150	100	100

The analysis of the filling percentage in both sides confirms that the filling has been symmetrical and by increasing the pressure the resulting length rises.

Simulations

The geometry shown in Figure 93 was implemented in Moldflow to simulate the polymer behavior during the filling of the short shots experiments. The piece and the channels were described by a Mesh 3D, represented in Figure 97, in which are 208152 tetrahedral elements. The mold temperature is 40°C.

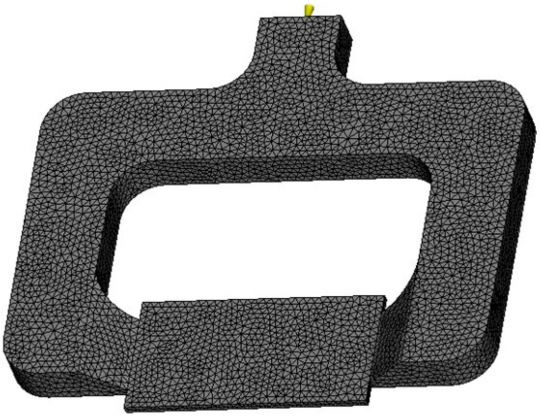

Figure 97. Mesh 3D used in Moldflow.

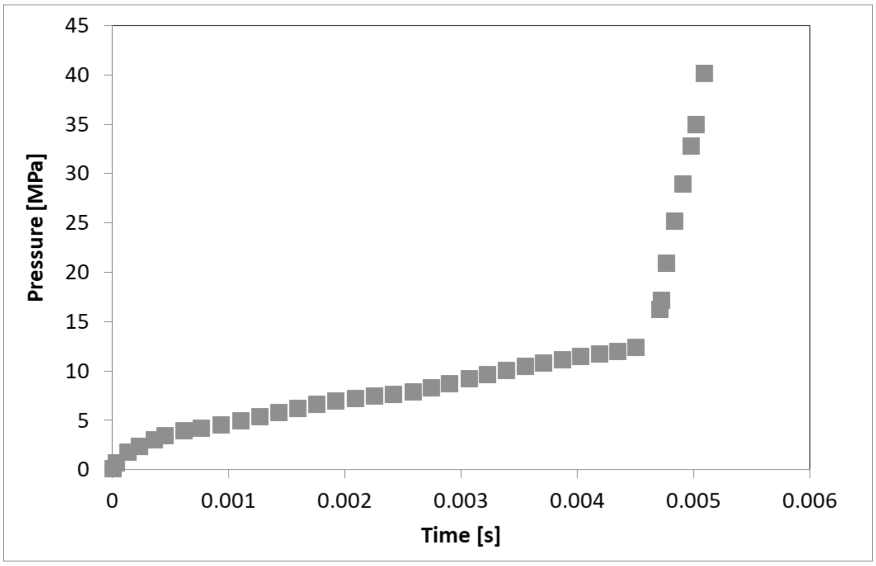

Figure 98. Pressure during the filling of the geometry represented in Figure 97.

The study highlighted that whatever is the flow rate considered, there is always a switchover point at which the slope of the curve pressure versus time changes (Figure 98). That point corresponds to the entrance of the cavity.

It is possible to assess the flow rate and determine for each test the filling of the channels. The Figures 99 and 100 show the comparison between the short shots and the quite good previsions made by Moldflow.

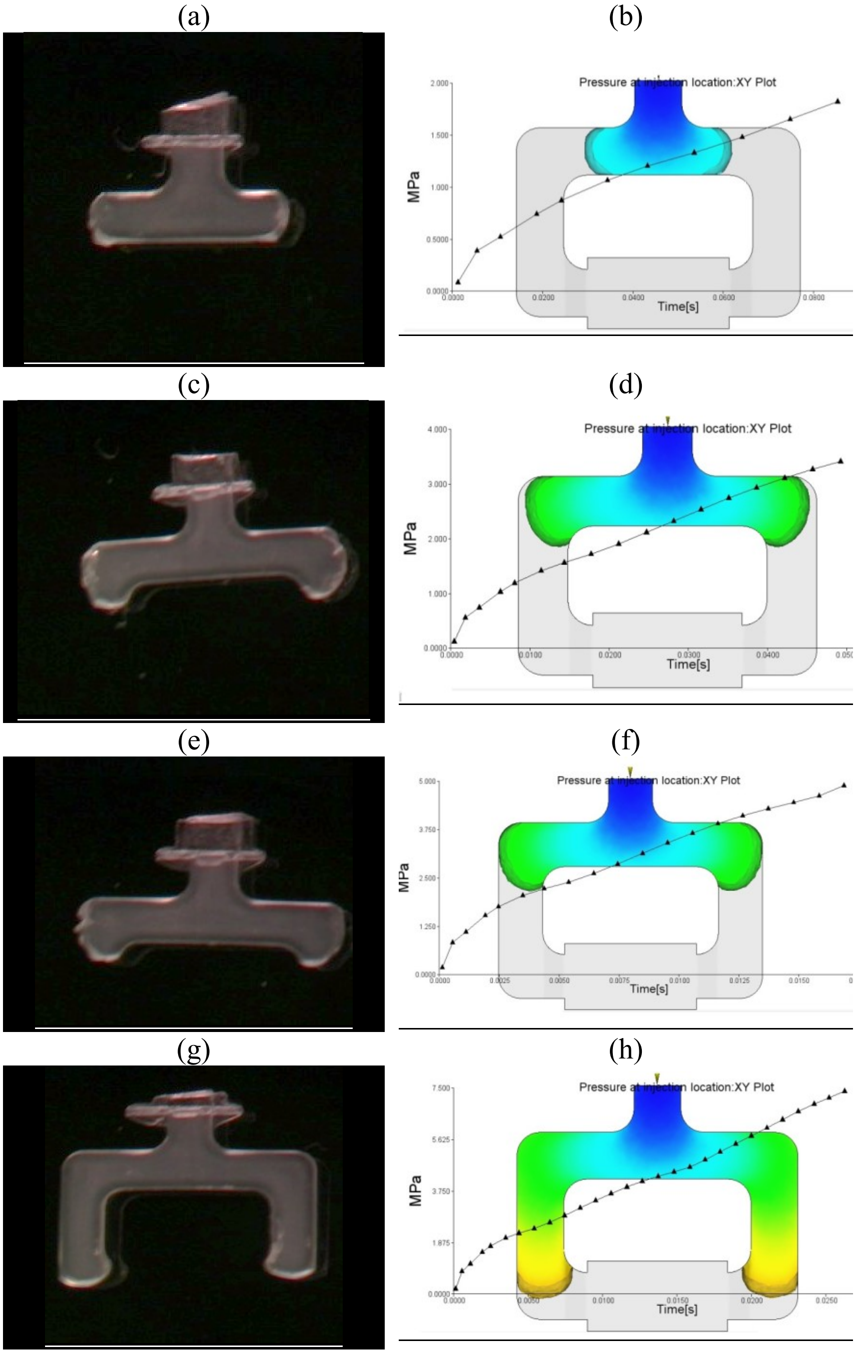

Figure 99. Comparison between short shots and simulations at 10 bar (a) experimental, (b) prevision, at 30 bar (c) experimental, (d) prevision,

at 50 bar (e) experimental, (f) prevision, at 70 bar (g) experimental, (h) prevision.

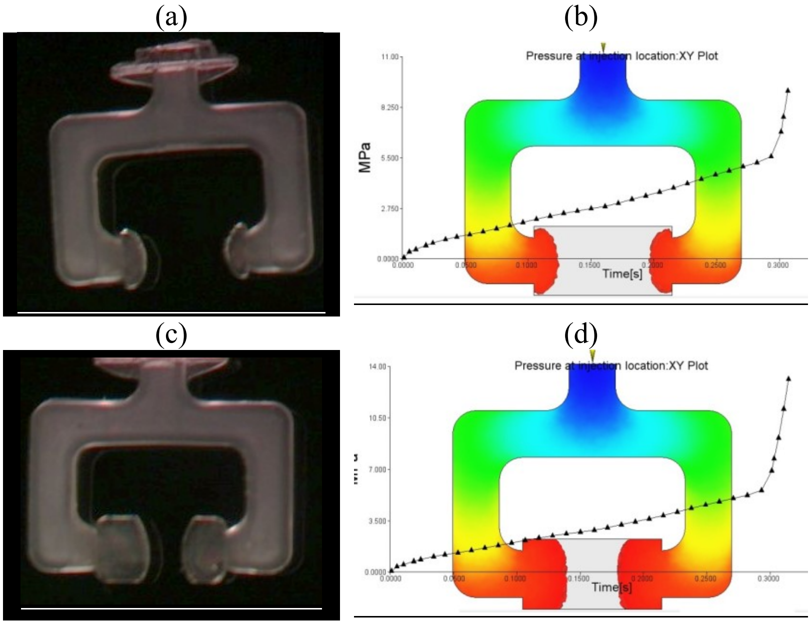

Figure 100. Comparison between short shots and simulations at 90 bar (a) experimental, (b) prevision, at 110 bar (c) experimental, (d) prevision.

Part II Effect of different cavity temperatures on the weld line

Experiments

By using the geometry described in the previous paragraph, the flow fronts are expected to meet in the center and weld lines in this critical area could be visible. To study the effect of different temperature in the cavity surface and in particular near the critical region in the center, a set of experiments was designed. In particular, the injection pressure, the melt temperature, the injection time as well as the packing pressure and the temperature of the mold were equal for all the tests and the value applied are shown in Table 16.

Table 16. Parameters used for all the tests.

Melt Temperature (°C)	230
Mold Temperature (°C)	40
Cavity Temperature (°C)	40 – 80 – 105 - 130
Injection Pressure (bar)	200
Injection/Packing time (s)	10
Packing Pressure (bar)	100
Cooling time (s)	10

The system for the temperature control was used to modify the temperature of the cavity during the filling and for a total time of 10 s that include also a part of the packing step. Four different temperatures were investigated and for each one at least six samples were produced. The temperatures adopted were: 40°C, 80°C, 105°C and 130°C. In the Figure 101 there is a schematic of the protocol for the use of the control of the temperature. The system used to regulate the temperature is the same described before.

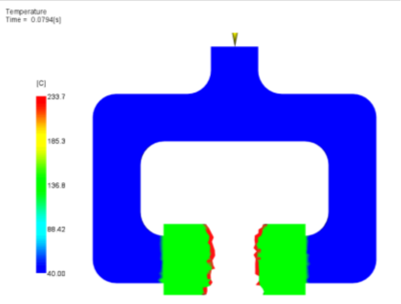

t=0 s Control ON

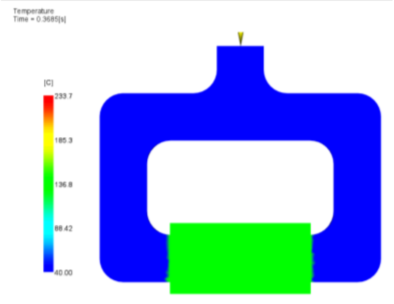

t≤10 s Control ON

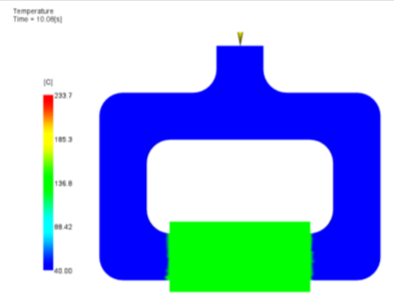

t>10s Control OFF

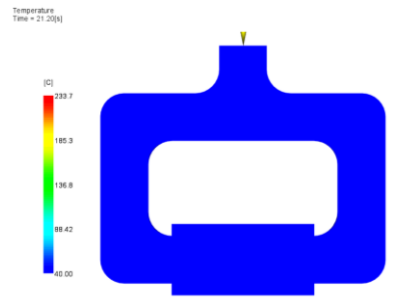

t= $t_{ejection}$ Control OFF

Figure 101. Protocol for the temperature control.

Thermal profile and weld line predictions

By means of Moldflow predictions of the temperature profiles and weld lines formation are possible. In particular, it is possible to monitor the temperature in the entire geometry with the time (Figure 102a) or select a tetrahedron and plot the property with the time (Figure 102b).

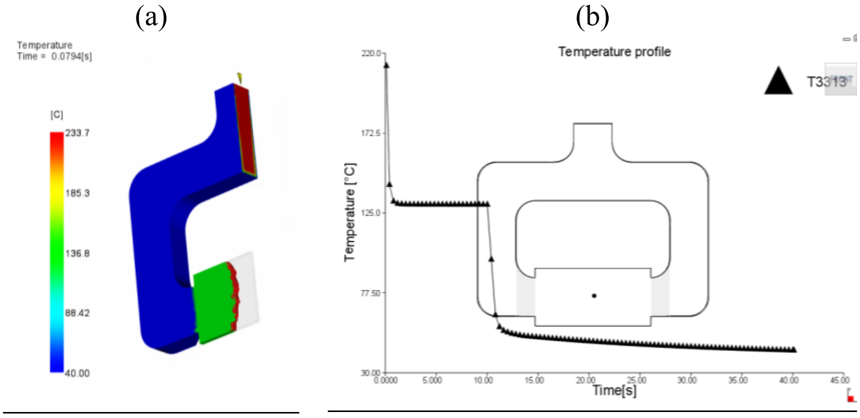

Figure 102. Study of the temperature evolutions: (a) 3D, (b) in the center of the cavity.

By selecting a tetrahedron in the center of the cavity, the temperature profiles were observed in the thickness of the part by changing the normalized thickness of the output. When the normalized thickness “nt” is equal to 1 the values refer to the surface, when it is zero value the temperature is calculated in the center. Figure 103 and Figure 105 plot the values for the complete cycle while Figure 104 and Figure 106 refer to the filling.

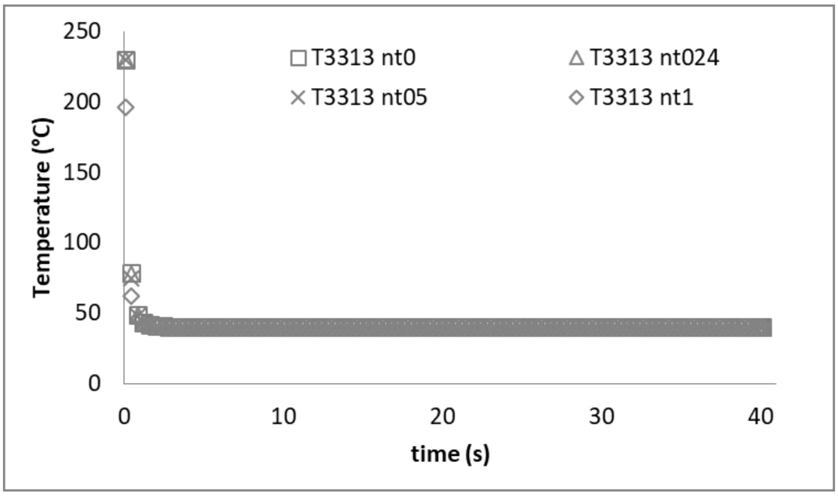

Figure 103. Temperature at different distances from the skin (Tcavity = 40°C).

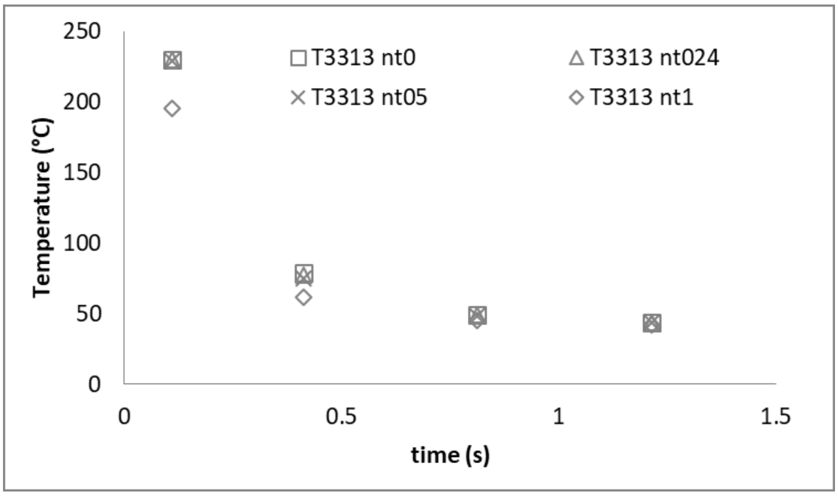

Figure 104. Temperature during the filling at different distances from the skin (Tcavity = 40°C).

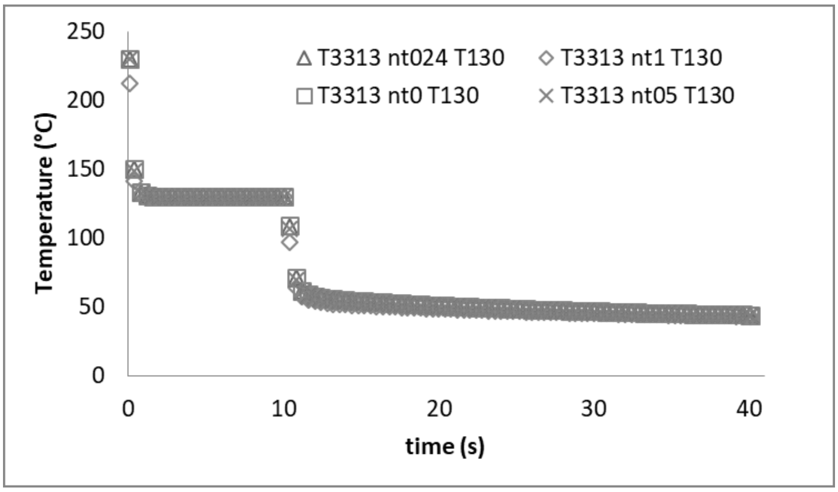

Figure 105. Temperature at different distances from the skin (Tcavity = 130°C x 10s).

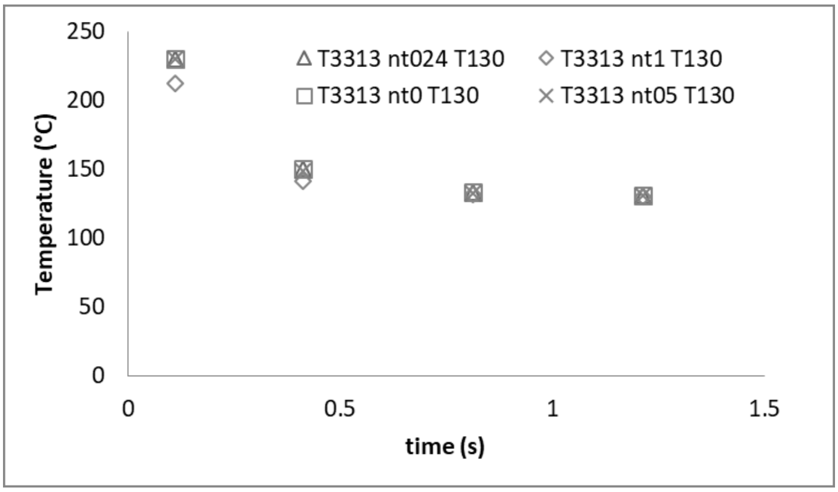

Figure 106. Temperature during the filling at different distances from the skin (Tcavity = 130°C x 10s).

These simulations confirmed that since the part is very thin in less than 1 second the temperature is the same along the thickness.

The weld line formation that is the analysis made by the simulator along the thickness (Figure 107) and the weld lines results that is the weld line on the surface (Figure 108) show that the defects involve not only the surface of the part but also the internal structure highlighting the need for the application of a technique to reduce the problem.

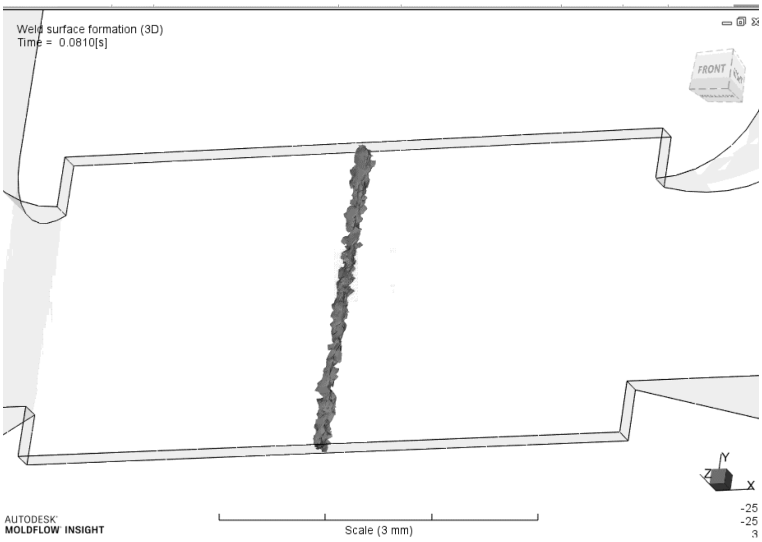

Figure 107. Weld lines surface formation.

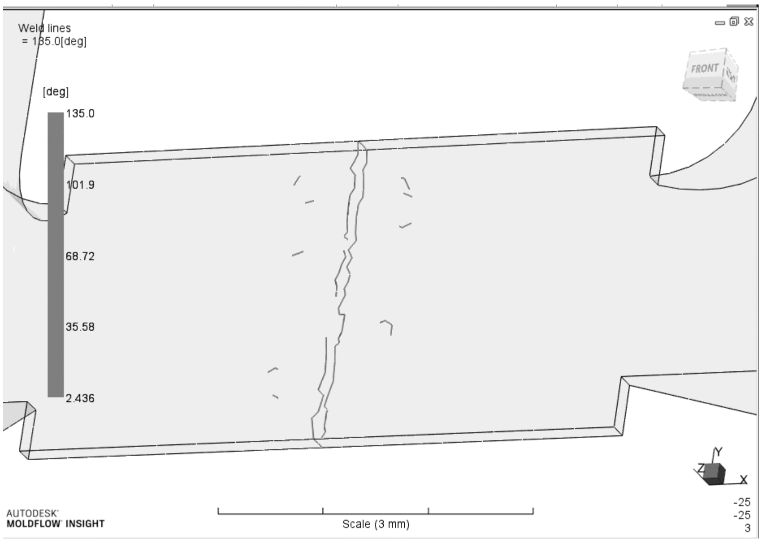

Figure 108. Weld lines (Moldflow).

Results

Temperature evolutions

The thermocouples located behind the two slabs of the cavity registered the temperature values that are acquired by Labview and exported for the analysis.

The Figures 109, 110 and 111 represent the measurements performed in some of the experiments carried out. They include a part of a few seconds for the preparation of the injection, the heating step and an isothermal one, on the left of each graph. Once the temperature desired is reached and the mold is closed, the polymer is injected. The entrance of the polymer into the cavity was also detected as an instantaneous increase of the temperature followed by 10 seconds of isothermal time at the set temperature. Then, the power supply is switched off and the part injected cooled down in 10 seconds.

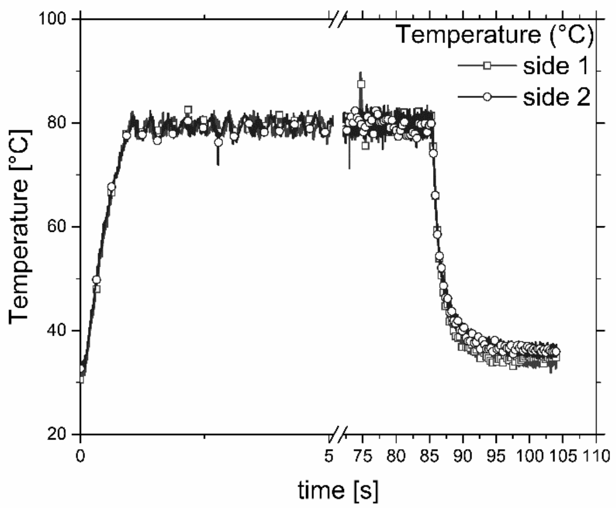

Figure 109. Temperature acquisitions during a test with a set Temperature of 80°C.

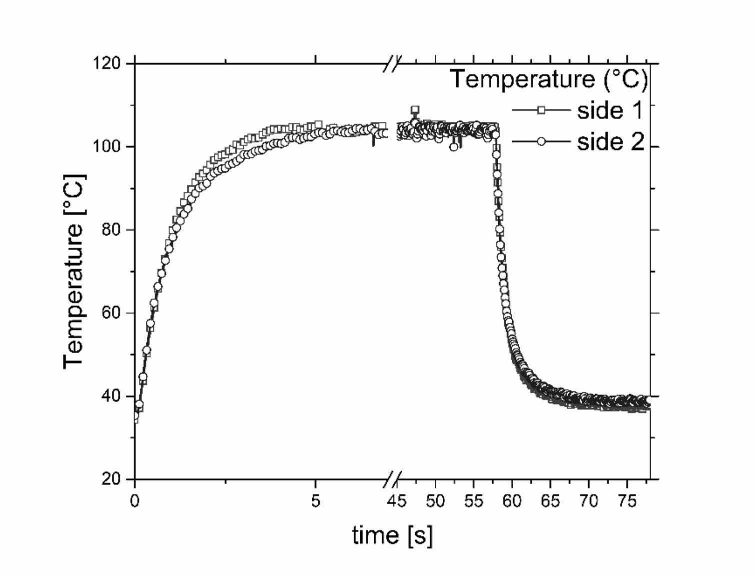

Figure 110. Temperature acquisitions during a test with a set Temperature of 105°C.

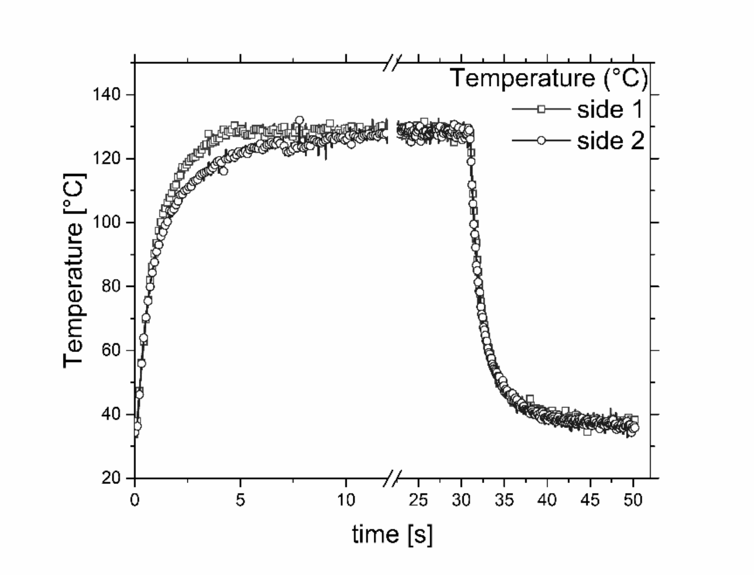

Figure 111. Temperature acquisitions during a test with a set Temperature of 130°C.

Optical Microscopy

Optical observations have been made on massive samples, to detect the weld line in the samples at different temperatures, and on slices cut from each sample to observe the weld line and the morphology along the thickness.

Massive samples

The effect of the different temperature of the cavity surfaces is immediately visible by placing the sample between crossed polarizers and transmit the light throughout it: the clear weld line in the center tends to disappear increasing the temperature. Although, the clear fringes that characterize the part injected in a cold cavity (Figure 112a) are not distinguishable when the polymer solidified after a time of permanence in the cavity at a high temperature (Figure 112d).

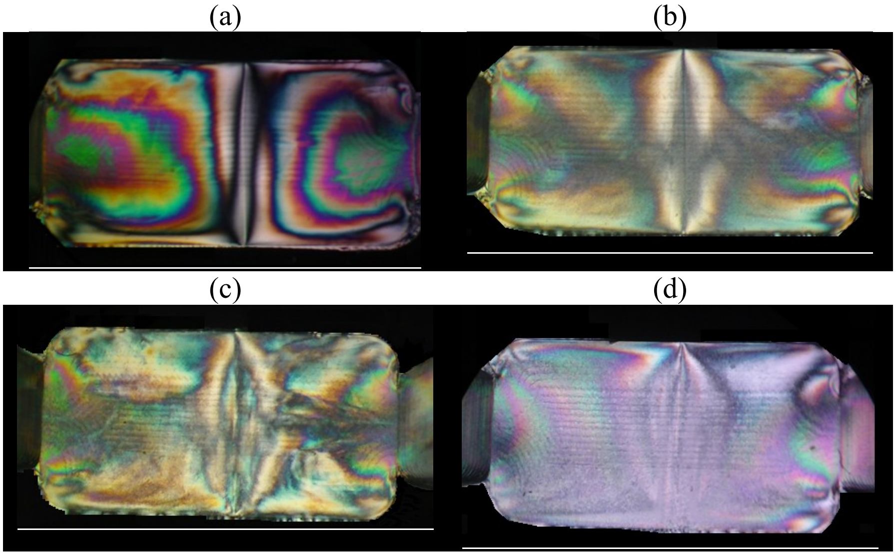

Figure 112. Overview of the samples produced at different conditions: (a) T=35°C, (b) T=80°C, (c) T=105°C, (d) T=130°C.

Slices

A deepest analysis of the morphology was carried out by obtaining thin slices from each sample. For this purpose, after embedding the part in a mixture of hardener and epoxy resin, a microtome Leica RM2265 equipped with a tungsten knife was used. The resin permitted to clamp the sample and cut very precise slices with different thicknesses, from 25 to 100 microns.

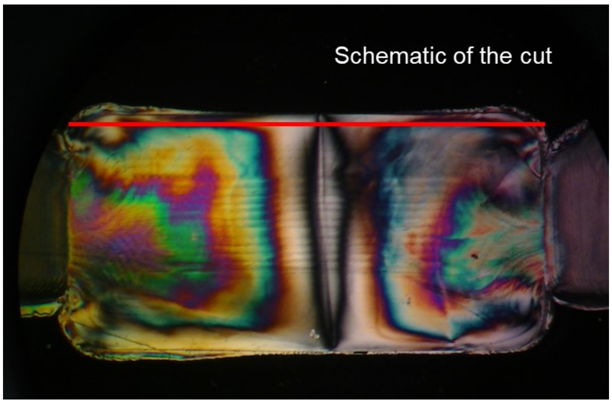

Figure 113. Schematic of the cut.

The slices, immersed in a low light refracting oil, were observed with different magnitudes by using the Olympus BX51 microscope. Images were taken in the complete length of the part.

All the samples show a skin-core morphology, typical of injection molded parts with a shear layer thicker near the gate and smaller and smaller moving towards the center where it fully disappears (Figure 114).

However, the observations revealed that increasing the temperature the thickness of the shear layer decreased and the core layer thickness increased (Figure 115).

From the Figure 116 it is noticeable that also the dimension of the crystalline structures are different, higher is the temperature and larger are the spherulites.

By focusing on the weld line region the comparison between all the samples show that the weld line is clearly visible at 35°C, 80°C and 105°C but seemed to disappear when the temperature was 130°C.

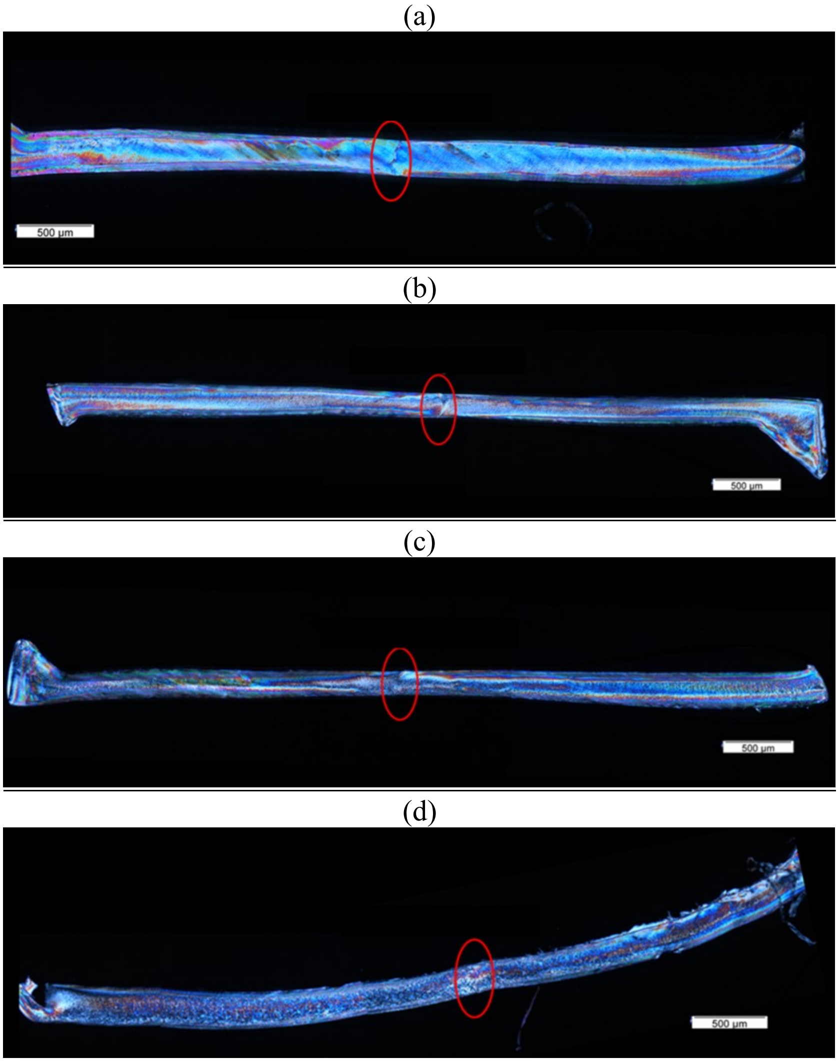

Figure 114. Low magnification (5x) polarized optical microscopy of the slices: (a) T=35°C, (b) T=80°C, (c) T= 105°C, (d) T=130°C.

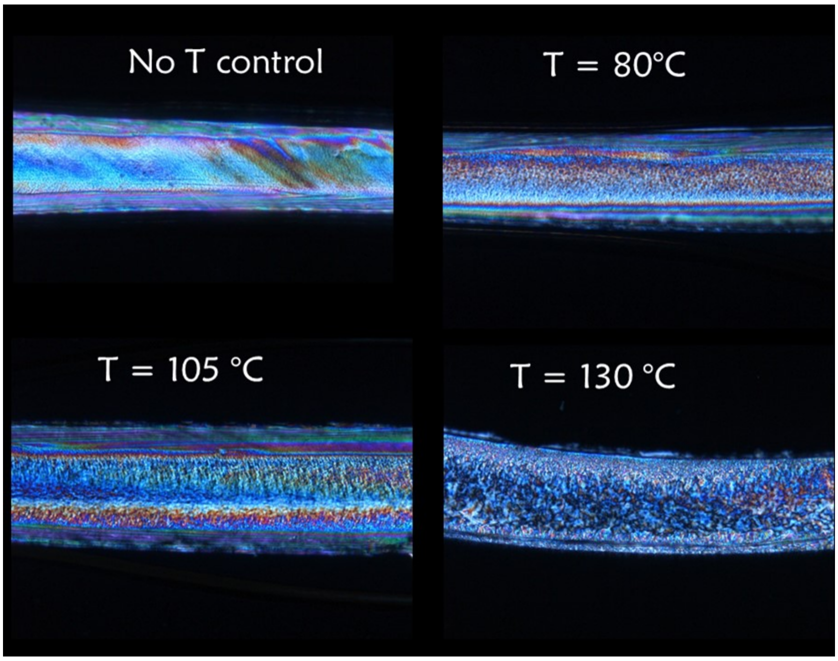

Figure 115. Medium magnification (10x) polarized optical microscopy of the slices (after the gate).

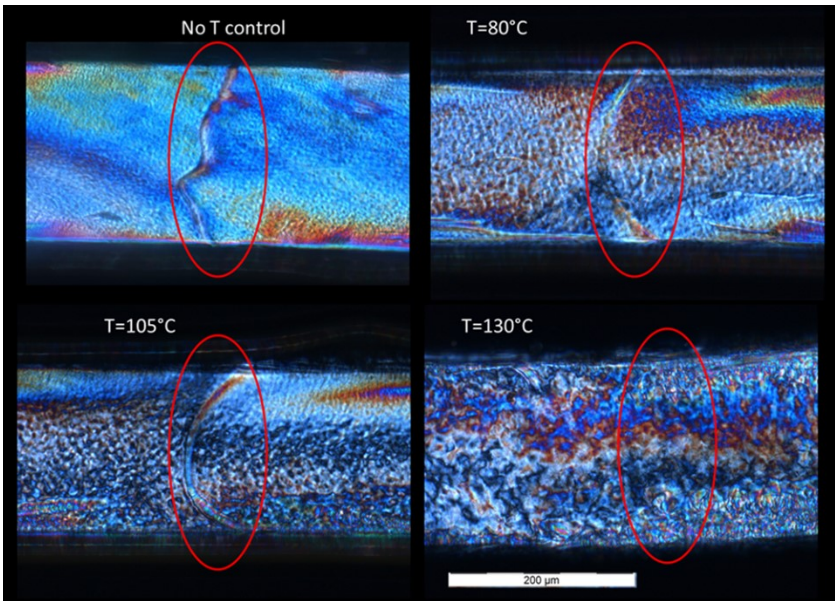

Figure 116. High magnification (20x) polarized optical microscopy of the slices (weld line area).

Mechanical tests

The effect of the cavity temperature on the mechanical properties of the micro-parts was studied by means of uniaxial tensile tests. A mechanical testing system (Biomomentum, Mach1), equipped with a 25 N load cell was adopted to perform the experiments at room temperature. Custom grips were used to fix the micro molded parts and the experiments were carried out with a tensile speed of 10 mm/min. In order to compare the mechanical properties of the samples elastic modulus, yield stress and strain at break were taken in consideration.

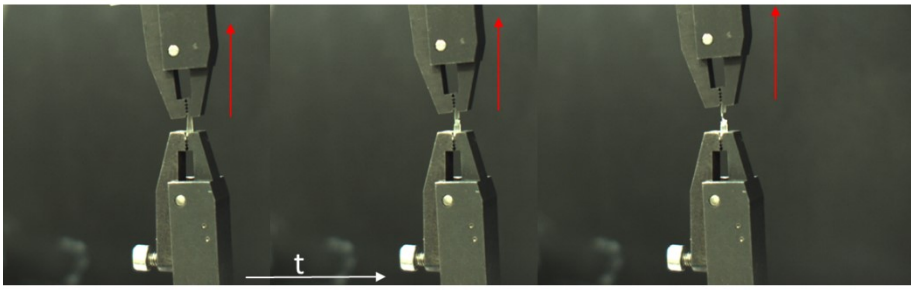

Figure 117. Images of a tensile test.

For each condition, five samples were tested and then the arithmetic average was considered for the comparison between the different cases. All parts broke at the weld line.

As shown in Figure 118 the behavior was typical of semicrystalline polymers with a yield followed by a cold drawing and a fracture.

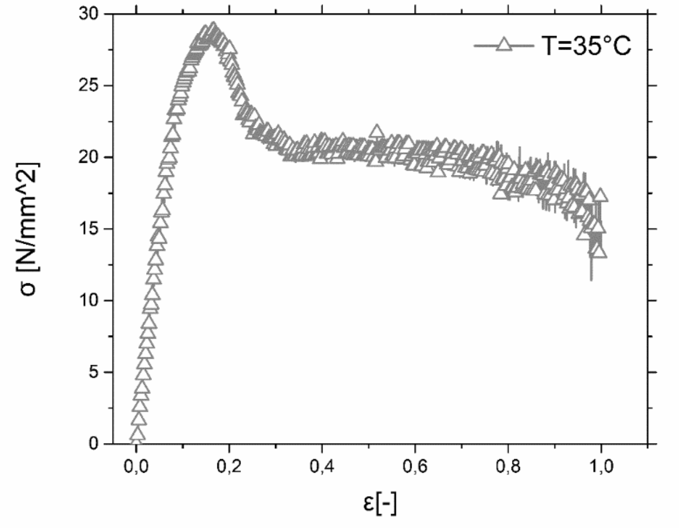

Figure 118. Stress and strain measurements T_{cavity}= 35°C.

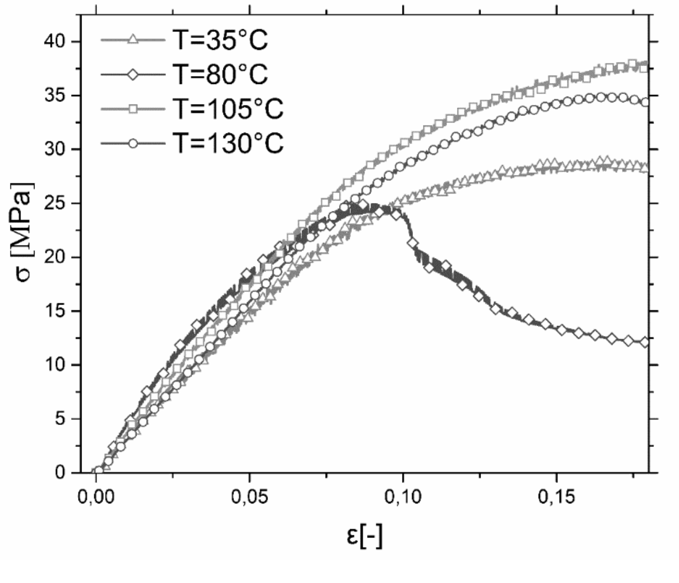

Figure 119. Comparison between the tensile tests up to the yield point.

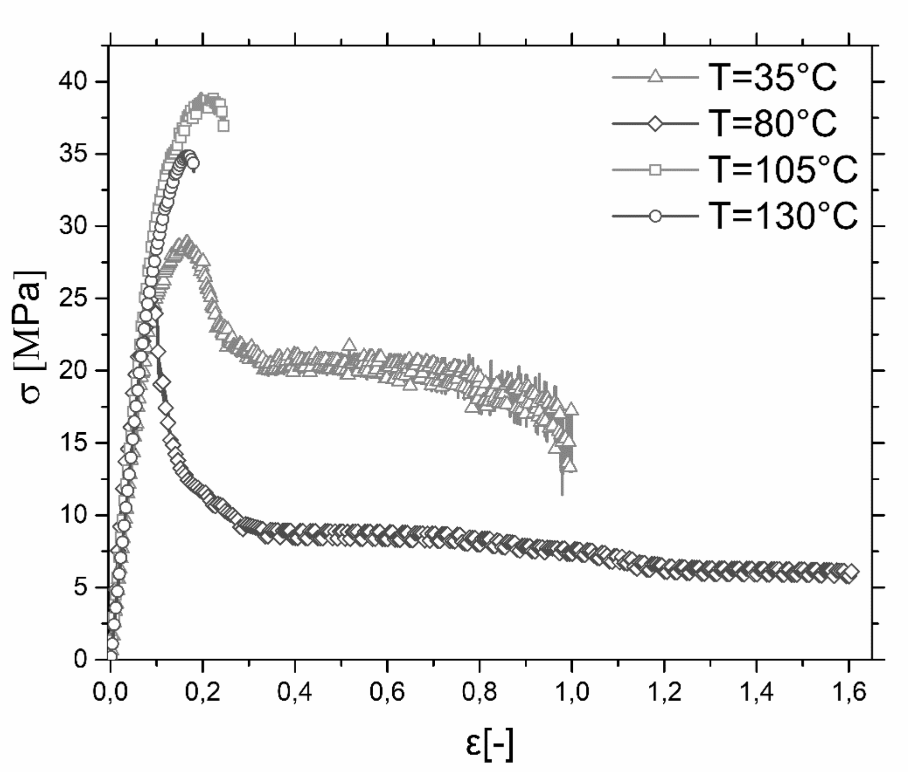

Figure 120. Comparison between the tensile tests until breakage.

The analysis of the tensile curves revealed that an increase of the temperature of the cavity can led to a slight increase of the elastic modulus that at 80°C is 22% higher than the lower temperature but is the highest value since increasing the temperature the modulus decreases (Table 17).

The yield stress, on the other hand, tends to increase with the temperature like the maximum stress having a maximum value at 105°C. The highest rigidity and strength of the parts corresponds to a lower ductility. The parts produced at 105°C and 130°C showed a lower extensibility followed by a brittle fracture.

The different behavior detected in the samples produced in different conditions of cavity temperature can be ascribed to two phenomena that obviously occur in the parts produced: the different welding of the two flow fronts and the different morphology developed along the thickness and the direction of the flow.

The morphological analysis conducted on the massive samples and the slices allowed the observation of the weld line gradual disappearance. In particular, when the temperature was 130°C the weld line was not visible revealing that the polymer fronts met and join not along a freezing line but in a rubbery state in which molecular chains from the two fronts can interact.

As shown before, the cavity temperature has a high impact on the morphology, the higher diameter of spherulites as well as a thinner shear layer are responsible of an increase in brittleness.

Table 17. Mechanical properties of the micro parts.

T(°C)	E (MPa)	σ_y(MPa)	σ_{max}(MPa)	ε_{max}
35	291	29	13.5	1.00
80	355	25	5.8	1.61
105	334	39	37.7	0.24
130	318	35	33.8	0.18

Conclusions

A preliminary analysis of the filling capabilities of an isotactic polypropylene was carried out in Moldflow. Short shots experiments of an isotactic polypropylene were used to verify that the flow behavior is well described by Moldflow studies. The geometry has a rectangular shape and is characterized by two gates. The study of the effect of the cavity temperature on the weld line formation was investigated. Four different temperatures were taken in consideration to condition the cavity surfaces during the filling and the packing for an amount of time of 10 seconds. After that, the parts solidified and were analyzed in terms of morphology and mechanical properties. The optical observations revealed that increasing the temperature the weld line becomes less visible. Also, the morphology is extremely affected by the temperature of the cavity: spherulites with higher diameter and bigger core layer. The complex phenomenon is demonstrated by the mechanical behavior of the parts, higher temperatures corresponded to higher modulus and yield stress but lower extensibility. The best performance is obtained not at the maximum temperature but seems to be a compromise between 80°C and 105°C.

Chapter VII. Innovative Design and Simulation Study of a mold for Rapid Temperature Control in Microinjection Molding

Introduction

The experiments shown in the previous chapters found that, by using the system developed, less than 10 s were required for the mold surface temperature to rise from 60°C to 160°C, and the same time is required to cool from 160°C to 60°C. In this chapter, the study of a different geometry of the mold was considered. In this case, the heating system previously developed will be coupled with a moving system of the inserts that allows reducing the cycle time further. For this purpose the process was studied by analyzing the effect of different materials, and related properties, in contact with the insert mold during different steps of the molding cycle. The innovative mold design is developed for a micro-injection molding machine of industrial scale.

In industrial scale machines for microinjection molding the injection system has to pursue different objectives. First of all, the shot has to be injected rapidly into the cavity to guarantee a complete filling of the high aspect ratio features and avoid the freezing of the material. The injection unit, moreover, has to be able to reach the high injection pressures required for accurate feature replication. Moreover, the reproducibility of the results are fundamental injection to obtain highly repeatable properties of the parts.

The manufacturers of the micro molding machine tried to fulfil the demands. In Table 18 is a list of micro molding machines commercially available and their main characteristics (Giboz, Copponnex and Mélé, 2007).

Table 18. List of micro molding machines commercially available and their main characteristics.

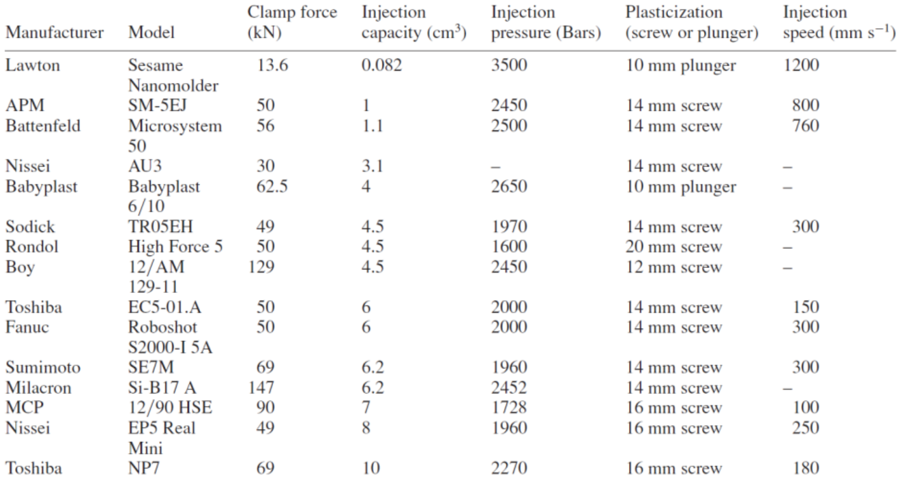

Manufacturer	Model	Clamp force (kN)	Injection capacity (cm^3)	Injection pressure (Bars)	Plasticization (screw or plunger)	Injection speed (mm s^{-1})
Lawton	Sesame Nanomolder	13.6	0.082	3500	10 mm plunger	1200
APM	SM-5EJ	50	1	2450	14 mm screw	800
Battenfeld	Microsystem 50	56	1.1	2500	14 mm screw	760
Nissei	AU3	30	3.1	–	14 mm screw	–
Babyplast	Babyplast 6/10	62.5	4	2650	10 mm plunger	–
Sodick	TR05EH	49	4.5	1970	14 mm screw	300
Rondol	High Force 5	50	4.5	1600	20 mm screw	–
Boy	12/AM 129-11	129	4.5	2450	12 mm screw	–
Toshiba	EC5-01.A	50	6	2000	14 mm screw	150
Fanuc	Roboshot S2000-I 5A	50	6	2000	14 mm screw	300
Sumimoto	SE7M	69	6.2	1960	14 mm screw	300
Milacron	Si-B17 A	147	6.2	2452	14 mm screw	–
MCP	12/90 HSE	90	7	1728	16 mm screw	100
Nissei	EP5 Real Mini	49	8	1960	16 mm screw	250
Toshiba	NP7	69	10	2270	16 mm screw	180

One of the most commercially successful micro molding machines is the Battenfeld Microsystem 50 (Coates *et al.*, 2006). This machine is equipped with servo electric driven components to achieve an accurate and repeatable process control, hold in a clean room. The Mycrosystem incorporates a extrusion screw with a diameter of 14 mm, mounted at an angle of 45° to the injection axis, that ensures homogeneity of the melt. The polymer is extruded into a metering chamber with a servo driven piston to accurately prepare a quantity of material (the maximum volume is 1100 mm^3 in 0.01 mm^3 increments). Another servo driven injection piston is designed to the injection of the shot with a velocity up to 1000 mm/s. The injection nozzle passes through the fixed half of the mold to the split plane to limit the amount of polymer needed to fill the feeding channels and guarantee that the melt is still at the desired temperature as it reaches the cavity. Since the injection and the cooling rates are so fast the mold can open within a second or two, and total cycle times are determined predominantly by the time taken for ejection and handling. Moreover, two separate molds can be mounted to a rotating moving plate, which allows a part to be produced, as the previously molded part is ejected from the cavity and increase the productivity.

For this machine, a new mold geometry was considered taking in consideration a mold assembly HASCO ® that can be manufactured according the design of the cavity and the necessary seats for the heaters, thermocouples and wires.

Design

By SolidWorks a mold cavity geometry of area equal to 40 mm^2 and a thickness of 200 µm was created in a small and removable insert.

Both sides of the mold had a removable insert. The cavity had a rectangular shape, it was 3.5 mm wide and 10.5 mm long, with a thickness of 0.2 mm (Figure 121).

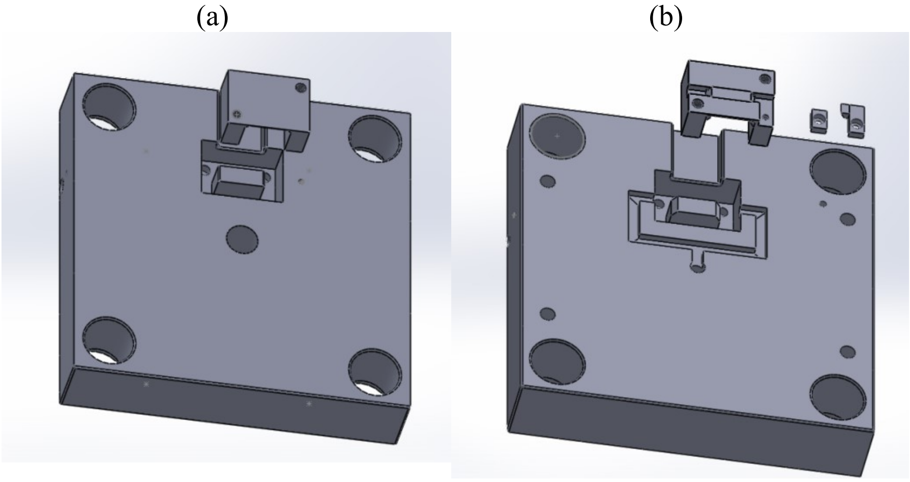

Figure 121. CAD mold design: (a) fixed half (b) moving half.

Temperature control was implemented using thin heating layers and thermocouples attached near the surface of the cavity. The innovative idea of this project is to minimize the thermal dispersion by developing a push-pull system for the cavity seat. With this new technique, when the mold plates are in the open position, a moving system allows a quick separation of the cavity seat from the rest of the mold. For the temperature control, two steps are considered: the heating and the cooling. When the mold is in the open position and the cavity seat is pulled from the mold, the heating step is activated. Because of the air gap between the mold and the cavity, large increases in cavity temperature are feasible in a few seconds. When the mold is closed, conversely, the cavity seat is pushed toward the mold reducing the air gap and permitting a rapid cooling. This step involves also the injection of the polymer in the cavity. The air gap can be tuned to 0 or 0.2 mm. This push-pull system for the cavity seat is created to minimize the thermal dispersion, during the heating just before the polymer injection in the cavity. When the mold plates are in the open position, the push-pull system allows a quick separation of the cavity seat from the rest of the mold up to 1 mm (Figure 122).

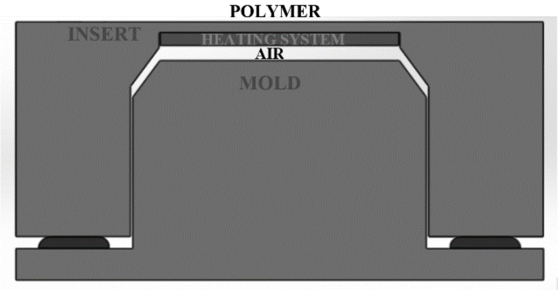

Figure 122. Sketch of the moving system.

Simulations

An evaluation of the heat transfer, by means of Moldflow simulations was carried out.

Basically, the cyclic heating/cooling process is a three-dimensional time-dependent heat conduction problem with convective boundary conditions.

The energy equation used for the mold domain is the basic heat conduction with heat source term described as:

$$\rho_m c_m \frac{\partial T_m}{\partial t} = \frac{\partial}{\partial x}\left(K_m \frac{\partial T_m}{\partial x}\right) + \frac{\partial}{\partial y}\left(K_m \frac{\partial T_m}{\partial y}\right) + \frac{\partial}{\partial z}\left(K_m \frac{\partial T_m}{\partial z}\right) + \dot{Q} \qquad \text{(eq.14)}$$

$$-K_m \frac{\partial T}{\partial n} = h_{air}(T_m - T_{air}) \qquad \text{(eq.15)}$$

$$-K_m \frac{\partial T}{\partial n} = h_c(T_m - T_c) \qquad \text{(eq.16)}$$

Where T_m is the mold temperature (°C), c_m, the specific heat (J kg^{-1} $°C^{-1}$), ρ_m density (kg/m^3) and K_m thermal conductivity (W m^{-1} $°C^{-1}$) of the mold.

The corresponding heat transfer coefficients for air and coolant are designated as h_{air} and h_c.

The volumetric heating power generated from Joule Effect is represented by the equation 4.

$$P = \frac{V^2}{R} \times \frac{1}{V_R} \qquad \text{(eq.17)}$$

$$G_{hr}(t) = \begin{cases} 1 \; if \; T_w < T_{sp} \; and \; 0 \le t \le t_{hr} \\ 0 \; if \; T_w > T_{sp} \; or \; t > t_{hr} \end{cases} \qquad \text{(eq.18)}$$

Where V, R and V_R are the applied voltage, the heating resistance and the volume of the heating resistance, respectively.

The thermal conductivity of the polymer is usually much smaller (by a factor of at least 10) than that of the material of the mold so the cooling time of the process is mostly affected by the rate the hot polymeric material releases the heat from its inner region to its outer surface. During the cooling stage, material solidifies because of the conductive heat transfer (Kenig and Kamal, 1970), (Himasekhar, Lottey and Wang, 1992). Since the parts are usually thin a local one dimension transient analysis is adequate for a three dimensional molded part. Furthermore, polymer may be either amorphous or semi-crystalline, and the properties like the specific heat may depend on temperature especially for semi-crystalline polymers (Kamal and Lafleur, 1984). The study carried out on the new mold, considers the heating step and the cooling step without the polymer in the cavity.

The insert-mold system is schematized as a multi-layer model as in Figure 123, using electrical resistances as a heat source and an air gap, which limit the heat flow towards the mold. The layers and their properties considered are listed in Table 19.

Table 19. Layers and properties considered in the simulations

Layer	**Material**	**ρ [g/cm^3]**	**c_p [J/kg K]**	**k [W/m K]**	**Thickness [mm]**
Insert	Steel P20	7.8	460	29	0.300
Thermocouple	Polyimide	2.138	1090	2.74	0.155
Heater	Default properties within Moldflow	default	default	default	0.140
Air gap	Air	1.292	1005	0.026	0 - 1
Mold	Steel P20	7.8	460	29	10

The electrical resistances are grids of constantan foil sealed in a polyimide film with a nominal resistance of 120 Ω. The resistances cover the entire area of the cavity impression and the insert is not fixed to the rest of the mold so it automatically moves from the plate when the mold opens while in the closed position it is pushed into the seat to reduce the air gap to the desired value.

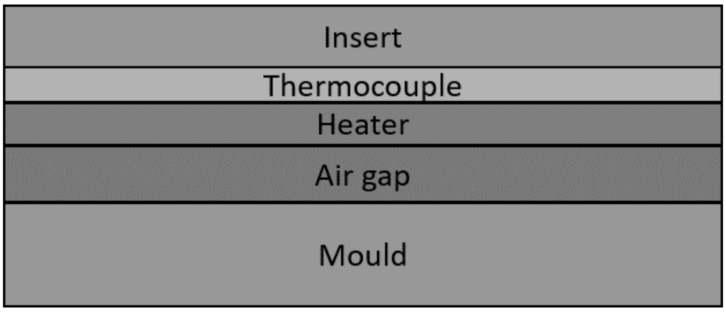

Figure 123. Schematic of the layers.

By using Moldflow software, a Cool FEM analysis of the mold with heating sources was conducted to evaluate the thermal response in both heating and cooling stage. The three dimensional (3D) mesh model of the mold and the layers for Cool FEM simulation are shown in the Figure 124 and 125, respectively.

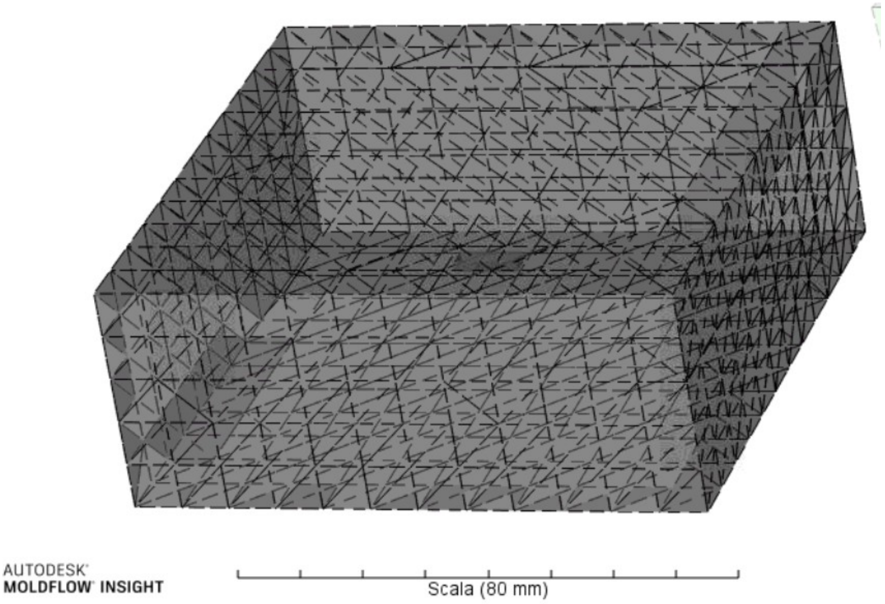

Figure 124. Mesh Model of the mold.

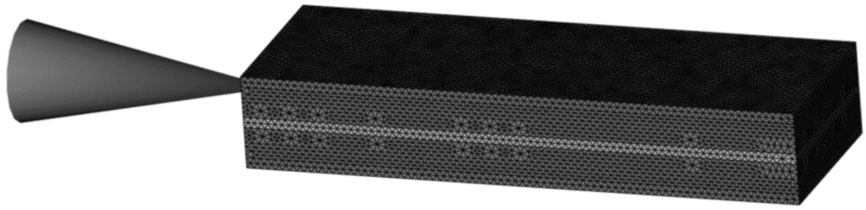

Figure 125. 3D mesh model for Moldflow simulations.

The simulations were conducted by fixing the boundary conditions:

- the initial mold temperature is the same as the ambient temperature, i.e. 25°C;
- the heat exchange between the mold surface and surrounding environment belongs to air free convection;
- the heat generated by each heater is equal to 110 kW/m^2, with the applied voltage of 12 V.

Heating step

For the heating step, the cycle time for the injection molding is set to 32 s. After that, the heater is kept active for 20 s. The Figures 126, 127 and 128 show the temperature evolutions calculated for the heating stage, obtained with different configuration of the system described in this work. The values reached depend on the thickness of the air gap.

If the air gap is set to zero and no insulation material is considered between the heater and the mold a small increase of the temperature is achieved. The simulation showed that the temperature rises to 61 °C with an initial temperature of 25°C.

An air gap of 0.2 mm permits to obtain in the central area of the cavity a temperature of 123°C (Figure 128) and a distance of 1 mm between the mold and the block represented by the insert and the heating system is required if an interfacial temperature of 150°C is necessary (Figure 128).

The temperature of the rest of the mold is weakly affected during the heating and the Figure 129 shows that while the cavity temperature is at 150°C the rest of the mold is essentially at 25°C confirming that the system modifies the temperature locally.

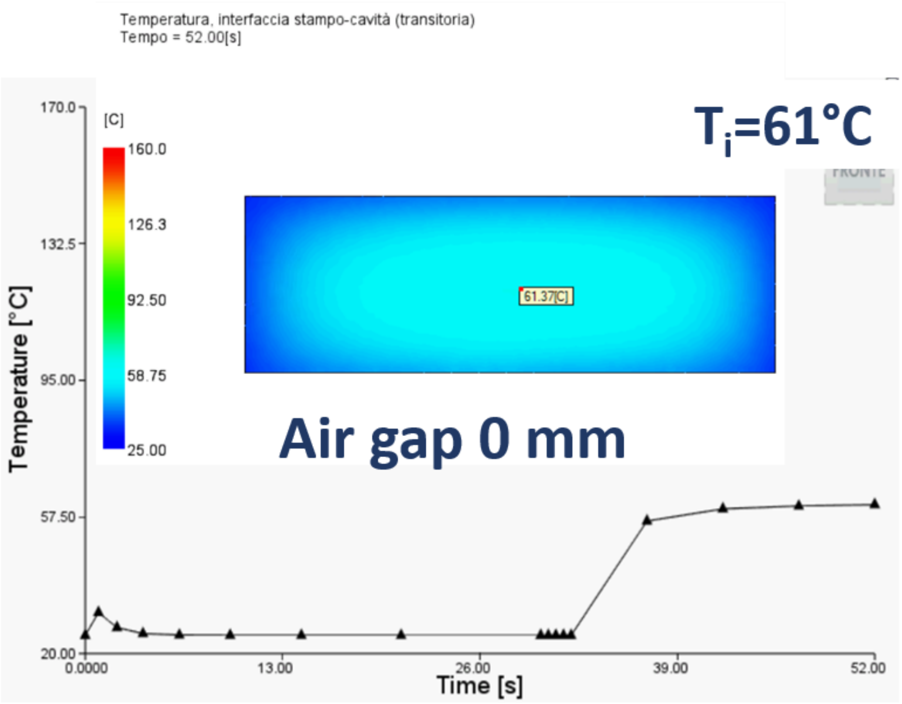

Figure 126. Temperature evolution during the heating at the interface polymer-steel when the air gap=0 mm.

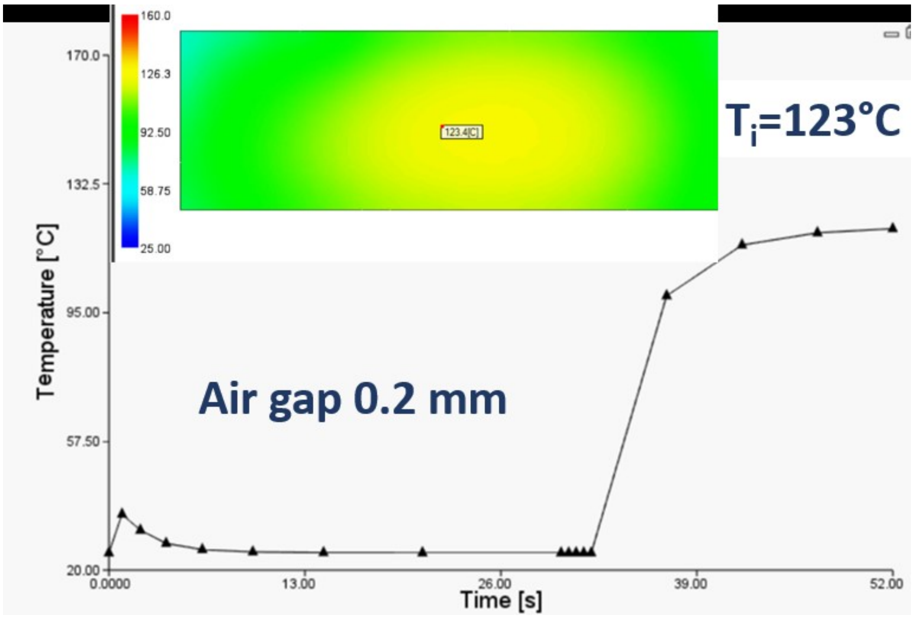

Figure 127. Temperature evolution during the heating at the interface polymer-steel when the air gap=0.2 mm.

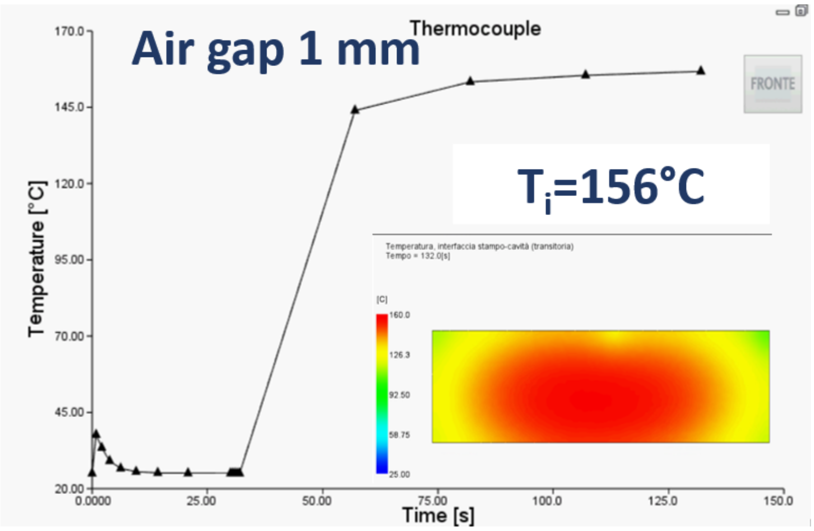

Figure 128. Temperature evolution during the heating at the interface polymer-steel when the air gap=1 mm.

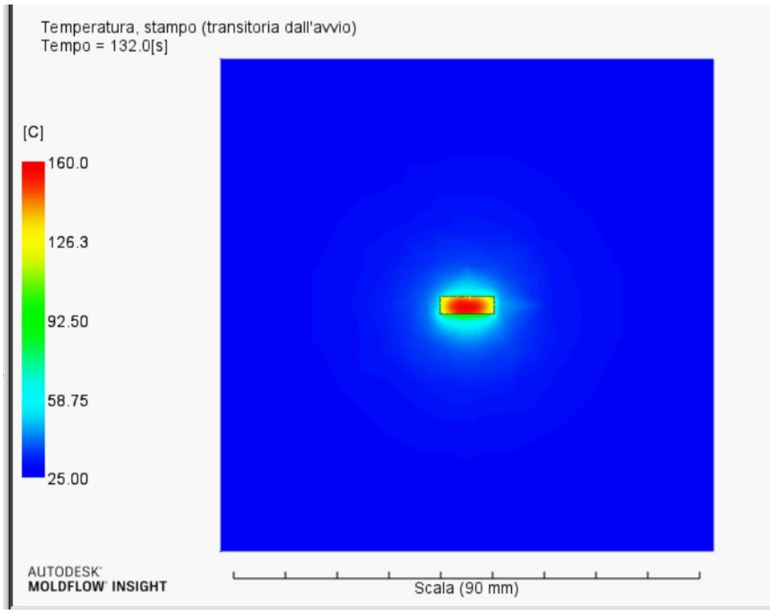

Figure 129. Mold temperature in the case of air gap = 1 mm.

Filling step

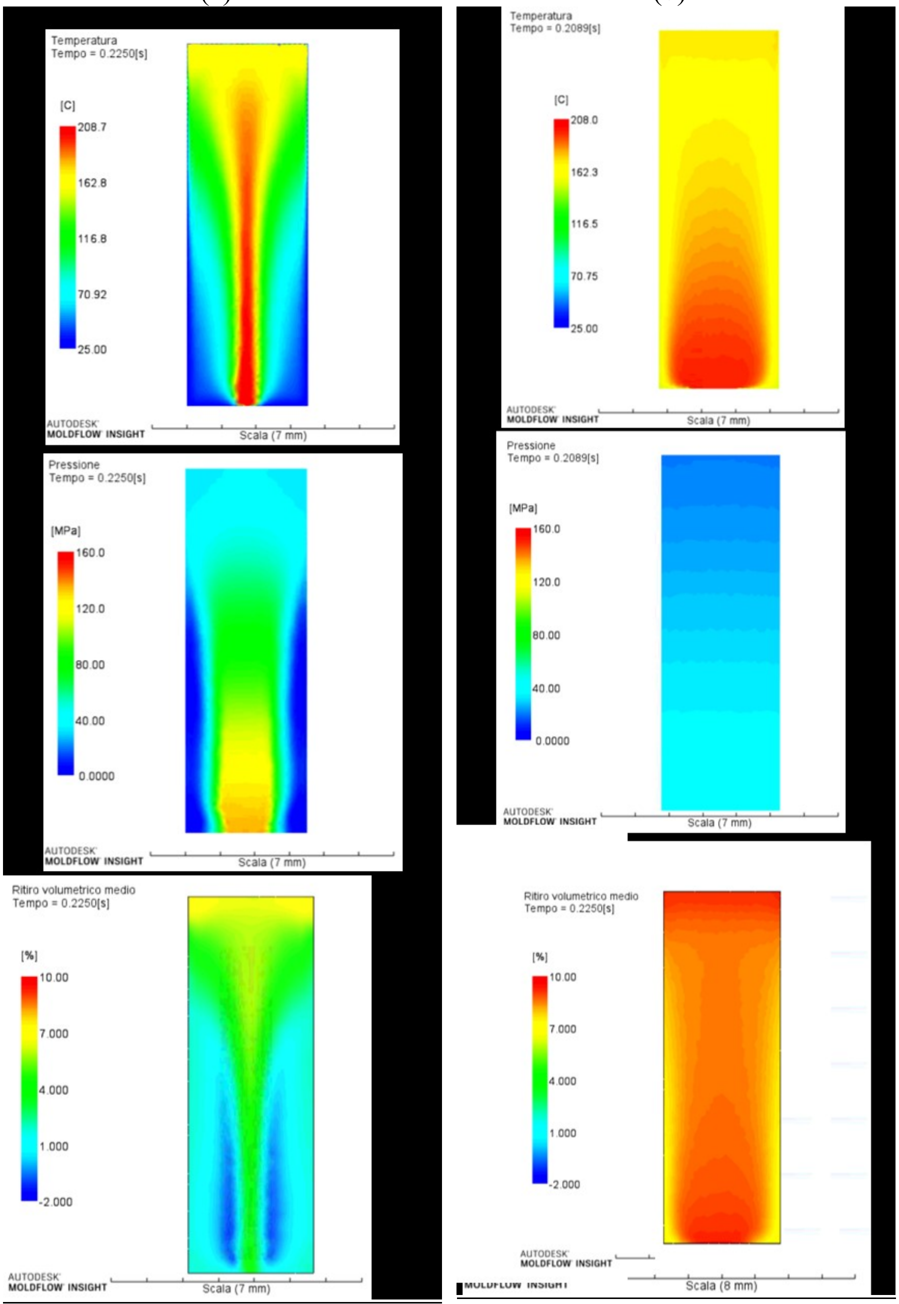

(a) (b)

Figure 130. Temperature, Pressure and shrinkage evolutions in the case of (a) T=25°C and (b) T=150°C.

The effects of different cavity temperatures was also investigated by considering a filling analysis in terms of temperature of the polymer, pressure and shrinkage evolution along the cavity.
For this study, the PLA 3251D, present in the Moldflow database was considered and a melt temperature of 180°C was selected.
The results, represented in Figure 130, confirmed that a higher temperature of the material the polymer is in contact might cause a delay in the solidification but with the evident consequences of highly homogeneous properties along the part. In the case *a,* the temperature of the cavity is equal to 25°C whereas in the case *b* it is 150°C. Because of the high viscosity of the polymer, the pressure, moreover, changes a lot in different points of the cavity for the case *a* with values that reach 150 MPa near the gate region whereas in the case *b* the material is clearly less stressed because the values required for the filling are lower than 50 MPa. This situation reflects the final properties of the product. The shrinkage, in fact, will be higher but completely homogeneous if the cavity temperature is 150°C with a very good dimensional stability.

Cooling step

The analysis of the cooling step was conducted by considering the mold in closed position and the cavity empty (without polymer). Thanks to the moving system, during this step it is possible to regulate the distance between the insert and the rest of the mold. As shown in Figure 131, when the mold is closed, if the air gap is zero value and the heater is ON, the temperature decreases of an amount of almost 100°C in about 1 s. If the gap between the mold and the heater equal to 1 mm and the heater is OFF, a temperature decrease of about 50°C will be obtained (Figure 132).

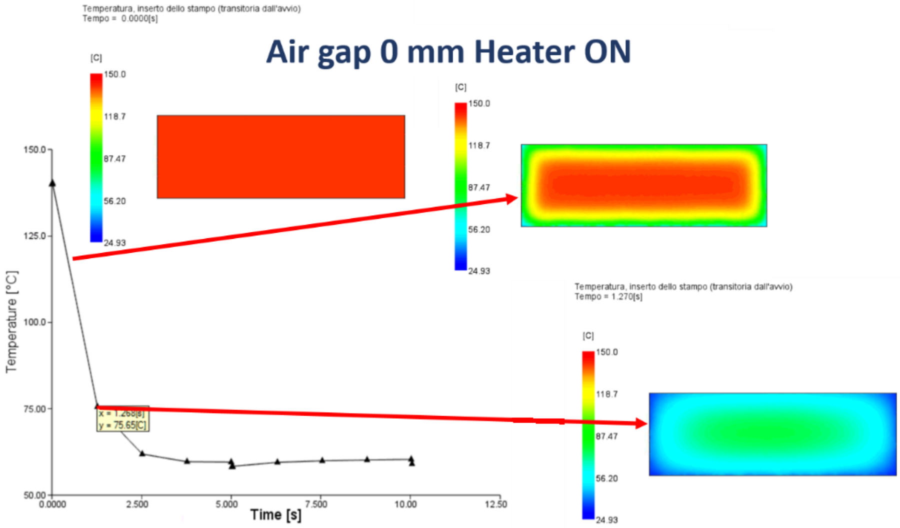

Figure 131. Temperature evolution during the cooling at the interface polymer-steel when the air gap=0 mm and the heater is switched ON.

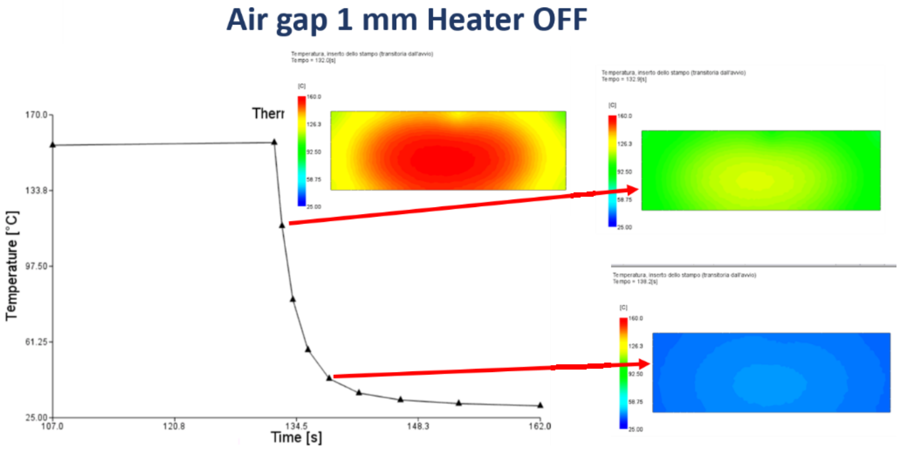

Figure 132. Temperature evolution during the cooling at the interface polymer-steel when the air gap=1 mm and the heater is switched OFF.

Conclusions

In this chapter, the idea of an advanced technique based on the rapid heating/cooling system and a push-pull mechanism was developed and studied. In particular, the design for a mold suitable for a Battenfield machine was carried out by SolidWorks. The drawing was imported in Moldflow for the mesh and the simulation analysis.

This study shows that during the heating step, the use of the system allows the reduction of the thermal dispersion and the achievement of a temperature increase of the more than one hundred degrees at the cavity surfaces when an air gap is considered. However, a slight increase is achieved when the air gap is zero and the layers are in contact with the mold. Furthermore, the high thermal conductivity of the steel permits to obtain a fast cooling when the mold is closed, it can be tuned by the heater activation and a very small air gap.

The investigation confirmed that the technique for the rapid temperature control is adaptable to a machine for industrial scale and by coupling the system with a moving system considerable time reductions for each step can be obtained, making the resulting cycle time very short.

Chapter VIII. Conclusions

The aim of this thesis is the development of a system that fulfils rapid temperature evolutions during the µIM and its application to influence the viscosity, the morphology and the weld line strength of semicrystalline polymers.

The device was created by adopting different thin layers, in particular, heating elements, thermocouples and insulation layers. A Labview code was written to acquire data and control the temperature at 10 kHz. The code regulates the switch for the current flow through the resistances that generate the heat by Joule effect. In order to study the influence of the physical properties and the thickness of each layer, simulations by a finite-element software were carried out. These simulations demonstrated that a steel slab between the resistance and the cavity does not cause any thermal difference between the value read by the thermocouples and the one on the cavity surface. Moreover, the rest of the mold is not affected by the local thermal variation so that in the cooling step the cavity surfaces reach the temperature of the rest of the mold in a few seconds.

Initially, the system was adopted for the µIM of a biodegradable polymer that shows interesting properties for different engineering sectors including the micro-scale applications: the poly-lactid acid (PLA). Having a relatively high viscosity, this polymer solidified after entering the thin cavity. Increasing the temperature of the cavity surfaces, the viscosity of the polymer decreased and the melt was able to fill up to the entire length heated by the resistances. Moreover, the PLA is characterized by a low crystallization rate. Calorimetric analysis on pellets of PLA permitted to study the crystallization behaviour in quiescent conditions and set the temperature value at 105 °C for the annealing steps during the process. In this manner, the system for the temperature control was adopted to influence the final crystallinity of the PLA, by applying isothermal steps at a particular temperature. The effect of the application of different time of annealing and different thermal history before the annealing were investigated. X-ray analysis and optical observations verified the effect of the annealing step on the microparts. Furthermore, the system was used to apply different thermal histories in different zones of the sample after the solidification in the microcavity and generate a crystalline phase and an amorphous one in the same part. Morphology modifications were analysed by means of optical observations, calorimetric analysis, X-ray and IR spectra showing that the system is able to generate a biphasic sample in which it is possible to obtain a profile of properties within the same part. The possibility to obtain a difference in the biodegradation rate in the same part was also verified.

To verify the potentiality of the system for the rapid temperature control it was adopted to study the effect on the weld line of a thermoplastic polymer widely used in industrial applications. The isotactic polypropylene (iPP) was considered and the effect of the application of different temperature of the cavity on the weld line formation was studied. Optical observations of slices obtained from each sample allowed a deep morphological analysis that clearly highlighted the disappearance of the weld line at higher temperature. Mechanical tests checked the tensile behaviour of the samples and revealed that the weld line elimination is not the only factor to be considered to understand the final properties. It has to be coupled to the morphology of the part to determine the effect of the different thermal histories on the performance of the micropart.

Successively, a new mold for the rapid temperature control was designed to study the possibility to make modifications and reduce the total cycle time. In particular, to minimize the thermal dispersion, a moving system for the cavity seat was designed. The idea was obtaining a system that allows a quick separation of the cavity seat from the rest of the mold when the mold plates are in the open position. Simulations conducted by Moldflow software verified that the air gap between the mold and the cavity permitted to obtain large increases in cavity temperature in a few seconds. When the mold is closed, conversely, the cavity seat pushed toward the mold put in contact the cavity and the rest of the mold allowing a rapid cooling. In addition, an evaluation of the heat transfer, by means of simulations was carried out. The study demonstrated that during the heating step, the use of the system allows the reduction of the thermal dispersion and the achievement of a temperature increase of the order of one hundred degrees at the cavity surfaces. Furthermore, the high thermal conductivity of the cavity permits to obtain a fast cooling when the mold is closed.

Future research

The thesis focused on the development of a method to rapidly change the temperature of the surface of the cavity without influencing the one of the rest of the mold. This method was applied to study the effect on the filling, the morphology and the weld line of semi-crystalline polymers. A study of the implementation of the technique in a mold for industrial scale was also presented.

Future research can involve different interesting developments of the work:

- Verifying the effect of rapid thermal variations in parts produced by polymers different from the ones used in this thesis and applying the same methods adopted in this work.
- Applying the system in more complex geometries to verify its adaptability. Due to the use of flexible elements it is expected that one can attach the thermocouples and the heaters to curved shapes.
- It could be very interesting the application of rapid temperature variations to study the replication capabilities of polymers when surfaces have features in the nano-meter scale. The surfaces of the cavity and the samples produced can be analyzed by means of a profilometer or Atomic Force Microscope.
- Investigate the effect of different cooling rates on the morphologies of semi-crystalline polymers. The Labview Code that was used for the experiments described in the thesis could be rewritten to regulate in different manner the cooling rate, in particular, it is possible to properly decrease it by switching on the power supply. Considerable differences in the morphology developed are expected in polymers characterized by a fast crystallization rate, like the isotactic polypropylene.
- Considering the method proposed in the chapter 7, the combination of the control system with a moving system for the different steps in the cycle could be developed to explore the properties of the parts.
- Using diffractometric analysis to investigate the morphology development in polypropylene when the temperature of the surfaces are between 80°C and 105°C.
- Verify the effect of thermal variation on the adhesion of co-injection molded micro-parts.
- Analyze the benefits of the soft micro-injection molding that requires the use of lower injection pressures compared to the conventional ones on the final properties and defects of the micro-parts.

Bibliography

Arias, V. *et al.* (2014) ‘Tuning the Degradation Profiles of Poly(l-lactide)-Based Materials through Miscibility’, *Biomacromolecules*. American Chemical Society, 15(1), pp. 391–402. doi: 10.1021/bm401667b.

Auras, R. A. *et al.* (2011) *Poly (lactic acid): synthesis, structures, properties, processing, and applications*. John Wiley & Sons.

Auras, R., Harte, B. and Selke, S. (2004) ‘An Overview of Polylactides as Packaging Materials’, *Macromolecular Bioscience*. John Wiley & Sons, Ltd, 4(9), pp. 835–864. doi: 10.1002/mabi.200400043.

Babu, R. P., O’Connor, K. and Seeram, R. (2013) ‘Current progress on bio-based polymers and their future trends’, *Progress in Biomaterials*, 2(1), p. 8. doi: 10.1186/2194-0517-2-8.

Belbella, A. *et al.* (1996) ‘In vitro degradation of nanospheres from poly(D,L-lactides) of different molecular weights and polydispersities’, *International Journal of Pharmaceutics*, 129(1), pp. 95–102. doi: https://doi.org/10.1016/0378-5173(95)04258-X.

Bociąga, E. *et al.* (2019) ‘The influence of the type of polypropylene and the length of the flow path on the structure and properties of injection molded parts with the weld lines’, *Polymer Engineering & Science*. John Wiley & Sons, Ltd, 59(8), pp. 1710–1718. doi: 10.1002/pen.25170.

Bojda, J. and Piorkowska, E. (2016) ‘Shear-induced nonisothermal crystallization of two grades of PLA’, *Polymer Testing*, 50, pp. 172–181. doi: https://doi.org/10.1016/j.polymertesting.2016.01.006.

Cai, H. *et al.* (1996) ‘Effects of physical aging, crystallinity, and orientation on the enzymatic degradation of poly(lactic acid)’, *Journal of Polymer Science Part B: Polymer Physics*. John Wiley & Sons, Ltd, 34(16), pp. 2701–2708. doi: 10.1002/(SICI)1099-0488(19961130)34:16<2701::AID-POLB2>3.0.CO;2-S.

Chen, S.-C. *et al.* (2012) ‘Mold temperature control using high-frequency proximity effect induced heating’, *International Communications in Heat and Mass Transfer*, 39(2), pp. 216–223. doi: https://doi.org/10.1016/j.icheatmasstransfer.2011.11.006.

Coates, P. D. *et al.* (2006) ‘Micromoulding – precision processing for controlled products’, in Menz, W., Dimov, S., and Fillon, B. B. T.-4M 2006-S. I. C. on M.-M. M. M. (eds). Oxford: Elsevier, pp. 13–15. doi: https://doi.org/10.1016/B978-008045263-0/50004-0.

Coccorullo, I., Pantani, R. and Titomanlio, G. (2003) ‘Crystallization kinetics and solidified structure in iPP under high cooling rates’, *Polymer*, 44(1), pp. 307–318. doi: https://doi.org/10.1016/S0032-3861(02)00762-0.

Crema, L., Sorgato, M. and Lucchetta, G. (2017) ‘Thermal optimization of deterministic porous mold inserts for rapid heat cycle molding’, *International Journal of Heat and Mass Transfer*, 109, pp. 462–469. doi:

https://doi.org/10.1016/j.ijheatmasstransfer.2017.02.023.
Dorgan, J. R. *et al.* (2001) ‘Polylactides: properties and prospects of an environmentally benign plastic from renewable resources’, *Macromolecular Symposia*. John Wiley & Sons, Ltd, 175(1), pp. 55–66. doi: 10.1002/1521-3900(200110)175:1<55::AID-MASY55>3.0.CO;2-K.
Drumright, R. E., Gruber, P. R. and Henton, D. E. (2000) ‘Polylactic Acid Technology’, *Advanced Materials*. John Wiley & Sons, Ltd, 12(23), pp. 1841–1846. doi: 10.1002/1521-4095(200012)12:23<1841::AID-ADMA1841>3.0.CO;2-E.
Duan, Z. and Thomas, N. L. (2014) ‘Water vapour permeability of poly(lactic acid): Crystallinity and the tortuous path model’, *Journal of Applied Physics*. American Institute of Physics, 115(6), p. 64903. doi: 10.1063/1.4865168.
Farah, S., Anderson, D. G. and Langer, R. (2016) ‘Physical and mechanical properties of PLA, and their functions in widespread applications — A comprehensive review’, *Advanced Drug Delivery Reviews*, 107, pp. 367–392. doi: https://doi.org/10.1016/j.addr.2016.06.012.
Finniss, A., Agarwal, S. and Gupta, R. (2016) ‘Retarding hydrolytic degradation of polylactic acid: Effect of induced crystallinity and graphene addition’, *Journal of Applied Polymer Science*. John Wiley & Sons, Ltd, 133(43). doi: 10.1002/app.44166.
Fischer, C. *et al.* (2017) ‘Influencing hardness and wear during the dynamic tempered microinjection molding process by considering isothermal holding time’, *Polymer Engineering & Science*. John Wiley & Sons, Ltd, 57(2), pp. 121–128. doi: 10.1002/pen.24394.
Fukushima, K., Feijoo, J. L. and Yang, M.-C. (2013) ‘Comparison of abiotic and biotic degradation of PDLLA, PCL and partially miscible PDLLA/PCL blend’, *European Polymer Journal*, 49(3), pp. 706–717. doi: https://doi.org/10.1016/j.eurpolymj.2012.12.011.
Gamez-Perez, J. *et al.* (2011) ‘Influence of crystallinity on the fracture toughness of poly(lactic acid)/montmorillonite nanocomposites prepared by twin-screw extrusion’, *Journal of Applied Polymer Science*. John Wiley & Sons, Ltd, 120(2), pp. 896–905. doi: 10.1002/app.33191.
Gao, S. *et al.* (2017) ‘Development of high efficiency infrared-heating-assisted micro-injection molding for fabricating micro-needle array’, *The International Journal of Advanced Manufacturing Technology*, 92(1), pp. 831–838. doi: 10.1007/s00170-017-0169-5.
Giboz, J., Copponnex, T. and Mélé, P. (2007) ‘Microinjection molding of thermoplastic polymers: a review’, *Journal of Micromechanics and Microengineering*. IOP Publishing, 17(6), pp. R96–R109. doi: 10.1088/0960-1317/17/6/r02.
Gleadall, A. *et al.* (2014) ‘Degradation mechanisms of bioresorbable polyesters. Part 1. Effects of random scission, end scission and autocatalysis’, *Acta Biomaterialia*, 10(5), pp. 2223–2232. doi:

https://doi.org/10.1016/j.actbio.2013.12.039.

Gorrasi, G. and Pantani, R. (2013) ‘Effect of PLA grades and morphologies on hydrolytic degradation at composting temperature: Assessment of structural modification and kinetic parameters’, *Polymer Degradation and Stability*, 98(5), pp. 1006–1014. doi: https://doi.org/10.1016/j.polymdegradstab.2013.02.005.

Gorrasi, G. and Pantani, R. (2017) ‘Hydrolysis and Biodegradation of Poly (lactic acid)’, in *Synthesis, Structure and Properties of Poly (lactic acid)*. Springer, pp. 119–151.

Guo, C. *et al.* (2012) ‘Morphological evolution of HDPE parts in the microinjection molding: Comparison with conventional injection molding’, *Journal of Applied Polymer Science*. John Wiley & Sons, Ltd, 126(2), pp. 452–462. doi: 10.1002/app.36698.

Gupta, B., Revagade, N. and Hilborn, J. (2007) ‘Poly(lactic acid) fiber: An overview’, *Progress in Polymer Science*, 32(4), pp. 455–482. doi: https://doi.org/10.1016/j.progpolymsci.2007.01.005.

Ha, J. U. and Xanthos, M. (2010) ‘Novel modifiers for layered double hydroxides and their effects on the properties of polylactic acid composites’, *Applied Clay Science*, 47(3), pp. 303–310. doi: https://doi.org/10.1016/j.clay.2009.11.033.

Harris, A. M. and Lee, E. C. (2008) ‘Improving mechanical performance of injection molded PLA by controlling crystallinity’, *Journal of Applied Polymer Science*. John Wiley & Sons, Ltd, 107(4), pp. 2246–2255. doi: 10.1002/app.27261.

Himasekhar, K., Lottey, J. and Wang, K. K. (1992) ‘CAE of mold cooling in injection molding using a three-dimensional numerical simulation’, *Journal of engineering for industry*. American Society of Mechanical Engineers Digital Collection, 114(2), pp. 213–221.

Hocking, P. J. *et al.* (1995) ‘Enzymatic Degradability of Poly(β-Hydroxybutyrate) as a Function of Tacticity’, *Journal of Macromolecular Science, Part A*. Taylor & Francis, 32(4), pp. 889–894. doi: 10.1080/10601329508010302.

Iannace, S. and Nicolais, L. (1997) ‘Isothermal crystallization and chain mobility of poly(L-lactide)’, *Journal of Applied Polymer Science*. John Wiley & Sons, Ltd, 64(5), pp. 911–919. doi: 10.1002/(SICI)1097-4628(19970502)64:5<911::AID-APP11>3.0.CO;2-W.

Iqbal, N. *et al.* (2019) ‘Critical specific work of flow for shear-induced formation of crystal nuclei in poly (l-lactic acid)’, *POLYMER CRYSTALLIZATION*. John Wiley & Sons, Ltd, 2(4), p. e10073. doi: 10.1002/pcr2.10073.

Jamshidian, M. *et al.* (2010) ‘Poly-Lactic Acid: Production, Applications, Nanocomposites, and Release Studies’, *Comprehensive Reviews in Food Science and Food Safety*. John Wiley & Sons, Ltd (10.1111), 9(5), pp. 552–571. doi: 10.1111/j.1541-4337.2010.00126.x.

Jeng, M.-C. *et al.* (2010) ‘Rapid mold temperature control in injection molding by using steam heating’, *International Communications in Heat and Mass Transfer*, 37(9), pp. 1295–1304. doi: https://doi.org/10.1016/j.icheatmasstransfer.2010.07.012.

Jiang, J. *et al.* (2015) ‘Effect of mold temperature on the structures and mechanical properties of micro-injection molded polypropylene’, *Materials & Design*, 88, pp. 245–251. doi: https://doi.org/10.1016/j.matdes.2015.09.003.

Jones, A. T., Aizlewood, J. M. and Beckett, D. R. (1964) ‘Crystalline forms of isotactic polypropylene’, *Die Makromolekulare Chemie*. John Wiley & Sons, Ltd, 75(1), pp. 134–158. doi: 10.1002/macp.1964.020750113.

de Jong, S. J. *et al.* (2001) ‘New insights into the hydrolytic degradation of poly(lactic acid): participation of the alcohol terminus’, *Polymer*, 42(7), pp. 2795–2802. doi: https://doi.org/10.1016/S0032-3861(00)00646-7.

Kamal, M. R. and Lafleur, P. G. (1984) ‘Heat transfer in injection molding of crystallizable polymers’, *Polymer Engineering & Science*. John Wiley & Sons, Ltd, 24(9), pp. 692–697. doi: 10.1002/pen.760240911.

Kenig, S. and Kamal, M. R. (1970) ‘Cooling molded parts-A rigorous analysis’, *SPE JOURNAL*, 26(7), p. 50.

Kim, S. *et al.* (2007) ‘Injection Molding Nanoscale Features with the Aid of Induction Heating’, *Polymer-Plastics Technology and Engineering*. Taylor & Francis, 46(11), pp. 1031–1037. doi: 10.1080/03602550701522344.

Kühnert, I. *et al.* (2018) ‘Processing of Poly(lactic Acid) BT - Industrial Applications of Poly(lactic acid)’, in Di Lorenzo, M. L. and Androsch, R. (eds). Cham: Springer International Publishing, pp. 1–33. doi: 10.1007/12_2017_30.

Lee, J. K., Lee, K. H. and Jin, B. S. (2001) ‘Structure development and biodegradability of uniaxially stretched poly(l-lactide)’, *European Polymer Journal*, 37(5), pp. 907–914. doi: https://doi.org/10.1016/S0014-3057(00)00213-5.

Li, G. *et al.* (2019) ‘Interfacial cylindrite of poly(lactic acid) induced by pulling a single glass fiber’, *European Polymer Journal*, 114, pp. 127–133. doi: https://doi.org/10.1016/j.eurpolymj.2019.02.016.

Li, S., Garreau, H. and Vert, M. (1990) ‘Structure-property relationships in the case of the degradation of massive poly ($α$-hydroxy acids) in aqueous media’, *Journal of Materials Science: Materials in Medicine*. Springer, 1(4), pp. 198–206.

Li, S. and McCarthy, S. (1999) ‘Influence of Crystallinity and Stereochemistry on the Enzymatic Degradation of Poly(lactide)s’, *Macromolecules*. American Chemical Society, 32(13), pp. 4454–4456. doi: 10.1021/ma990117b.

Li, X. *et al.* (2017) ‘Enhancing the joining strength of injection-molded polymer-metal hybrids by rapid heating and cooling’, *Journal of Materials Processing Technology*, 249, pp. 386–393. doi:

https://doi.org/10.1016/j.jmatprotec.2017.06.034.
Liparoti, S *et al.* (2019) 'Modeling of the Injection Molding Process Coupled with the Fast Mold Temperature Evolution', *JOURNAL OF THE ELECTROCHEMICAL SOCIETY*, 166(9), pp. B3148–B3155. doi: 10.1149/2.0291909jes.
Liparoti, Sara *et al.* (2019) 'Process Induced Morphology Development of Isotactic Polypropylene on the Basis of Molecular Stretch and Mechanical Work Evolutions', *Materials*. Multidisciplinary Digital Publishing Institute, 12(3), p. 505. doi: 10.3390/ma12030505.
Liu, F. *et al.* (2012) 'Morphological comparison of isotactic polypropylene parts prepared by micro-injection molding and conventional injection molding', *Polymers for Advanced Technologies*. John Wiley & Sons, Ltd, 23(3), pp. 686–694. doi: 10.1002/pat.1946.
Liu, J. *et al.* (2017) 'Numerical and experimental investigations on polymer melt flow phenomenon in a vario-thermal mold cavity', *Journal of Applied Polymer Science*. John Wiley & Sons, Ltd, 134(33), p. 45193. doi: 10.1002/app.45193.
Lostocco, M. R. and Huang, S. J. (1998) 'The hydrolysis of poly(lactic acid)/ poly(hexamethylene succinate) blends', *Polymer Degradation and Stability*, 61(2), pp. 225–230. doi: https://doi.org/10.1016/S0141-3910(97)00138-9.
Lucchetta, G., Fiorotto, M. and Bariani, P. F. (2012) 'Influence of rapid mold temperature variation on surface topography replication and appearance of injection-molded parts', *CIRP Annals*, 61(1), pp. 539–542. doi: https://doi.org/10.1016/j.cirp.2012.03.091.
Ma, Z. *et al.* (2014) 'Flow induced crystallization in isotactic polypropylene during and after flow', *Polymer*, 55(23), pp. 6140–6151. doi: https://doi.org/10.1016/j.polymer.2014.09.039.
Madhavan Nampoothiri, K., Nair, N. R. and John, R. P. (2010) 'An overview of the recent developments in polylactide (PLA) research', *Bioresource Technology*, 101(22), pp. 8493–8501. doi: https://doi.org/10.1016/j.biortech.2010.05.092.
Meister, S. and Drummer, D. (2013) 'Investigation on the Achievable Flow Length in Injection Moulding of Polymeric Materials with Dynamic Mould Tempering', *SCIENTIFIC WORLD JOURNAL*. doi: 10.1155/2013/845916.
Monnier, X. *et al.* (2017) 'Local and segmental motions of the mobile amorphous fraction in semi-crystalline polylactide crystallized under quiescent and flow-induced conditions', *Polymer*, 126, pp. 141–151. doi: https://doi.org/10.1016/j.polymer.2017.08.021.
Mulligan, J. and Cakmak, M. (2005) 'Nonlinear Mechanooptical Behavior of Uniaxially Stretched Poly(lactic acid): Dynamic Phase Behavior', *Macromolecules*. American Chemical Society, 38(6), pp. 2333–2344. doi: 10.1021/ma048794f.
Murariu, M. *et al.* (2014) 'Chapter 21 - Pathways to Biodegradable Flame Retardant Polymer (Nano)Composites', in Papaspyrides, C. D. and Kiliaris,

P. B. T.-P. G. F. R. (eds). Amsterdam: Elsevier, pp. 709–773. doi: https://doi.org/10.1016/B978-0-444-53808-6.00021-4.

Pantani, R. *et al.* (2005) 'Modeling of morphology evolution in the injection molding process of thermoplastic polymers', *Progress in Polymer Science*, 30(12), pp. 1185–1222. doi: https://doi.org/10.1016/j.progpolymsci.2005.09.001.

Pantani, R. *et al.* (2007) 'Morphology evolution during injection molding: Effect of packing pressure', *Polymer*, 48(9), pp. 2778–2790. doi: https://doi.org/10.1016/j.polymer.2007.03.007.

Pantani, R. *et al.* (2010) 'Crystallization kinetics of virgin and processed poly(lactic acid)', *Polymer Degradation and Stability*. Elsevier Ltd, 95(7), pp. 1148–1159. doi: 10.1016/j.polymdegradstab.2010.04.018.

Pantani, R., Balzano, L. and Peters, G. W. M. (2012) 'Flow-Induced Morphology of iPP Solidified in a Shear Device', *Macromolecular Materials and Engineering*. John Wiley & Sons, Ltd, 297(1), pp. 60–67. doi: 10.1002/mame.201100158.

Pantani, R. and Sorrentino, A. (2013) 'Influence of crystallinity on the biodegradation rate of injection-moulded poly(lactic acid) samples in controlled composting conditions', *Polymer Degradation and Stability*, 98(5), pp. 1089–1096. doi: https://doi.org/10.1016/j.polymdegradstab.2013.01.005.

Pantani, R., Speranza, V. and Titomanlio, G. (2012) 'Orientation distribution in injection molding: a further step toward more accurate simulations', *Rheologica Acta*, 51(11), pp. 1041–1050. doi: 10.1007/s00397-012-0660-8.

Pantani, R., Speranza, V. and Titomanlio, G. (2017) 'Effect of flow-induced crystallization on the distribution of spherulite dimensions along cross section of injection molded parts', *European Polymer Journal*, 97, pp. 220–229. doi: https://doi.org/10.1016/j.eurpolymj.2017.10.012.

Perego, G., Cella, G. D. and Bastioli, C. (1996) 'Effect of molecular weight and crystallinity on poly(lactic acid) mechanical properties', *Journal of Applied Polymer Science*. John Wiley & Sons, Ltd, 59(1), pp. 37–43. doi: 10.1002/(SICI)1097-4628(19960103)59:1<37::AID-APP6>3.0.CO;2-N.

Raquez, J.-M. *et al.* (2013) 'Polylactide (PLA)-based nanocomposites', *Progress in Polymer Science*, 38(10), pp. 1504–1542. doi: https://doi.org/10.1016/j.progpolymsci.2013.05.014.

Salmerón Sánchez, M. *et al.* (2007) 'Effect of the Cooling Rate on the Nucleation Kinetics of Poly(l-Lactic Acid) and Its Influence on Morphology', *Macromolecules*. American Chemical Society, 40(22), pp. 7989–7997. doi: 10.1021/ma0712706.

De Santis, F. and Pantani, R. (2016) 'Development of a rapid surface temperature variation system and application to micro-injection molding', *Journal of Materials Processing Technology*, 237, pp. 1–11. doi: https://doi.org/10.1016/j.jmatprotec.2016.05.023.

De Santis, F., Pantani, R. and Titomanlio, G. (2011) 'Nucleation and crystallization kinetics of poly(lactic acid)’, *Thermochimica Acta*, 522(1), pp. 128–134. doi: https://doi.org/10.1016/j.tca.2011.05.034.

De Santis, F., Volpe, V. and Pantani, R. (2017) ‘Effect of molding conditions on crystallization kinetics and mechanical properties of poly(lactic acid)’, *Polymer Engineering & Science*. John Wiley & Sons, Ltd, 57(3), pp. 306–311. doi: 10.1002/pen.24414.

Sawyer, D. J. (2003) ‘Bioprocessing – no longer a field of dreams’, *Macromolecular Symposia*. John Wiley & Sons, Ltd, 201(1), pp. 271–282. doi: 10.1002/masy.200351130.

Speranza, V. *et al.* (2017) ‘Replication of micro and nano-features on iPP by injection molding with fast cavity surface temperature evolution’, *Materials & Design*, 133, pp. 559–569. doi: https://doi.org/10.1016/j.matdes.2017.08.016.

Speranza, V., De Meo, A. and Pantani, R. (2014) ‘Thermal and hydrolytic degradation kinetics of PLA in the molten state’, *Polymer Degradation and Stability*, 100(1). doi: 10.1016/j.polymdegradstab.2013.12.031.

Srithep, Y., Nealey, P. and Turng, L.-S. (2013) ‘Effects of annealing time and temperature on the crystallinity and heat resistance behavior of injection-molded poly(lactic acid)’, *Polymer Engineering & Science*. John Wiley & Sons, Ltd, 53(3), pp. 580–588. doi: 10.1002/pen.23304.

Stloukal, P. *et al.* (2015) ‘The influence of a hydrolysis-inhibiting additive on the degradation and biodegradation of PLA and its nanocomposites’, *Polymer Testing*, 41, pp. 124–132. doi: https://doi.org/10.1016/j.polymertesting.2014.10.015.

Su, Q., Zhang, N. and Gilchrist, M. D. (2016) ‘The use of variotherm systems for microinjection molding’, *Journal of Applied Polymer Science*. John Wiley & Sons, Ltd, 133(9). doi: 10.1002/app.42962.

Tang, S. De *et al.* (2013) ‘The Method of Improving Precision of Micro Injection Molding Machine Temperature Control’, *Applied Mechanics and Materials*. Trans Tech Publications Ltd, 372, pp. 354–359. doi: 10.4028/www.scientific.net/AMM.372.354.

Tjader, T., Seppala, J. and Jaaskelainen, P. (1998) ‘Effect of material characteristics of polyolefins on weld line morphology and its correlation to mechanical properties’, *Journal of Materials Science*, 33(4), pp. 923–931. doi: 10.1023/A:1004399409082.

Tosello, G. (2015) ‘Micromanufacturing Engineering and Technology; Qin, Y., Ed’. Elsevier: Amsterdam, The Netherlands.

Tsuji, H. (2003) ‘In vitro hydrolysis of blends from enantiomeric poly(lactide)s. Part 4: well-homo-crystallized blend and nonblended films’, *Biomaterials*, 24(4), pp. 537–547. doi: https://doi.org/10.1016/S0142-9612(02)00365-4.

Tsuji, H. (2010) ‘Hydrolytic Degradation’, *Poly(Lactic Acid)*. (Wiley Online Books), pp. 343–381. doi: doi:10.1002/9780470649848.ch21.

Vadori, R., Mohanty, A. K. and Misra, M. (2013) ‘The Effect of Mold

Temperature on the Performance of Injection Molded Poly(lactic acid)-Based Bioplastic', *Macromolecular Materials and Engineering*. John Wiley & Sons, Ltd, 298(9), pp. 981–990. doi: 10.1002/mame.201200274.

Valentina, I. *et al.* (2018) 'Poly (Lactic Acid)-Based Nanobiocomposites with Modulated Degradation Rates', *Materials*. Multidisciplinary Digital Publishing Institute, 11(10), p. 1943.

Wang, Y. *et al.* (2014) 'Unusual structural evolution of poly(lactic acid) upon annealing in the presence of an initially oriented mesophase', *Soft Matter*. The Royal Society of Chemistry, 10(10), pp. 1512–1518. doi: 10.1039/C3SM52611A.

Weir, N. A. *et al.* (2004) 'Degradation of poly-L-lactide. Part 2: Increased temperature accelerated degradation', *Proceedings of the Institution of Mechanical Engineers, Part H: Journal of Engineering in Medicine*. IMECHE, 218(5), pp. 321–330. doi: 10.1243/0954411041932809.

Wenig, W. and Stolzenberger, C. (1996) 'The influence of molecular weight and mould temperature on the skin-core morphology in injection-moulded polypropylene parts containing weld lines', *Journal of Materials Science*, 31(9), pp. 2487–2493. doi: 10.1007/BF01152966.

Whiteside, B. R. *et al.* (2004) 'Micromoulding: process measurements, product morphology and properties', *Plastics, Rubber and Composites*. Taylor & Francis, 33(1), pp. 11–17. doi: 10.1179/146580104225018346.

Wong, Y. S., Stachurski, Z. H. and Venkatraman, S. S. (2008) 'Orientation and structure development in poly(lactide) under uniaxial deformation', *Acta Materialia*, 56(18), pp. 5083–5090. doi: https://doi.org/10.1016/j.actamat.2008.06.027.

Wu, C.-H. and Liang, W.-J. (2005) 'Effects of geometry and injection-molding parameters on weld-line strength', *Polymer Engineering & Science*. John Wiley & Sons, Ltd, 45(7), pp. 1021–1030. doi: 10.1002/pen.20369.

Xiao, H. *et al.* (2010) 'Kinetics and crystal structure of poly(lactic acid) crystallized nonisothermally: Effect of plasticizer and nucleating agent', *Polymer Composites*. John Wiley & Sons, Ltd, 31(12), pp. 2057–2068. doi: 10.1002/pc.21004.

Xie, L. *et al.* (2010) 'A mechanism influencing micro injection molded weld lines of hybrid nano filled polypropylene', *Microsystem Technologies*, 16(11), pp. 1855–1859. doi: 10.1007/s00542-010-1090-0.

Xie, L. *et al.* (2013) 'A novel approach to realize the local precise variotherm process in micro injection molding', *Microsystem technologies*. Springer, 19(7), pp. 1017–1023.

Xie, L., Ziegmann, G. and Jiang, B. (2009) 'Reinforcement of micro injection molded weld line strength with ultrasonic oscillation', *Microsystem Technologies*, 16(3), p. 399. doi: 10.1007/s00542-009-0928-9.

Xie, P. *et al.* (2017) 'Carbide-bonded graphene coating of mold insert for rapid thermal cycling in injection molding', *Applied Thermal Engineering*, 122, pp. 19–26. doi: https://doi.org/10.1016/j.applthermaleng.2017.04.159.

Yang, S.-P. and Young, W.-B. (2004) ‘Microinjection Molding with LIGA-Like Process’, *International Polymer Processing*. Hanser Verlag, 19(2), pp. 180–185. doi: 10.3139/217.1814.

Yao, D., Kimerling, T. E. and Kim, B. (2006) ‘High-frequency proximity heating for injection molding applications’, *Polymer Engineering & Science*. John Wiley & Sons, Ltd, 46(7), pp. 938–945. doi: 10.1002/pen.20548.

Zhang, L., Zhou, W. and Yi, A. Y. (2017) ‘Rapid localized heating of graphene coating on a silicon mold by induction for precision molding of polymer optics’, *Opt. Lett.* OSA, 42(7), pp. 1369–1372. doi: 10.1364/OL.42.001369.

Zhang, X. *et al.* (1994) ‘An Investigation of Poly(lactic acid) Degradation’, *Journal of Bioactive and Compatible Polymers*. SAGE Publications Ltd STM, 9(1), pp. 80–100. doi: 10.1177/088391159400900105.

Zhao, H. *et al.* (2017) ‘Transition from the hierarchical distribution to a homogeneous formation in injection molded isotactic polypropylene (iPP) with dynamic mold temperature control’, *Polymer Testing*, 60, pp. 299–306. doi: https://doi.org/10.1016/j.polymertesting.2017.04.012.

Zhao, Z.-G. *et al.* (2018) ‘Structure and Property of Microinjection Molded Poly(lactic acid) with High Degree of Long Chain Branching’, *INDUSTRIAL & ENGINEERING CHEMISTRY RESEARCH*, 57(33), pp. 11312–11322. doi: 10.1021/acs.iecr.8b01597.